A novel approach for studying programmed cell death in living plant tissues

Mark, Christina

Publication date:
2015

Document Version
Publisher's PDF, also known as Version of record

A novel approach for studying programmed cell death in living plant tissues

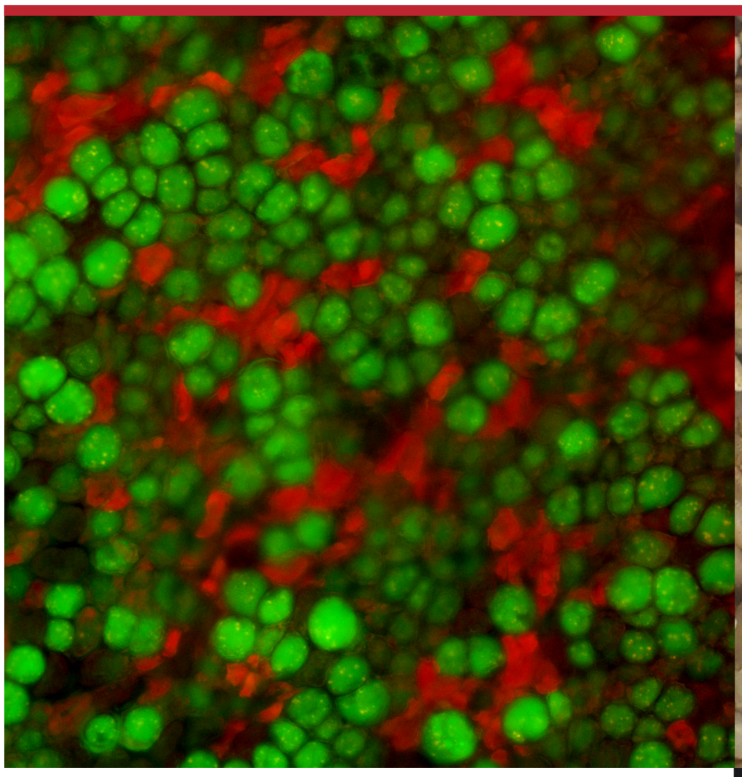

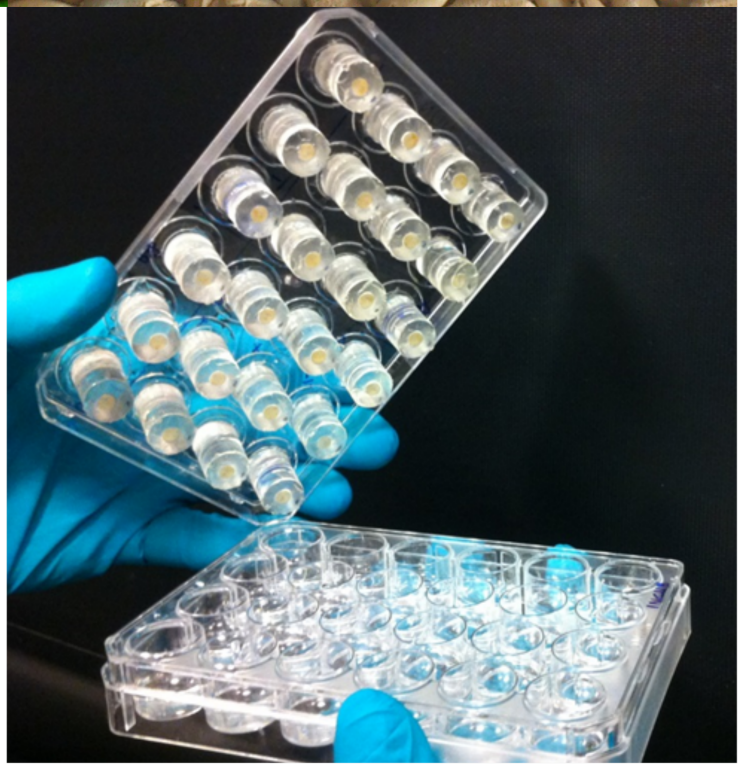

Christina Mark
PhD thesis
February 2015

DTU Systems Biology
Department of Systems Biology

DTU Nanotech
Department of Micro- and Nanotechnology

A novel approach for studying programmed cell death in living plant tissues

Christina Mark
PhD thesis
February 2012 – February 2015
Department of Systems Biology
Technical University of Denmark

Supervisors:

Associate professor Martin Dufva
Department of Micro- and Nanotechnology

Associate professor Christine Finnie
Department of Systems Biology

Front page illustrations:

Top left: FDA/MM 4-64 stained barley aleurone cells
Top right: Barley grains
Bottom right: Developed 24-well incubation system (photo: Kinga Zór)

Preface

This PhD thesis presents the results of my PhD project carried out in a cross-disciplinary collaboration between Department of Systems Biology and Department of Micro- and Nanotechnology, Technical University of Denmark, from February 2012 to February 2015 under supervision of Associate Professor Christine Finnie, Dept. of Systems Biology, and Associate Professor Martin Dufva, Dept. of Micro- and Nanotechnology.
Transient expression by particle bombardment was performed at Department of Molecular Biology and Genetics, Research Center Flakkebjerg, Aarhus University, under the supervision of Associate Professor Henrik Brinch-Pedersen.
All electrochemical measurements was performed by Postdoc Kinga Zór, Department of Micro- and Nanotechnology. Design and development of the 24-well incubation system for immobilised plant tissues was performed in collaboration with Kinga Zór.
The PhD project was funded by the Technical University of Denmark and the Danish Council for Independent Research (Natural Sciences).

The work has resulted in the following manuscripts, which are included in this thesis:

Mark, C.*, Zór, K.*, Heiskanen, A., Dufva, M., Emnéus, J., and Finnie, C. Electrochemical measurement of the intra- and extracellular redox environment in intact plant tissue responding to phytohormones. Manuscript submitted to Bioelectrochemistry (Part II).

Zór, K.*, **Mark, C.***, Heiskanen, A., Madsen, C. K., Dufva, M., Emnéus, J., Brinch-Pedersen, H., and Finnie, C. Easy immobilisation of living plant tissue, enabling higher throughput and parallelization of assays: Time course analysis of programmed cell death in barley aleurone layers. Manuscript in preparation, intended for submission to Plant Methods (Part IV).

* Shared first authorship.

Acknowledgements

I have received help and advice from a number of people throughout my PhD studies and I would therefore like to thank the following:

- Postdoc Kinga Zór (Dept. of Micro- and Nanotechnology) for a fantastic collaboration, for measuring an unbelievable amount of samples for me, and for always having the time to discuss results, future experimental designs, this thesis, and life in general.
- My supervisor Assoc. Prof. Christine Finnie (Dept. of Systems Biology) for answering all my stupid questions and guiding me, even during her maternity leaves.
- My supervisor Assoc. Prof. Martin Dufva (Dept. of Micro- and Nanotechnology) for posing critical questions to my results and for always keeping a positive outlook on less-than-good situations.
- Technicians Birgit Andersen (formerly Dept. of Systems Biology, now Dept. of Plant and Environmental Sciences, Copenhagen University) and Karina Jansen (Dept. of Systems Biology) for helping out with an immeasurable number of practicalities in the lab.
- Assoc. Prof. Henrik Brinch-Pedersen and Postdoc Claus Krogh Madsen (Dept. of Molecular Biology and Genetics, Research Center Flakkebjerg, Aarhus University) for supervising and assisting my work with transformation by particle bombardment.
- Postdoc Christina Rønn Ingvardsen and technicians Lis Bagnkop Holte and Inger Holme (Dept. of Molecular Biology and Genetics, Research Center Flakkebjerg, Aarhus University) for technical assistance and guidance in connection with the transformation by particle bombardment.
- My friends Postdocs Lea Benedicte Skov Hansen (Dept. of Systems Biology), Marie Sofie Møller (Dept. of Biochemistry and Structural Biology, Lund University, and Dept. of Systems Biology) and Casper Wilkens (Dept. of Chemistry and Bioscience, Aalborg University) for using their weekend to critically read, comment and improve this thesis.
- Friends and family of every kind for listening to all my complaints, for cheering me up, and for feigning an interest in or understanding of what this PhD mumbo-jumbo was all about
- And finally, my boyfriend Philippe Holt for happily looking at my results from new angles and discussing them with me, for knowing exactly when I needed a break and then making me take it, and for always believing in me.

Abstract

Programmed cell death (PCD) is a highly regulated process in which cells are killed as part of developmental programmes or as defence mechanisms against pathogens, but the process is less well understood in plant cells compared to animal cells. Reactive oxygen species (ROS) are involved in PCD in plants, but the relationship between and mechanisms behind ROS and PCD has not yet been fully elucidated due to the involvement of complex signalling networks. Elucidation of these mechanisms and signalling pathways will allow manipulation of cell death in plants, which could help to improve yield and quality of crops and thus contribute to solving the increasing food demands of the planet. Examples of this could be the development of cultivars with enhanced and/or faster response to pathogen attacks, or cultivars with increased grain filling and hence increased starch content through delayed cell death of the endosperm.
The barley aleurone layer is a generally accepted model system for studying phytohormone signalling, enzyme secretion, and PCD during seed germination. However, two main issues affect PCD-related research in the barley aleurone layer: Firstly, the current knowledge about ROS signalling and the cellular redox environment in aleurone layers undergoing PCD is mainly based on analyses of cell extracts, which do not evaluate the overall cellular redox environment in intact plant cells. Secondly, analyses based on cell extracts are end-point measurements, which are limited by the fact that each analysis is performed on a different pool of samples, as each tissue sample or population of cells can only be analysed at a single time point. This is of great importance for studies of time-dependent processes such as PCD, as time course experiments can be affected by biological and experimental diversity between independent samples, which could distort the interpretation of the results. Time course experiments on the same tissue or population of cells can be enabled by the use of assays that do not destroy cellular integrity, which could also facilitate the combination of multiple assays. However, time course studies with analysis of multiple parameters using different detection techniques remain challenging, as the different assays under consideration may be incompatible, and some assays may affect the plant tissue and therefore influence the outcome of simultaneous or subsequent analyses.

A previously described optical method was used to monitor PCD, while a previously described method for electrochemical detection of intracellular redox activity was tested and optimised for use with the aleurone layers. The electrochemical method had not previously been used in plant biology, and provided new insight by determining both the intra- and extracellular reducing capacity in living cells rather than using cell extracts. The reducing capacity of aleurone cells was shown to increase over time in parallel with the increase in cell death. Use of the flavoenzyme inhibitor diphenyleneiodonium chloride (DPI) provided evidence that the gibberellic acid-induced increase in reducing capacity is dependent on the plasma membrane-bound NADPH oxidase. A preliminary proteomics investigation also showed indirect effects of DPI on the abundance of glyceraldehyde-3-phosphate dehydrogenase 2 but not on the very similar paralogue

glyceraldehyde-3-phosphate dehydrogenase 1. Further investigations are needed to clarify these effects and to determine which other enzymes are affected by DPI.
A 24-well multiplate incubation system for immobilised plant tissues was developed to allow time course studies on the same tissues and to enable parallel use of multiple non-destructive assays. Immobilisation of the tissues in the lid of a 24-well plate facilitated easy combination of multiple assays by movement of the plate lid, lessened the workload by decreasing the amount of aleurone layers to be dissected 25-fold, and enabled a higher throughput. The system was used for parallel time course studies of cell viability, intracellular reducing capacity and transient expression profiles in immobilised tissue under multiple incubation conditions. Immobilisation resulted in decreased rates of cell death due to the lower exposure of immobilised tissues to the incubation buffer, but tendencies for both cell viability and reducing capacity remained the same for both non-immobilised and immobilised tissues. The parallel studies of cell viability and reducing capacity also revealed that PCD is induced by different mechanisms for tunicamycin, an inducer of protein unfolding in the endoplasmic reticulum, and the NO scavenger 2-(4-carboxyphenyl)-4,4,5,5-tetramethylimidazoline-1-oxyl-3-oxide.

Using optical and electrochemical detection techniques, this project has obtained new knowledge of increases in intra- and extracellular reducing capacity taking place in parallel with PCD, and proposed this increased reducing capacity as a mechanism for holding the 'oxidative window' for germination open. The involvement of the NADPH oxidase or other flavoenzymes in determining the level of gibberellic acid-induced reducing capacity was also shown using the inhibitor DPI. The new incubation system for immobilised aleurone layers enabled simple, user-friendly handling of plant tissue incubations and facilitated transient expression studies in plant tissues by particle bombardment as well as time course studies on the same population of cells combining multiple non-destructive assays. The immobilised approach allowed single transformed cells to be followed over time and provided an insight into the cell-to-cell variability of the actual transformation event, yielding a more detailed picture of transient expression profiles compared to traditional approaches.
Future applications of this type of setup could be used for other types of plant tissues such as leaves or germinating embryos for studying the effects of e.g. biotic and abiotic stresses or for screening of compounds for biological effects. Due to the ease of use and many possibilities of assay combinations, the setup has great potential in the area of plant science.

Sammenfatning

Programmeret celledød (PCD) er en stramt reguleret proces hvorunder celler dør som en del af udvikling og vækst eller som en del af forsvarsmekanismer mod patogener, men forståelse for processen er mindre i planteceller sammenlignet med dyreceller. Reaktive iltforbindelser (ROS) er involveret i PCD i planter, men forholdet mellem og mekanismerne bag ROS og PCD endnu ikke fuldt belyst som følge af de komplekse signaleringsnetværk, der er involveret. Belysning af disse mekanismer og signalveje vil muliggøre manipulation af celledød i planter, hvilket kan bidrage til at forbedre udbyttet og kvaliteten af afgrøder og dermed bidrage til at løse planetens stigende fødevarebehov. Eksempler på dette kunne være kornsorter med øget og/eller hurtigere respons til patogene angreb, eller kornsorter med øget stivelsesindhold gennem forsinket celledød af endeosperm-celler.
Bygkerners aleuroncellelag er et generelt accepteret modelsystem til undersøgelse phytohormonsignalering, enzymsudskillelse og PCD under frøspiring. To hovedspørgsmål påvirker imidlertid PCD-relateret forskning i aleuronlaget: For det første er den aktuelle viden om ROS signalering og det cellulære redox miljø i aleuronlag under frøspiring og PCD hovedsagelig baseret på analyser af celleekstrakter, hvilket forhindrer vurdering af det samlede cellulære redox-miljø i intakte planteceller. For det andet muliggÃ¸r celleekstrakter kun slutpunktsmålinger, som er begrænset af det faktum, at hver analyse udføres på en ny pulje af prøver, da hver vævsprøve eller population af celler kun kan analyseres på ét enkelt tidspunkt. Dette er af stor betydning for studier af tidsafhængige processer såsom PCD, da tidsafhængige eksperimenter kan påvirkes af den biologiske og eksperimentelle diversitet mellem prøver, hvilket kan forvride fortolkningen af resultaterne. Tidsafhængige forsøg på det samme væv eller den samme population af celler kan muliggøres ved anvendelse af analyser, der ikke ødelægger cellulær integritet, hvilket også vil muliggøre kombinationen af flere analyser. Tidsafhængige studier med analyse af flere parametre er dog fortsat udfordrende, da forskellige ønskelige analyser kan være uforenelige, og da nogle analyser kan påvirke plantevævet og dermed resultatet af samtidige eller efterfølgende analyser.

En tidligere beskrevet optisk metode blev anvendt til at observere PCD, mens en tidligere beskrevet metode til elektrokemisk bestemmelse af intracellulær redox-aktivitet blev testet og optimeret til brug med aleuronlag. Den elektrokemiske metode har ikke tidligere været anvendt indenfor plantebiologi og resulterede i ny indsigt ved at bestemme både intra- og ekstracellulær reducerende kapacitet i levende celler frem for at bruge celleekstrakter. Den reducerende kapacitet i aleuronceller viste sig at stige over tid i takt med en stigning i celledød. Anvendelse af flavoenzym-inhibitoren diphenyleneiodonium klorid (DPI) afslørede, at den gibberellinsyre-inducerede stigning i reducerende kapacitet afhænger af den plasmamembran-bundne NADPH oxidase. Et indledende proteom-studie viste også indirekte effekter af DPI på glyceral-dehyd-3-phosphat dehydrogenase 2 men ikke på paralogen glyceraldehyd-3-phosphat dehydrogenase 1.

Yderligere undersøgelser er nødvendige for at afklare disse effekter og for at kortlægge hvilke andre enzymer, der er påvirket af DPI.
Et 24-brønds, multiplade inkubationssystem for immobiliseret plantevæv blev udviklet for at muliggøre tidsafhængige undersøgelser af det samme væv og for at muliggøre parallelt brug af flere ikke-destruktive analyser. Immobilisering af plantevæv i låget på en multiplade med 24 brønde muliggjorde simpel kombination af flere analyser ved bevægelse af pladelåget og mindskede arbejdsbyrden ved at nedsætte mængden af aleuronlag der skulle dissekeres til 1/25 af det oprindelige antal. Systemet blev anvendt til parallelle, tidsafhængige undersøgelser af celledød, intracellulær reducerende kapacitet og transiente ekspressionsprofiler i immobiliseret væv under flere inkubationsbetingelser. Immobilisering af aleuronlag resulterede i reduceret celledødshastighed som følge af lavere eksponering af det immobiliserede væv til inkubationsbufferen, mens tendenser for både celledød og reducerende kapacitet forblev den samme for både ikke-immobiliserede og immobiliserede væv. De parallelle undersøgelser af celledød og reducerende kapacitet afslørede også, at PCD induceres af forskellige mekanismer for tunicamycin, der inducerer proteinudfoldning i det endoplasmatiske reticulum, og 2-(4-carboxyphenyl)-4,4,5,5-tetramethylimidazoline-1-oxyl-3-oxid, der eliminerer nitrogenmonoxid.

Ved hjælp af optiske og elektrokemiske analyseteknikker har dette projekt frembragt ny viden om stigninger i intra- og ekstracellulær reducerende kapacitet, der finder sted sideløbende med stigninger i PCD, og fremsat en hypotese om at denne øgede reducerende kapacitet er en mekanisme til at holde det 'oxidative vindue' for frøspiring åbent. NADPH oxidase eller andre flavoenzymer blev påvist at være involverede i den gibberellinsyre-inducerede reducerende kapacitet ved hjælp af inhibitoren DPI. Det nye inkubationssystem for immobiliserede aleuronlag muliggjorde enkel, brugervenlig håndtering af plantevævsinkubationer, transiente ekspressionsundersøgelser ved partikelbombardement samt tidsafhængige undersøgelser af den samme population af celler med kombinering af flere ikke-destruktive analyser. Den immobiliserede fremgangsmåde tillod at enkelte transformerede celler kunne følges over tid og gav dermed et indblik i celle-til-celle variationen af selve transformationen, hvilket gav et mere detaljeret billede af transiente ekspressionsprofiler sammenlignet med traditionelle fremgangsmåder.
Fremtidige anvendelser af denne type setup forventes at kunne bruges til andre typer plantevæv såsom blade eller spirende kimplanter til undersøgelse af blandt andet biotisk og abiotisk stress eller til screening af molekyler for biologiske effekter. På grund af den høje brugervenlighed og de mange muligheder for analysekombinationer har det udviklede inkubationssystem et stort potentiale inden for plantevidenskab.

List of Symbols and Abbreviations

A	Absorbance
C	Number of conditions for aleurone layer incubation
D	Dilution factor for spectrophotometrical redox assay
N	Number of samples for aleurone layer incubation
P	Number of parameters for aleurone layer incubation
R	Number of replicates for aleurone layer incubation
TP	Number of time points for aleurone layer incubation
ϵ	Molar extinction coefficient of BPDS
c	FoC concentration
l	Length of the spectrophotometer cuvette
ABA	Abscisic acid
AsA	Ascorbic acid (ascorbate)
BPDS	Bathophenanthroline disulfonate
cPTIO	2-(4-carboxyphenyl)-4,4,5,5-tetramethylimidazoline-1-oxyl-3-oxide
DPI	Diphenyleneiodonium chloride
FDA	Fluorescein diacetate
Fe^{2+}	Ferrous ion
Fe^{3+}	Ferric ion
FiC	Ferricyanide, $[Fe(CN)_6]^{3-}$
FoC	Ferrocyanide, $[Fe(CN)_6]^{4-}$
FTU	Phytase activity unit
GA	Gibberellic acid (gibberellin A_3)
GAPDH1	Glyceraldehyde-3-phosphate dehydrogenase 1
GAPDH2	Glyceraldehyde-3-phosphate dehydrogenase 2
GFP	Green fluorescent protein

H_2O_2	Hydrogen peroxide
$HO^{\bullet}$	Hydroxyl radical
M	Menadione
$M^{\bullet -}$	Menadione semiquinone radical
MH_2	Menadiol
MM 4-64	*N*-(3triethylammoniumpropyl)-4-(6-(4-(diethylamino)phenyl)hexatrienyl) pyridinium dibromide
MRE	Menadione reducing enzyme
MS	Mass spectrometry
NaN_3	Sodium azide
$NO^{\bullet}$	Nitric oxide radical
$O_2^{\bullet -}$	Superoxide radical
PCD	Programmed cell death
PDMS	Polydimethylsiloxane
PMMA	Polymethyl methacrylate
QR	Quinone reductase
ROS	Reactive oxygen species
SD	Standard deviation
SNAP	*S*-nitroso-*N*-acetylpenicillamine
SNP	Sodium nitroprusside
T	Tunicamycin
TMT	Tandem mass tag
U	α-amylase activity unit
UT	Untreated

List of Figures

List of Tables

Contents

Part I

Introduction

Programmed cell death (PCD) is a highly regulated process in which cells are killed as part of developmental programmes or as defence mechanisms against pathogens, but the process is less well understood in plant cells compared to animal cells [1–3]. Reactive oxygen species (ROS), such as hydrogen peroxide (H_2O_2), superoxide radical ($O_2^{\bullet -}$), and hydroxyl radical ($HO^{\bullet}$), are involved in PCD in plants, but the relationship between and mechanisms behind ROS and PCD has not yet been fully elucidated due to the involvement of complex signalling networks [1, 4]. Elucidation of these mechanisms and signalling pathways will allow manipulation of cell death in plants, which could help to improve yield and quality of crops and thus contribute to solving the increasing food demands of the planet [5, 6]. Examples of this could be the development of cultivars with enhanced and/or faster response to pathogen attacks, or cultivars with increased grain filling and hence increased starch content through delayed cell death of the endosperm.
The barley aleurone layer is a generally accepted model system for studying phytohormone signalling, enzyme secretion, and PCD during seed germination [7–9]. However, two main issues affect PCD-related research in the barley aleurone layer: Firstly, the current knowledge about ROS signalling and the cellular redox environment in aleurone layers undergoing PCD is mainly based on quantifications of H_2O_2 [7, 9], determinations of quantities and activities of selected redox-active enzymes [9–17], and gene expression profiles [9, 14, 18, 19] in cell extracts. Unfortunately, such studies do not evaluate the overall cellular redox environment in intact plant cells. Secondly, analyses based on cell extracts are end-point measurements, which are limited by the fact that each analysis is performed on a different pool of samples, as each tissue sample or population of cells can only be analysed at a single time point. This is of great importance for studies of time-dependent processes such as PCD, as time course experiments can be affected by biological and experimental diversity between independent samples. Time course experiments on the same tissue or population of cells can be enabled by the use of assays that do not destroy cellular integrity, which could also facilitate the combination of multiple assays. However, time course studies with analysis of multiple parameters using different detection techniques remain challenging, as the different assays under consideration may be incompatible, and some assays may affect the plant tissue and therefore influence the outcome of simultaneous or subsequent analyses.

I.1 Scientific aims

The main scientific aim of this PhD project has been to expand the current knowledge of ROS signalling and PCD in plant cells through the use of the barley aleurone layer as a biological model system. To this end, the intermediate aims has been to answer the following questions:

- Can redox activity/redox homeostasis be measured in intact plant tissue?
- How does cell viability and redox activity correlate in the aleurone layer?
- How does transient expression of GFP controlled by target enzyme promoters correlate with cell viability in the aleurone layer?
- How does cell viability and redox activity change in the aleurone layer in response to phytohormones or other effector compounds?
- What is the role of the plasma membrane-bound NADPH oxidase in redox homeostasis?
- Can the same living plant tissue be studied over time using detection techniques that do not destroy cellular integrity?
- Can multiple non-destructive techniques be combined to measure multiple parameters in such time course studies?

Based on these aims, this project has focused on the application of optical and electrochemical detection techniques in combination with the development of a novel incubation system for time course studies of immobilised aleurone layers. The first part of the project therefore focused on the optimisation and application of non-destructive detection techniques for determination of cell viability and redox activity in living cells. The second part of the project focused on the development of an incubation system that would allow combination of multiple non-destructive techniques for time-dependent investigations of cell viability, redox activity, and transient expression in parallel in living plant tissue.
This introduction (Part I) presents background information relevant to the work performed and covers the barley aleurone layer as a biological system, the current knowledge of PCD in plant cells and the involvement of ROS, the techniques used for detection of cell viability, redox activity, and transient expression, and finally the development of an incubation system for immobilised plant tissues.

I.2 Barley (*Hordeum vulgare*)

Barley (*Hordeum vulgare* L.) has been grown as a domesticated crop since 8.000 BC, and it is assumed that it was originally used for human consumption. The barley plant is able to grow under harsher conditions than any other cereal, which still today makes it a main food source in extreme climates. However, the use of barley for human consumption declined since the 19th century, as the use of rice, wheat and maize increased [20, 21]. The preference for other types of cereals over barley can be attributed the difficulties of e.g. milling barley into flour like wheat or polishing it like rice, as well as to the final food products from barley being of lesser quality and appearance compared to other cereals. Today, approximately two-thirds of the barley crop is used for feed, while one-third is used for malting and only about 2% is used for human consumption [20].
Nowadays, the use of barley is increasing again due to developing emerging awareness of the nutritional properties of barley grains, as studies have shown that regular consumption leads to a decrease in blood cholesterol levels and an increased insulin response in diabetics [20, 21]. Other nutritional benefits include a low amount of lipids combined with high levels of complex carbohydrates and dietary fibres. Although much is known of the nutritional and chemical properties of barley grains, effective processing of barley grains into products applicable for food production is still a developing area [20, 21]. Fortunately, promising results have been obtained from studies of baked foods prepared from other cereals mixed with a certain percentage of barley flour [20].

I.2.1 Structure and chemical composition of barley grains

The main components of the barley grain are the embryo and the endosperm surrounded by the aleurone layer, the pericarp and the seed coat (Figure I.1). The embryo is placed on the dorsal side at the base of the grain, separated from the endosperm by the scutellum, and a shallow crease runs from the base to the apex on the ventral side of the grain [21, 22].
Barley is a genetically very diverse cereal, but in general barley grains consist of about 70% starch, 5-10% β-glucans, 10-20% proteins, 2-3% free lipids and approximately 2.5% minerals. By far, the largest portion of the starch can be found in the endosperm of the grain. The amylose content of barley starch varies greatly between different types of barley, resulting in diverse properties of end-products such as noodles, since high amylose contents lead to harder noodles compared to wheat-based noodles [20, 21, 23]. β-glucans are also most prominent in the endosperm, where they constitute up to 75% of the cell walls, but are also the major constituent of aleurone cell walls. Consumption of β-glucans from barley has been linked tightly to lower blood cholesterol levels and increased lipid metabolism [20, 21]. The other major component of both aleurone and endosperm cell walls is arabinoxylans [20, 21]. During germination (Section I.2.2, page 5), both β-glucans and arabinoxylans of aleurone cell walls are rapidly degraded and secreted to support growth of the embryo [24]. Most of the proteins in barley are the storage glycoproteins hordeins,

as the endosperm serves as an energy storage for the embryo during germination (Section I.2.2, page 5) [20,21,25]. Barley lipids are mainly triacylglycerol and phospholipids, while barley minerals encompass mainly phosphorus, potassium and calcium with the highest concentrations in the embryo and the lowest in the endosperm [21].

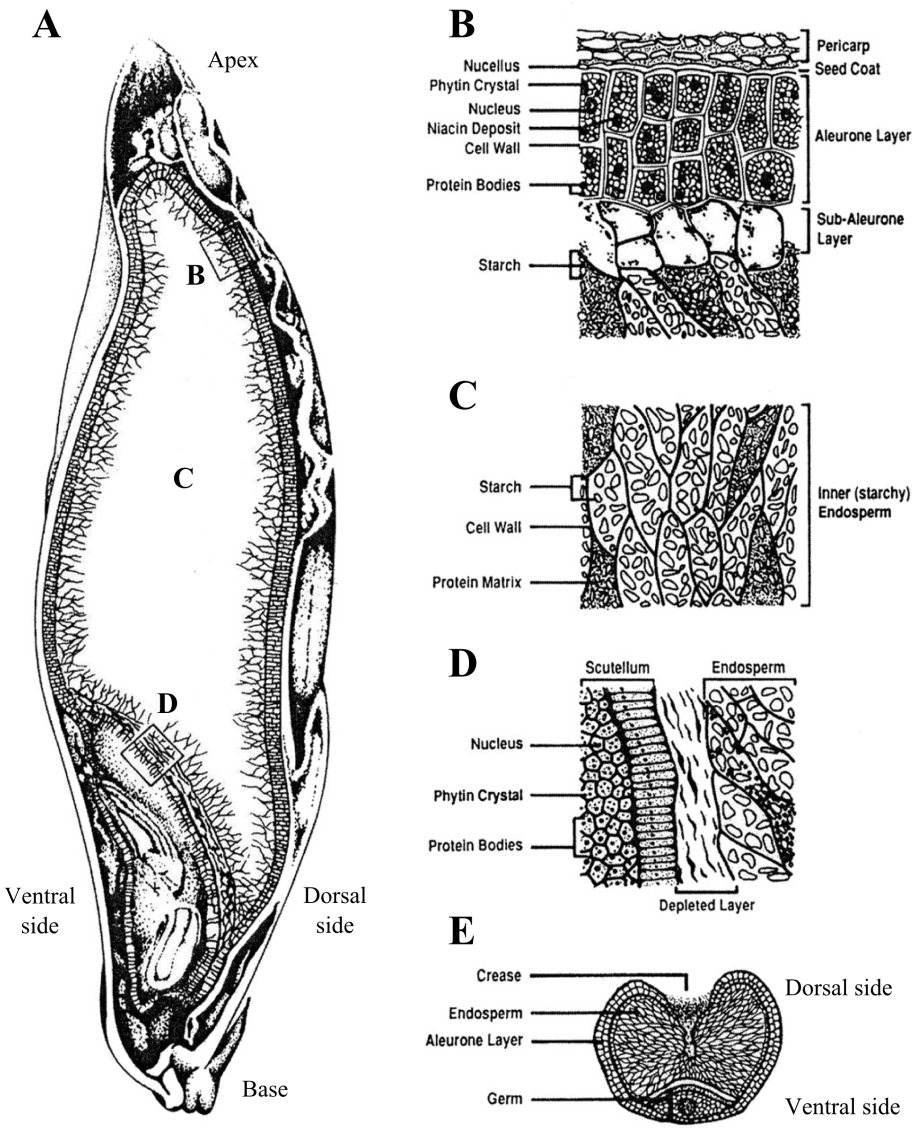

Figure I.1: Barley grain with enlarged cross sections

A: Longitudinal cross section of a barley grain with seed coat. **B:** Aleurone layer with pericarp and sub-aleurone layer. **C:** Endosperm. **D:** Border of endosperm and scutellum. **E:** Lateral cross section of a barley grain (germ = embryo). Figure adapted from [21].

I.2.2 Maturation and germination of barley grains

Maturation of grains is the process in which grains are filled with starch reserves and subsequently desiccated, while the grain is still attached to the barley plant. Grain filling takes place by rapid cell division and expansion of endosperm cells of a fertilised grain, which then synthesise starch and storage proteins in large amounts. The outer 2-3 cell layers of the endosperm differentiates into the aleurone layer, while the embryo develops separately [8, 23]. As the grain is filled and desiccated, the endosperm cells undergo non-autolytic PCD (Section I.3.2, page 8), i.e. they do not disintegrate but remain as starch-filled dead cells until germination [3, 8, 23, 24]. The seed coat including the pericarp also undergo PCD during grain maturation, but the aleurone layer and the embryo survive the desiccation process and remain in a desiccated state until germination [8, 23, 24].
Germination (Figure I.2A) begins when the grain takes up water (imbibition) under favourable conditions, which initiates metabolic activity in the embryo and the aleurone layer [3, 8, 23, 32]. The phytohormone gibberellic acid (GA, Figure I.3) is produced and secreted by the embryo, inducing synthesis of hydrolytic and cell wall-degrading enzymes in the aleurone layer from protein storage vacuoles in these cells [3, 8, 23, 24]. GA binds to the receptor GID1, inducing breakdown of the gene repressor SLN1 (Figure I.2B). Without this repressor, the transcription factor GAMyb is produced, leading to production of hydrolytic enzymes [9, 27–31]. The produced enzymes are released into the endosperm for degradation of cell walls and mobilisation of starch for embryo development. Having depleted their reserves for protein production, the

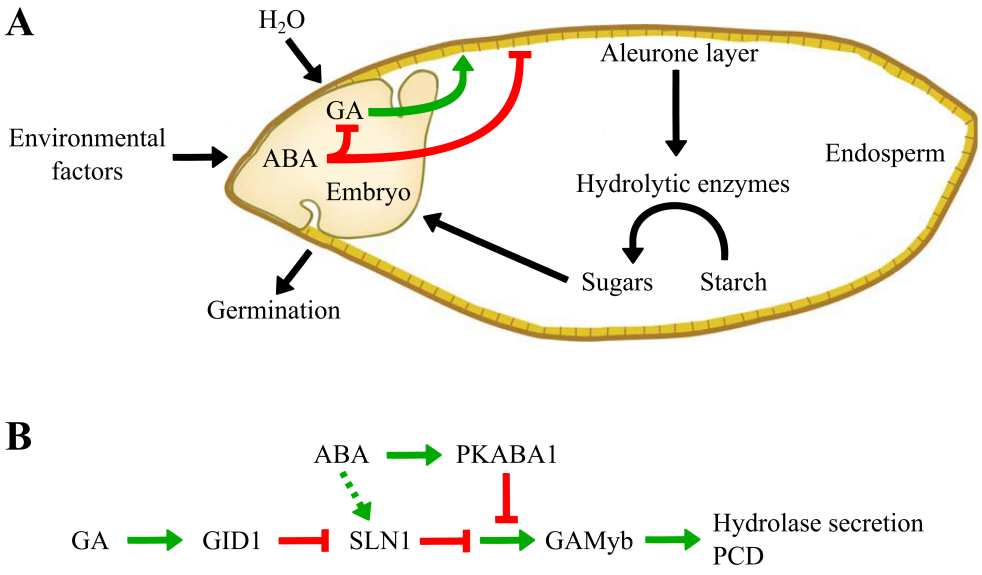

Figure I.2: Gibberellic acid and abscisic acid signalling in germination of barley grains

A: Signalling in the barley grain. **B:** Signalling in the barley aleurone cell. GA: Gibberellic acid. ABA: Abscisic acid. GID1: GA-receptor. SLN1: Gene repressor. GAMyb: Transcription factor. PKABA1: Protein kinase. Figures adapted from or inspired by [9, 26–31].

aleurone cells undergo PCD at the end of the germination process [3,8,23].
The phytohormone abscisic acid (ABA, Figure I.3) has an antagonistic effect to GA (Figure I.2), as it halts germination and enzyme production to keep the grains in the desiccated state. ABA is produced by the embryo already during grain maturation to prevent germination of grains still attached to the barley plant and to induce proteins that help the embryo and aleurone layer to survive the desiccated state [8,30,33]. ABA suppresses the action of GA by induction of the protein kinase PKABA1, which inhibits expression of GAMyb, and is also believed to stabilise the gene repressor SLN1, further inhibiting the effects of GA (Figure I.2B) [9,27–31]. Another aspect of the antagonistic effects of GA and ABA is the ability of both compounds to inhibit biosynthesis of the other in the embryo [27,30,31].

I.2.3 The aleurone layer as an experimental model system

The aleurone layer is a widely accepted model system for studying phytohormone signalling, enzyme secretion, and PCD during grain germination for several reasons: First, the aleurone layer has very specific responses to GA and ABA from exogenous sources, as GA induces germination, while ABA maintains dormancy. The practicality of this in an experimental setup is further underlined by the fact that the aleurone layer does not produce these phytohormones endogenously, resulting in easy control of induction or prevention of germination [8,18,34]. Second, the production and secretion of α-amylases is induced by GA but not ABA, and successful induction of germination is therefore easily monitored through the presence or activity of α-amylases in the incubation medium [8,34]. Third, the aleurone layer consists of only one cell type, resulting in uniform responses from the entire layer to phytohormone treatment [8,34]. Fourth, due to the thickness of the barley aleurone layer of 2-3 cell layers [8,23] it is mechanically robust and can thus be easily isolated from the other grain tissues [8]. In contrast, wheat aleurone layer consists of only a single cell layer [8], making it more difficult to isolate for *in vitro* incubations. Fifth, the aleurone layer can be maintained in *in vitro* incubations as either intact tissue [8,18,34,35] or as single aleurone cells in the form of protoplasts [18,19,36].

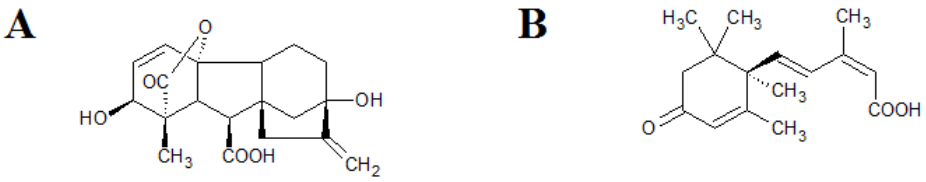

Figure I.3: Chemical structures of GA and ABA

A: Gibberellic acid (GA). **B:** Abscisic acid (ABA).

I.3 Programmed cell death in plant cells

PCD is an integral part of plant development and survival, as it is involved in a range of processes such as grain germination, tissue development, and defence against pathogens [6, 37–39], but knowledge of PCD in animals is far better than that in plants [1, 2, 19]. Recent discoveries have proposed the classification of plant PCD into two main categories, autolytic and non-autolytic (Figure I.4), which resemble the animal PCD classes autophagy and necrosis, respectively, whereas the third type of PCD observed in animal cells, apoptosis, has not been identified in plants [1, 2]. As in animals, the classes of plant PCD are based on cell morphology changes (Figure I.4), and they are categorised by one main feature occurring at the end of the PCD process: Rupture of the tonoplast, the membrane that surrounds the main lytic vacuole, followed by clearance of the cytoplasm distinguishes autolytic PCD from non-autolytic PCD [2]. Biochemical events that seem to be common for both types of PCD include elevated levels of ROS and Ca^{2+}, leading to release of cytochrome *c* from the mitochondria into the cytoplasm [37, 38, 40–42]. This results in a positive feedback loop, as the release of cytochrome *c* into the cytoplasm leads to further ROS generation (Section I.4, page 10) [40].

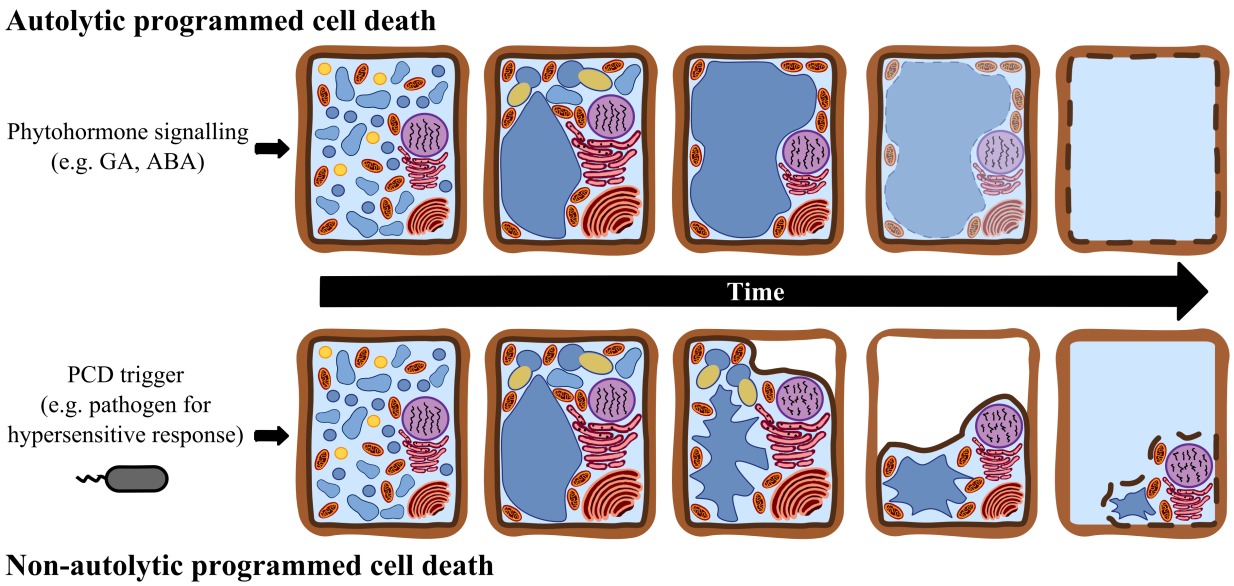

Figure I.4: Programmed cell death is autolytic or non-autolytic

See Sections I.3.1 and I.3.2, page 8, for details. Vacuoles: Blue. Peroxisomes and glyoxysomes: Yellow. Nucleus: Purple. Endoplasmic reticulum with ribosomes and Golgi: Red/pink. Mitochondrion: Orange. Figure inspired by [38, 43–45].

I.3.1 Autolytic programmed cell death

Aleurone cells undergo autolytic PCD (Figure I.4), which occurs mainly in relation to plant development. As resumption of metabolism in aleurone cells is induced by water imbibition and GA-production by the embryo, aleurone cells contain a large number of protein storage vacuoles in addition to its organelles [2, 24]. These vacuoles serve as carbohydrate and mineral reserves during grain maturation, but during germination the vacuoles become lytic as the stored proteins are broken down and used for synthesis of hydrolytic enzymes. The vacuoles merge and swell, taking up an ever larger proportion of the cytoplasm. The endoplasmic reticulum and the Golgi apparatus also increase in size and complexity, as these are the main sites involved in protein synthesis and packaging of proteins for their final destinations, especially of secreted proteins. A certain amount of hydrolytic enzymes are not secreted into the endosperm but instead enter the lytic vacuoles to degrade stored reserves for synthesis of new enzymes [24]. As stored reserves are depleted, the enzyme production decreases along with protein synthesis-related organelles such as ribosomes and the endoplasmic reticulum, while remaining storage vacuoles coalesce with the main lytic vacuole. As the cells reach this highly vacuolate stage, rapid degradation of nuclear DNA begins. Finally, the tonoplast surrounding this vacuole ruptures, releasing the hydrolytic enzymes into the remaining cytoplasm, which is quickly degraded. The process is finished as the plasma membrane becomes permeable and the cells collapse unto themselves [2, 24, 38, 44].

I.3.2 Non-autolytic programmed cell death

Non-autolytic PCD in plants (Figure I.4) has been described under three main circumstances; during the hypersensitive response to pathogen attacks, during attacks by necrotrophic pathogens, and in the endosperm of cereals during grain maturation. This type of PCD is defined by the absence of a rapid clearing of the cytoplasm, although permeabilisation or even rupture of the tonoplast can happen, just as with autolytic PCD [2].

Upon infection with a pathogen plants can react with the hypersensitive response, which creates a ring of dead cells around the site of penetration, blocking the advance of the pathogen. PCD is preceded by an increase in cytoplasmic Ca^{2+} concentration and an oxidative burst, in which the NADPH oxidase plays an important role, yielding a rapid production of high levels of ROS and the nitric oxide radical ($NO^{\bullet}$) [2, 16, 38, 44, 46]. Physiologically, PCD is preceded by nuclear DNA degradation, blebbing of the lytic vacuole and plasma membrane, and disappearance of organelles [2, 16, 38, 44].

The hypersensitive response is, however, useless in battling necrotrophic pathogens that feed off dead plant tissue. In these cases, the pathogens themselves are the cause of PCD through the secretion of toxic molecules that induce an oxidative burst in the plant cells. An example of this is release of oxalic acid by the fungi *Botrytis cinerea* and *Sclerotinia sclerotiorum*, which induces increased levels of H_2O_2, leading to PCD [2].

The mechanism of PCD in endosperm cells during grain maturation is unfortunately unknown.

Tonoplast rupture, or even permeabilisation of the tonoplast, has not been detected, although a decline in DNA content and a loss of plasma membrane integrity has been shown. Despite the loss of membrane integrity, the dead endosperm cells remain intact until germination, as described above. This type of cell death is developmental rather than related to pathogen attacks, but has been categorised as non-lytic due to the absence of tonoplast rupture and cytoplasm clearance [2].

I.3.3 Determinations of programmed cell death in intact cells

A popular option for determining cell viability of plant cells is fluorescence microscopy with the combination of fluorescein diacetate (FDA, Figure I.5A) for staining living cells [7,11–13,36,47–53] and *N*-(3-triethylammoniumpropyl)-4-(6-(4-(diethyl-amino)phenyl)hexatrienyl) pyridinium dibromide (MM 4-64, Figure I.5B) for staining dead cells [7, 12, 13, 36, 47, 48, 52]. FDA is non-fluorescent, but upon uptake by living cells it is deacetylated to the green fluorescent dye fluorescein, which is retained within the cytoplasm of living cells due to its charge [12, 36, 52]. MM 4-64 is lipophilic and accumulates in the intracellular membranes of dead cells, where it fluoresces orange-red. The dye is accumulated rapidly in dead cells due to their permeable plasma membranes, while it only partitions slowly into living cells [12, 36].
Cell viability can also be determined using Evans blue [11, 54] or the SYTOX dyes [53, 55], both of which cannot pass the intact plasma membranes of live cells. The water-soluble compounds 2,3,5-triphenyltetrazolium chloride (TTC) and 3-(4,5-dimethylthiazo-2-yl)-2,5-diphyltetrazolium bromide (MTT), on the other hand, are reduced in living cells to an insoluble red and purple formazan, respectively [16, 56, 57].
Due to the non-destructive nature of the FDA-MM 4-64 double fluorescent probe system, the application of this technique for cell viability determinations of living plant tissues was one of the focus points of this thesis. Part II: Article Manuscript #1 (page 25) presents results obtained with the FDA-MM 4-64 cell viability assay in traditional incubations of aleurone layers, while Part IV:

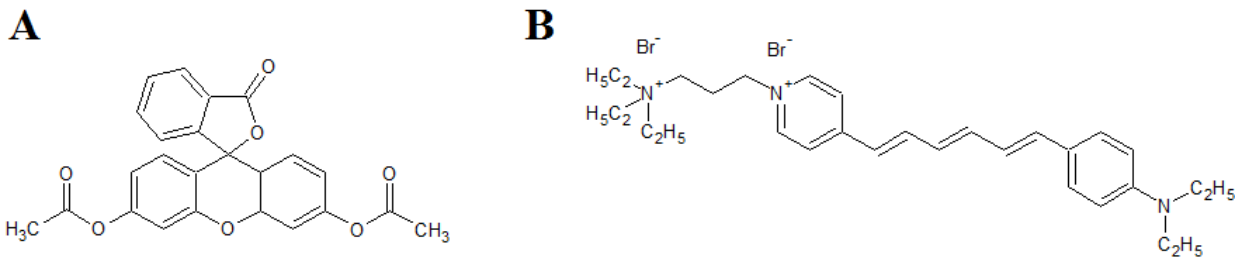

Figure I.5: Chemical structures of FDA and MM 4-64

A: Fluorescein diacetate (FDA). **B:** *N*-(3-triethylammoniumpropyl)-4-(6-(4-(diethylamino)phenyl)hexatrienyl) pyridinium dibromide (MM 4-64).

Article Manuscript #2 (page 61) and Part V: Other results related to Article Manuscript #2 (page 79) introduces results obtained with the FDA-MM 4-64 cell viability assay in the developed incubation system for immobilised aleurone layers.

I.4 Reactive oxygen species in programmed cell death

Due to the complexity of ROS signalling in relation to PCD, this section is in not an extensive and in-depth description of the topic. Instead, it is intended merely as an introduction to the interplay between ROS and PCD in aleurone layers, highlighting the most relevant aspects in relation to the work described in this thesis. To this end, Figure I.7 depicts a simplified model for the complex involvement of ROS in PCD with the details described in the text.
Plant cells in general contain five to ten times more genes encoding enzymes involved in regulation of redox homeostasis and protection of cells against oxidative stress than bacteria and mammalian cells [4, 59, 60]. Redox active enzymes and ROS have been shown to play a major role in a number of processes including abiotic stress, pathogen defence, tissue development, grain germination and, as mentioned, PCD [4, 36, 59–61]. As in animal cells, ROS in plant cells are produced as by-products of normal metabolic processes through incomplete reduction of

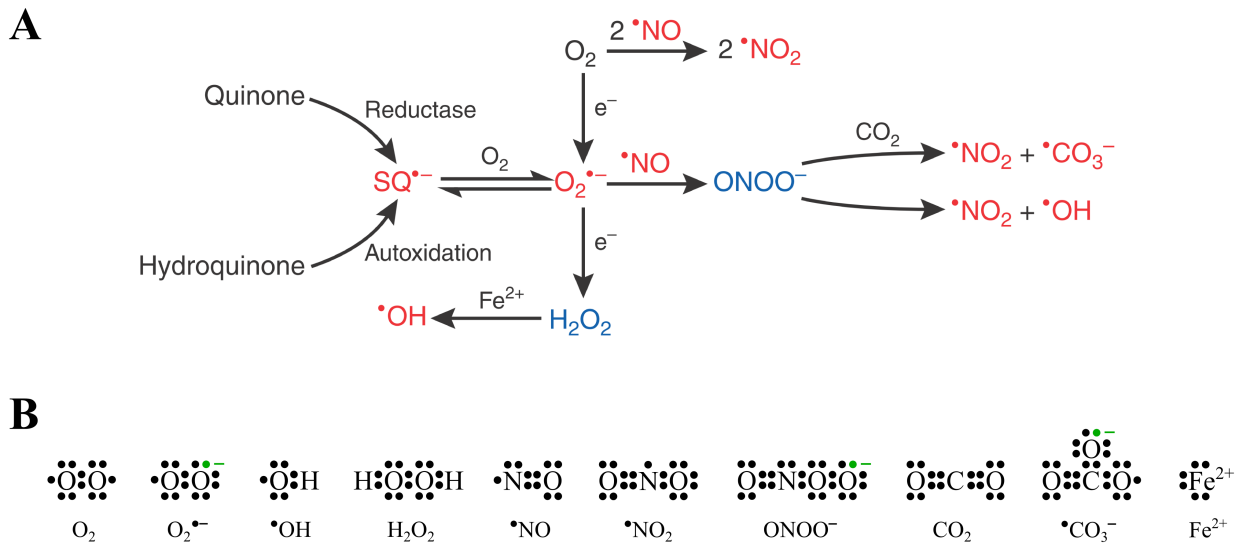

Figure I.6: Chemical reactions of reactive oxygen species

A: See text for details. $O_2^{\bullet -}$: Superoxide radical. H_2O_2: Hydrogen peroxide. $^{\bullet}OH$: Hydroxyl radical. $NO^{\bullet}$: Nitric oxide radical. $ONOO^-$: Peroxynitrite. $^{\bullet}NO_2$: Nitrogen dioxide radical. CO_2: Carbon dioxide. $^{\bullet}CO_3^-$: Carbonate radical anion. Fe^{2+}: Ferrous iron ion. $SQ_2^{\bullet -}$: Semiquinone-like radicals, generated by enzymatic reduction of quinones such as ubiquinone or menadione. One-electron oxidants (radicals) are shown in red; two-electron oxidants are shown in blue. Figure and text adapted from [58]. **B:** Lewis electron dot structures for compounds in A (except for quinones and derivatives). Extra electrons responsible for negative charges are marked in green.

O_2 (Figure I.6) [1, 4, 60, 61]. The highly reactive superoxide radical ($O_2^{\bullet -}$) is typically produced through transfer of a single electron from over-reduced quinones or quinone-containing protein complexes to O_2 [58, 60, 62, 63]. $O_2^{\bullet -}$ dismutates to H_2O_2, either spontaneously or by the enzymatic action of superoxide dismutase [58,60,63]. While H_2O_2 is both more stable and less reactive than $O_2^{\bullet -}$, it can react with metal ions such as iron or copper to produce $HO^{\bullet}$, which is capable of damaging all types of biomolecules [58, 60, 63, 64]. In addition to superoxide dismutase, ROS levels are controlled by other scavenging enzymes such as catalases and peroxidases [4, 12, 60], and by reactions with antioxidants such as ascorbic acid or glutathione [58, 60].
The effects of ROS are concentration dependent; at low levels they can act as signalling molecules or as inducers of ROS scavenging enzymes, while they can induce oxidative stress and PCD at high levels [4, 37, 61, 65]. However, the effects are also dependent on the interactions of ROS with other signalling molecules, including lipid messengers and phytohormones [1, 4, 61, 66], and on the type of ROS, as the chemical properties of the ROS in question determine which signalling pathways are induced [1]. Another piece of this already complex puzzle is the timing of ROS production, as prolonged exposure of plant cells to H_2O_2 triggers non-autolytic cell death, whereas a short, high-concentration pulse of H_2O_2 induces autolytic PCD [1, 65]. An example of the complexity of ROS signalling is the interactions of $NO^{\bullet}$ with H_2O_2 and $O_2^{\bullet -}$ in regulation of PCD, as addition of $NO^{\bullet}$ generators can result in both induction and prevention of damaging ROS ef-

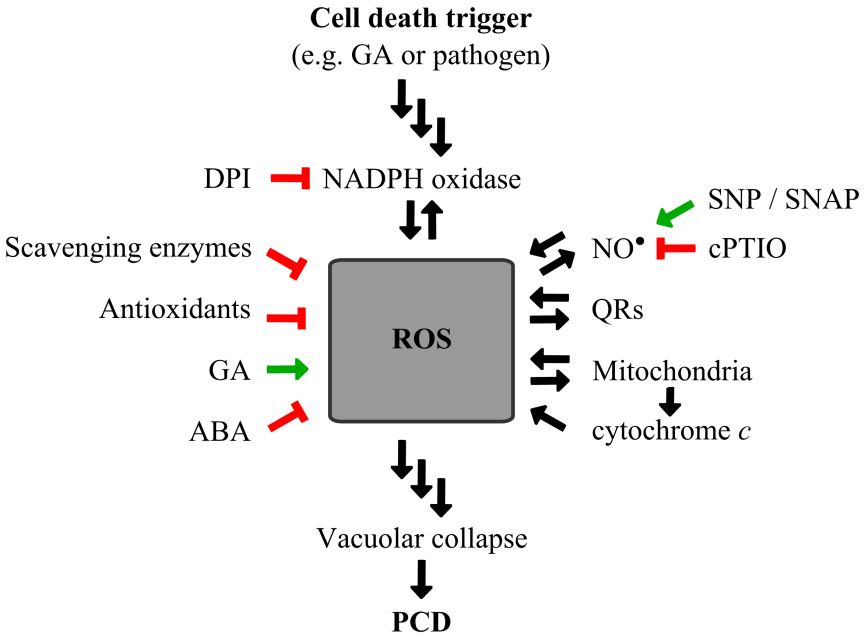

Figure I.7: A simplified model for reactive oxygen species in programmed cell death

See text for details. ROS: Reactive oxygen species. PCD: Programmed cell death. GA: Gibberellic acid. ABA: Abscisic acid. DPI: Diphenyleneiodonium chloride. $NO^{\bullet}$: Nitric oxide radical. SNP: Sodium nitroprusside. SNAP: *S*-nitroso-*N*-acetylpenicillamine. cPTIO: 2-(4-carboxyphenyl)-4,4,5,5-tetramethylimidazoline-1-oxyl-3-oxide. QRs: Quinone reductases. Figure adapted from [37, 50].

fects (Figure I.7) [1, 4]. $NO^{\bullet}$ is produced by NO synthase or nitrate reductase, and the molecule can react with other radicals, such as $O_2^{\bullet -}$ (Figure I.6), eliminating these while forming reactive nitrogen species such as peroxynitrite ($ONOO^-$) or nitrogen dioxide radical ($NO_2^{\bullet}$) [4, 47, 60, 67]. As with ROS, levels of reactive oxygen species are also controlled by scavenging enzymes and antioxidants [60].

The production of H_2O_2, a major by-product of germination-related metabolism, has been shown to be induced after only 3 h of aleurone layer incubation with GA [9]. In photosynthetic plant cells, chloroplasts are the major contributors to ROS production, but aleurone cells are devoid of chloroplasts, and ROS production, especially H_2O_2, in these cells therefore originates from mitochondria, peroxisomes and glyoxysomes [4, 13, 16, 65, 68, 69]. Another function of the mitochondria is the release of cytochrome *c* into the cytosol in response to elevated levels of ROS and Ca^{2+}, which leads to further ROS production (Figure I.7) [37, 38, 40–42]. The membrane-bound flavoenzyme NADPH oxidase (Figure I.7) has been shown to contribute to H_2O_2 production through production of extracellular $O_2^{\bullet -}$ which dismutates to H_2O_2 [4, 14, 37, 65, 69] and diffuses or is transported into the cells [4, 66]. The role of NADPH oxidase is further underlined by the demonstration of reduced ROS levels, reduced α-amylase production, and delayed germination induced by the flavoenzyme inhibitor diphenyleneiodonium chloride (DPI, Figure I.7) [14, 61, 65]. Similarly, cytosolic and intracellularly active, plasma membrane-bound quinone reductases (QRs) have been shown to be involved in ROS production (Figure I.7) [70–72].

Reduced amounts and activities of ROS-scavenging enzymes such as superoxide dismutase, catalase, and ascorbate peroxidase have been demonstrated in GA-treated barley aleurone layers prior to PCD, whereas ABA-treated layers retained ROS scavenging ability and cell viability [12, 16, 32, 69]. These effects were delayed in aleurone layers treated with $NO^{\bullet}$ donors such as sodium nitroprusside (SNP) and *S*-nitroso-*N*-acetylpenicillamine (SNAP) in addition to GA (Figure I.7) [47]. Both cell viability and amounts of catalase and superoxide dismutase declined less rapidly for aleurone layers incubated in the presence of $NO^{\bullet}$ donors [47], whereas the presence of both SNAP and the $NO^{\bullet}$ scavenger 2-(4-carboxyphenyl)-4,4,5,5-tetramethylimidazoline-1-oxyl-3-oxide (cPTIO) restored the rates of decline of both viability to that of aleurone layers treated with GA alone [47, 48]. Furthermore, treatment with both GA and $NO^{\bullet}$ donors increased the production levels of α-amylase above those for GA only treatment [47].

In summary, the balance between oxidative and reductive processes will determine whether or not germination-related metabolism and subsequent PCD of the aleurone layer will occur. Connecting ROS to germination, Bailly et al. [61] defined the concept of an 'oxidative window' as:

> *a critical level of ROS not to overcome, which would otherwise prevent germination, and a ROS threshold level, below which germination (radicle protrusion) cannot occur.*

The combined effects of cellular oxidative and reductive processes determine whether this window is open or closed (Figure I.8). Increased H_2O_2 levels combined with decreased activities of ROS scavenging enzymes is therefore predicted to shift the overall redox balance above the

upper threshold of the 'oxidative window' towards conditions of oxidative stress, which will ultimately lead to PCD [1,61,66].

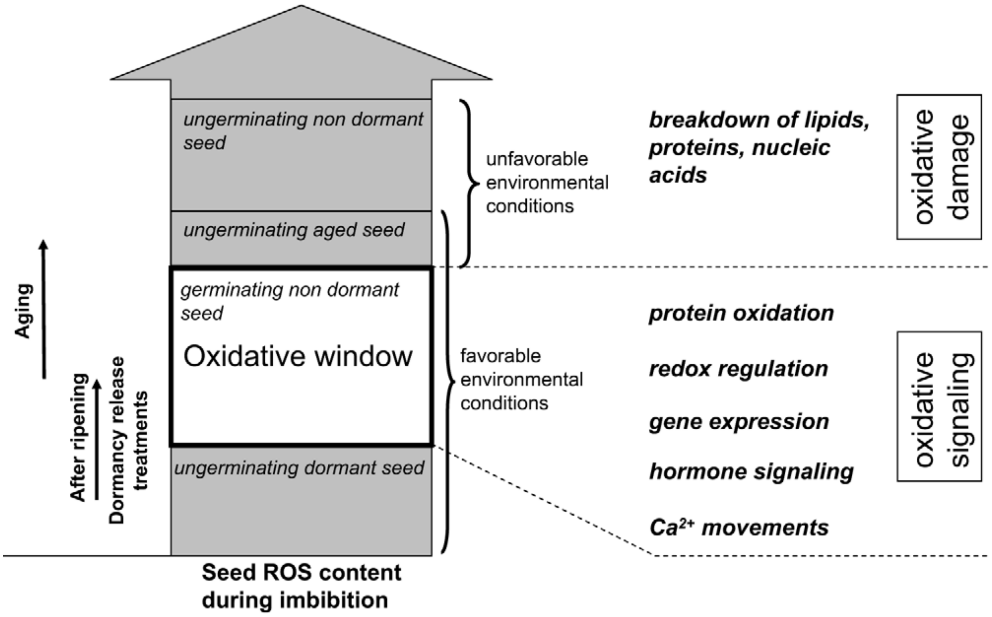

Figure I.8: The oxidative window: a model to account for the dual role of ROS in seed physiology

The amount of ROS in seeds during their imbibition is represented as boxes. Seed germination is only possible when the ROS content is enclosed in the oxidative window. Below this window, i.e. in dormant seeds, the amount of ROS during imbibition is too low for allowing germination. Alleviation of dormancy (by after-ripening, in the dry state, or by dormancy alleviation treatments, during imbibition) leads to an increase of the cellular level of ROS during seed imbibition thus ensuring germination completion, owing to the ROS signalling role, as mentioned on the right part of the figure. Above this window, ROS content is too high, because seeds are aged or placed in inappropriate environmental conditions during their imbibition (ROS sensing of environmental cues). In this case, ROS become deleterious and cause cellular oxidative damage that prevent or delay germination. Figure and text from [61].

I.4.1 Determinations of redox activity

Due to the importance of PCD for a range of biological processes and the complex ROS signalling involved in PCD, monitoring of redox changes occurring during processes leading to PCD could lead to a better understanding of the relationships linking ROS and PCD. Elucidation of these mechanisms and signalling pathways could enable manipulation of cell death in plants, which would be of great importance for agriculture and post-harvest industries by increasing yield and by improving quality and shelf-life of crops and crop-derived products [5,6].
The current knowledge about aleurone layer redox environment, i.e. evaluations of the overall reducing or oxidising capacity, is mainly based on quantifications of H_2O_2 [7,9], determinations of quantities and activities of selected redox active enzymes [9–17], and gene expression profiles [9,14,18,19], all of which are performed on cell extracts. Methods based on cell extracts do not give a complete understanding of cellular redox homeostasis, resulting in a lack of studies

evaluating the overall redox environment in intact plant cells. Even though plant plasma membrane redox reactions have been monitored electrochemically on living plant cells [49,73], to the best of my knowledge there is currently no method reported that allows intra- and extracellular as well as membrane-related redox activity measurements in intact plant tissues. Enabling detection in intact living tissues and cells could provide additional information closer to *in vivo* conditions than cell lysate-based methods.

I.4.2 Electrochemical determinations of intracellular redox activity in intact cells

Electrochemical techniques have been successfully applied for evaluations of intracellular redox activity in living intact mammalian [74–76], yeast [77–81] and bacterial [82, 83] cells. Most of these methods employ a mediator that is able to enter living cells, where it can be reduced before exiting the cell again. The reduced mediator (or a second mediator present in the extracellular environment that is reduced upon contact with the first mediator) is then quantified electrochemically by either potentiometry [75], voltammetry [77,82], or amperometry [76,78–80,82]. In short, potentiometry measures the electric potential in volts of a solution without the application of a current, whereas both voltammetry and amperometry measures the current in amperes as the function of an applied variable (voltammetry) or fixed (amperometry) potential [84].
A popular option is the menadione-ferricyanide (M-FiC) double mediator system, which probes intracellular redox activity through the availability of NAD(P)H (Figure I.9). The principle of intracellular probing is based on the lipid-soluble quinone, M, which can pass through the cell membrane into the cytosol, where it is reduced by menadione reducing enzymes (MRE), such

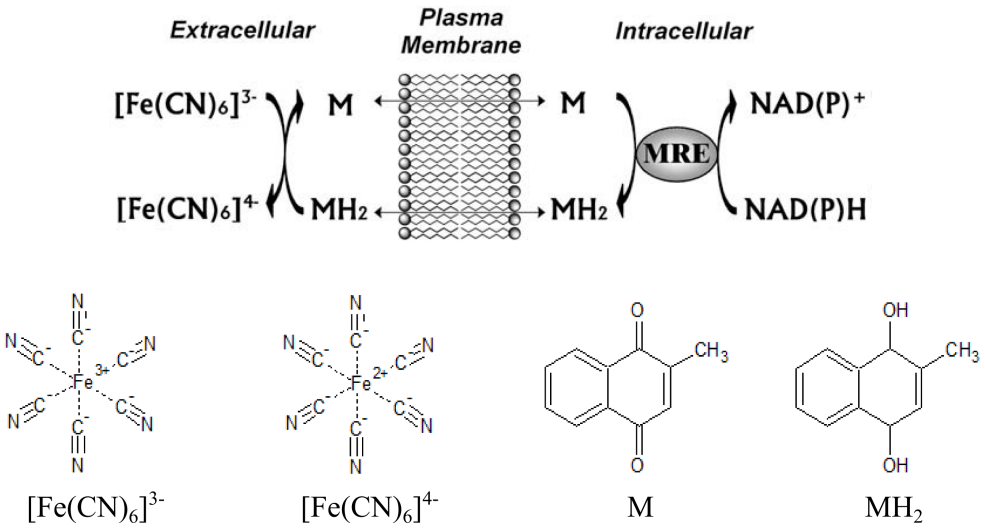

Figure I.9: Principle of redox activity measurements with the M-FiC double mediator system

$[Fe(CN)_6]^{3-}$: Ferricyanide (FiC). $[Fe(CN)_6]^{4-}$: Ferrocyanide (FoC). M: Menadione. MH_2: Menadiol. MRE: Menadione reducing enzymes. Figure adapted from [79].

as quinone reductases (QR), to menadiol (MH_2). The quantification of MH_2 is enabled via its re-entrance to the extracellular environment, where it reduces FiC (which is unable to pass the cell membrane) to ferrocyanide (FoC), while simultaneously being re-oxidised to M. The amount of FoC generated is therefore directly proportional to the overall reducing capacity of the cells and is subsequently detected electrochemically [75–80]. Though several studies have identified MREs in *Saccharomyces cerevisiae* [79], the knowledge about the identities and roles of MREs in plant cells is more limited. QRs have not yet been characterised in the barley aleurone layer, but the existence of cytosolic, mitochondrial, and intracellularly active plasma membrane-bound QRs has been shown in several plants [70, 72, 85–88]. In addition, Viljoen et al. [89] demonstrated that QRs can convert changes in H_2O_2 levels to changes in the NAD(P)H:NAD(P)$^+$ ratio, which should enable probing of the cellular redox environment (especially the NAD(P)H:NAD(P)$^+$ ratio) of aleurone layers through quinone reducing capability.
As Chalmers et al. [49] successfully employed FiC on its own for the detection of plasma membrane-related redox changes in plant cells, and due to the non-destructive nature of the method, the application of the M-FiC double mediator system in living plant tissues for the first time was one of the focus points of this thesis. Part II: Article Manuscript #1 (page 25) presents results obtained with the M-FiC redox activity assay in traditional incubations of aleurone layers, while Part IV: Article Manuscript #2 (page 61) introduces results obtained with the M-FiC redox activity assay in the developed incubation system for immobilised aleurone layers.

I.5 Transformation of plant cells

Genetic transformation of cells, tissues, or whole plants has been widely used in plant biology since the 1980s [90, 91], both for the development of improved crops and for the study of gene functions and expressions [92]. A number of different approaches for transformation exists, classified as either indirect or direct. Indirect approaches utilise bacterial or viral infections for transfer of plasmids encoding a gene of interest into the plant cell, while direct methods physically penetrate the cell wall of the plant cell to introduce the plasmid in question [90–94].
The most widely used indirect approach uses either of the plant pathogens *Agrobacterium tumefaciens* or *Agrobacterium rhizogenes* to transfer the gene of interest to a plant host cell. Agrobacteria carry a Ti-plasmid from which a small segment, the T-DNA, is transferred to the plant host cell and inserted into the nuclear genome. Transformation with a gene of interest can therefore be performed by inserting this gene into the T-DNA of a Ti-plasmid, cloning the plasmid into Agrobacteria, and subsequently infecting the plant tissue of interest with the bacterial culture [90–94]. Despite its otherwise high efficiency, the method is not very efficient in cereals, as these plants are not natural hosts of Agrobacteria [90–92].
The most commonly used direct approaches are electroporation and biolistics, but unfortunately electroporation has the disadvantages of low efficiency, low reproducibility, and only being applicable to protoplasts. The technique enhances pore formation in the plasma membrane, which

in protoplasts facilitates transport of the gene of interest in the form of naked plasmids into the host cell. However, for cells in plant tissues the cell wall prevents this transport despite pore formation in the plasma membrane [91, 92, 94]. Biolistics, or particle bombardment, was originally developed as an alternative to Agrobacteria for transformation of cereals, as it overcomes the problem of the cell wall by simply 'firing' the gene of interest into the cells. Gold or tungsten particles are coated with plasmids carrying the gene of interest, and subsequently the particles are accelerated into the plant cells or tissues of interest. The particles are believed to pass through the cells, while the DNA becomes dislodged on the way through the plant cells and remain inside the cells. The technique unfortunately suffers from low efficiency just as electroporation, but has the distinct advantages of being applicable to most types of tissues and plants [90–92, 94].

I.5.1 Transient expression in barley aleurone layers

Barley aleurone layers have been transformed by particle bombardment since the early 1990s, first in the form of embryoless half-grains with the seed coat removed [28, 29, 97–107] and from the early 2000s also as isolated aleurone layers [108–114]. For isolated layers, the predominant method of transformation uses the PDS-1000/He (previously named DuPont PDS-1000) biolistic helium gun offered by Bio-Rad Laboratories [108, 110–114]. With this system (Figure I.10), the

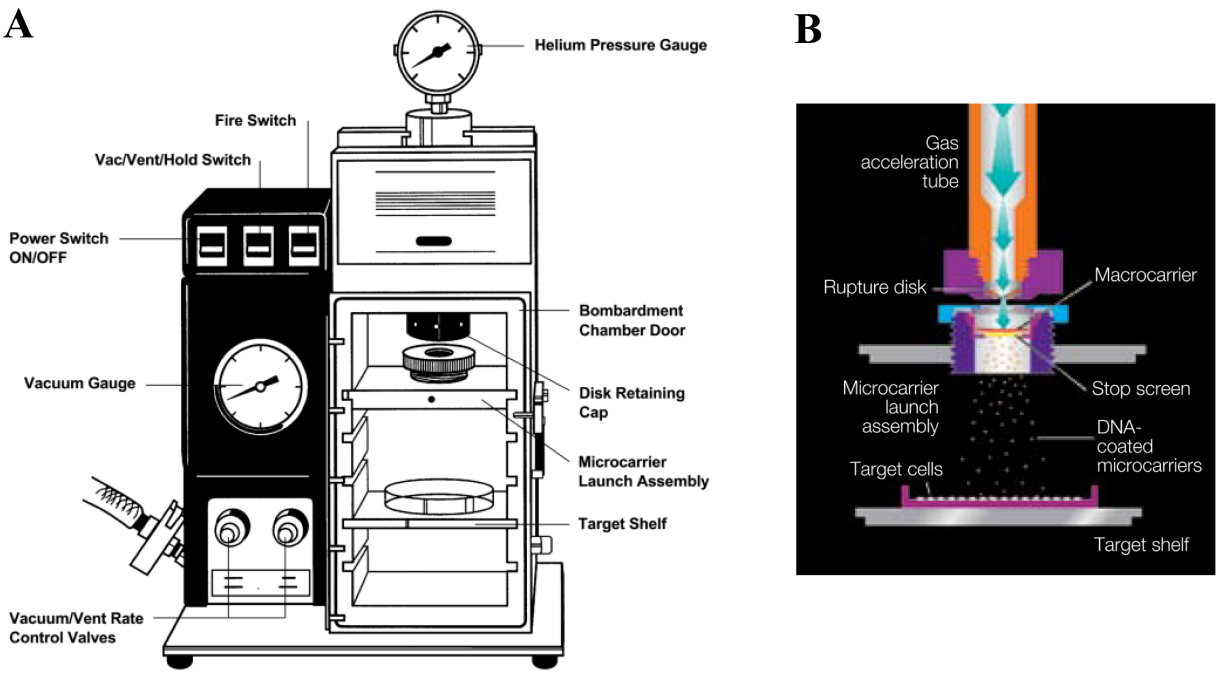

Figure I.10: Biolistic PDS-1000/He Particle Delivery System

A: Front view of the PDS-1000/He system. **B:** Schematic representation of the PDS-1000/He system upon activation. Arrows indicate the direction of helium flow. Figures and text from [95, 96].

coated particles are placed in the launch assembly, while the aleurone layers are placed on the target shelf in the bombardment chamber at the desired distance from the assembly. A vacuum is applied to the chamber, and when the instrument is fired, helium builds up in the acceleration tube until the specific pressure of the rupture disk is reached and the disk burst. This releases a helium shock wave, which shoots the coated particles into the chamber and further into the aleurone cells [95,96]. Transient expression in aleurone layers is usually evaluated by fusing the promoter of the gene of interest to a reporter gene, typically β-glucuronidase [28,29,97–107,110–114] or the green fluorescent protein (GFP) [29,107–109,112,113]. The expression of the gene of interest is then assayed by histochemical staining or determination of enzymatic activity in the case of β-glucuronidase, or by fluorescence microscopy in the case of GFP. Compared to GFP, the usage of β-glucuronidase as the reporter gene has the distinct disadvantage of both detection techniques destroying cellular integrity, as enzymatic activity is determined in cell extracts [28, 29,97,99–102,104,107], and histochemical staining requires fixation of the tissue, killing the cells [103,110–115].
The use of particle bombardment for time course studies of GA-induced expression of target enzymes was one of the focus points of this thesis. To the best of my knowledge, such expression profiles over time has not previously been achieved with transient expression. Part IV: Article Manuscript #2 (page 61) presents results obtained with transient expression of GFP controlled by the α-amylase (*AMY1*) and phytase (*PAPhy_b*) promoters in the developed incubation system for immobilised aleurone layers.

I.6 Developing a novel incubation system for aleurone layers

A standard method for incubation of barley aleurone layers does not seem to exist, and surprisingly many research articles lack detailed information on the exact setup and conditions used for aleurone layer incubations (Table I.1). Information on the incubation liquid is typically the most detailed with a few investigations using water but the most common is a solution of 10 or 20 mM $CaCl_2$, as Ca^{2+} ions have been shown to be necessary for enzyme secretion in aleurone layers [17]. In some instances the buffer is stabilised with 20 mM succinate or 1 mM acetate, but most articles do not mention any stabiliser. Concentrations of GA applied to induce germination typically ranges from 1 to 10 μM, while concentrations of ABA used to maintain dormancy of the aleurone layers encompass a wider span from 5 to 50 μM. Most articles do not list the vessels used for incubation, but examples of incubation vessels are as different as Erlenmeyer flasks and flat-bottomed multiwell plates as used in our group[1] (12-well), although not mentioned by neither Barba-Espín et al. [7] nor Finnie et al. [8]. Conditions are also often lacking exact information, as only some authors mention the ratio between aleurone layers and incubation buffer, and those mentioned are again very different. Other types of incubation details only supplied by some authors include temperature, shaking, and the addition of antimicrobials.

[1] Agricultural and Environmental Proteomics, Department of Systems Biology, Technical University of Denmark

Table I.1: Aleurone layer incubation conditions

Incubation media	Concentrations of GA [μM]	Concentrations of ABA [μM]	Vessel	Ratio of aleurone layers to incubation media [x layers : y mL]	Temperature [°C]	Shaking [rpm]	Anti-microbial agents	Study
H_2O	1	*						[35]
H_2O / calcium succinate	10	50			RT			[108]
10 mM $CaCl_2$	5	5						[36]
10 mM $CaCl_2$, 1 mM acetate, pH 4.8	1	*			25			[116]
10 mM $CaCl_2$	1	*			22		cefotaxime, nystatin	[9]
10 mM $CaCl_2$	5	10						[17]
20 mM $CaCl_2$	1	*		10:1 / 10:2	28			[34]
20 mM $CaCl_2$, 20 mM sodium succinate, pH 4.2	5	*	12-well plate[1]	approx. 10^2:2	RT	gentle[3]	ampicillin[1], nystatin[1]	[7]
20 mM $CaCl_2$, 20 mM sodium succinate, pH 4.2	5	5	12-well plate[1]	approx. 10^2:2	RT	150[1]	ampicillin[1], nystatin[1]	[8]
20 mM $CaCl_2$	5	5						[47]
20 mM $CaCl_2$	5	5		35:10 / 10:3				[48]
20 mM $CaCl_2$	5	5						[12, 13]
20 mM $CaCl_2$	5	5			RT	125		[16]
20 mM $CaCl_2$	10	20	Erlen-meyer flask (25 mL)	20-40:1.5-2.5 / 5:2	RT	50		[52]

*Not used in this study. [1]Unpublished information. [2]100 mg. [3]Approximately 150 rpm (unpublished information).

The absence of exact information is probably (part of) the cause of the lack of a standard method of incubation for aleurone layers, making it difficult to replicate and compare results. This adds to the inconsistency caused by the limitations of end-point analyses mentioned briefly in Part I (page 1); most analyses performed in aleurone layer investigations are based on end-point measurements, often destroying cellular integrity [7–9, 12, 13, 16, 17, 34–36, 47, 48]. For such end-point analyses only one measurement per incubation is performed on the aleurone layers per time point, whereas multiple analyses can be performed on the incubation buffer depending on its volume. For the analysis of more than one parameter, replicates of the same experiment will therefore have to be performed, resulting in biological diversity between between independent samples affecting the outcome. Another issue of end-point analyses is the high amount of samples required, as each analysis parameter and each time point requires a separate set of aleurone layer incubations. Both the effects of biological diversity between independent samples and the amount of sample preparation required is therefore the most severe for time course studies.
The effect of biological diversity between independent samples can be eliminated, or at least minimised, if multiple non-destructive analyses are performed on the same set of aleurone layers, which will also lower the amount of samples needed to only one set of aleurone layer incubations. Taking all these factors into account, we[2] saw the need for developing a new method of incubation for aleurone layers that would allow continuous, non-destructive measurements on the same set of aleurone layer incubations over time with a lower work load.

I.6.1 A multiwell plate approach

The typical incubation setup used in our[3] group consists of replicates of 10 aleurone layers (approximately 100 mg) in 2 mL incubation buffer [7, 8] placed in separate wells of flat-bottomed 12-well incubation plates incubated at room temperature on a shaker at approximately 150 rpm. Already, the use of multiwell plates enables a number of different incubation conditions; with three biological replicates of each experiment, the typical approach is four different conditions (e.g. GA, ABA, GA+ABA, and an untreated sample), if only one parameter is to be analysed at the end of the experiment. Other combinations in the 12-well plate could be one parameter at four different time points under the same condition, four parameters at one time point under the same condition, or maybe 2 parameters at one time point under two different conditions. However, despite the flexibility of the 12-well multiplate setup, the number of samples (N) required increases rapidly with number of desired replicates (R), conditions (C), parameters (P), and time points (TP):

$$N = R \cdot C \cdot P \cdot TP$$

[2] Work performed in collaboration with Kinga Zór, Bioanalytics, Department of Micro- and Nanotechnology, Technical University of Denmark
[3] Agricultural and Environmental Proteomics, Department of Systems Biology, Technical University of Denmark

An example of just three replicates, two conditions, two analysis parameters, and three time points will therefore require $N = 3 \cdot 2 \cdot 2 \cdot 3 = 36$ samples and is hence both time and resource consuming, as a total of 360 aleurone layers should be dissected during sample preparations. Employing non-destructive analyses eliminates the need for replicates of aleurone layer incubations for each analysis due to both multiple parameters and multiple time points - though only for assays that are not mutually exclusive. Analyses can be mutually exclusive e.g. if buffers are not compatible, or if one analysis affects the outcome of another analysis. If assays are mutually exclusive, only the need for replicates due to multiple time points can be eliminated, whereas the need for replicates due to multiple analysis parameters cannot. The above formula for calculation of required sample numbers can therefore be simplified to the following for non-compatible and compatible analysis parameters, respectively:

$$N = R \cdot C \cdot P$$

$$N = R \cdot C$$

It had previously been decided to lower the work load required for sample preparation by decreasing the amount of aleurone layers per well from 10 to 5, and to avoid changing the ratio of aleurone layers to incubation buffer the buffer volume had been decreased from 2 to 1 mL. Using this ratio in the 12-well setup, the cell viability assay (Section I.3.3, page 9) and the redox activity assay (Section I.4.2, page 14) were tested and optimised as described in Part II (page 25). However, even though the assays are non-destructive and not mutually exclusive, this setup did not allow measurements on the same set of aleurone layers at multiple time points. For the cell viability assay, it proved impossible to identify the same cells of the same aleurone layers for imaging at different time points due to the suspension of the aleurone layers in the wells, which would also prevent the desired time course studies of transient expression of target enzymes by fluorescence microscopy (Section I.5.1, page 16). For the redox activity assay, adding the redox mediators directly to the incubation buffer would prevent the incubation to be continued (thus allowing only one time point), and moving the aleurone layers to new wells with the redox mediators and back to the original wells after the assay turned out to be very laborious and therefore only added to the work load. The solution to these problems proved to be immobilisation of single, whole aleurone layers.

I.6.2 An immobilised approach

Immobilisation strategies for cultivations of plant cells have been used extensively in the industry [117–119], and although single barley aleurone protoplasts have been immobilised [120, 121], nothing similar had yet been implemented for whole barley aleurone layers, to the best of our knowledge. In established methods, immobilisation of cells has been achieved by attachment to carrier surfaces, or by entrapment in porous polymer gels or in membranes [117–119]. The

attachment of plant cells to carrier surfaces has the distinct advantage compared to entrapment strategies of improved mass transfer of both nutrients to the cells and products from the cells, as the immobilisation matrix does not surround the cells [117]. Another advantage of attachment is that growth of cells immobilised in a matrix can lead to disintegration of the immobilisation matrix and possibly release of the cells into the incubation media [118]. The latter consideration is not a concern in connection with incubation of the aleurone layer, as these cells do not divide [7–9, 13, 36], but may be of concern for other types of plant tissue. Examples of immobilised plant tissues such as leaves, shoots, embryos and especially roots exist [117–119, 122, 123] but are much less implemented and used than single cell immobilisation methods.
Based on these considerations attachment was chosen as the optimal technique for immobilisation of the aleurone layers. However, immobilising the layers at the bottom of the wells of a 12-well multiplate facing upwards and into the incubation buffer would not work for the cell viability assay or the transient expression studies, as the microscope used for imaging was inverted and therefore only would image the seed coat on the outer side of the aleurone layers rather than the aleurone cells themselves. This setup would also not solve either of the problems with the redox activity assay, as redox mediators would still have to be added to the incubation buffer, or the incubation buffer removed before addition of the redox mediators - both options excluding the possibility of multiple time points. Instead, immobilisation of single, whole aleurone layers in the lid of the multiplate facing downwards towards the bottom of the wells was chosen. This would allow the use of the inverted microscope and hence the imaging of the same cells over time, as each imaging position could be stored in the microscope software for future time points. Immobilisation in the multiplate lid would also work for the redox activity assay, as immobilised aleurone layers could simply be lifted out of the plate with the incubation buffer and into another plate with the redox mediators for the assay and then moved back into the incubation buffer after completion of the assay for continued incubation. This would also allow for redox measurements on the aleurone layers alone (without incubation buffer), which had already been determined to be the most precise measurements (Part II, page 25).
Clearly, the aleurone layers could not be immobilised directly onto the lid of a multiwell plate, as this would not allow for immersion of the layers into the incubation buffer. However, immobilisation of the aleurone layers on pillars attached to lid would result in immersion of the aleurone layers into the buffer. Cylindrical pillars of polydimethylsiloxane (PDMS) were therefore cast in a flat-bottomed 48-well plate. The choice of the silicone-based PDMS was mainly due to its optical transparency and bio-compatibility but also due to the material being inexpensive, unreactive to most reagents, and easy to mold into a desired shape [124, 125]. A study on the growth of *Arabidopsis thaliana* roots in an incubation unit cast from PDMS further underlines the bio-compatibility of the material [126]. The PDMS pillars would be attached to the lid of a 12-well plate with a double-sided silicone adhesive (INT TA106, Intertronics, Oxfordshire, UK), as this had previously been applied to assemble polymer-based incubation units for cell culture [80, 127, 128]. Single, whole aleurone layers would then be immobilised at the end of the

pillars facing downwards towards the bottom of the wells and into the incubation buffer. To keep the system simple the double-sided silicone adhesive would also be used to attach the aleurone layers to the PDMS pillars.
Although the system would now work well with the cell viability assay and the transient expression studies, it became obvious that the previous approach for non-immobilised aleurone layers of normalisation of redox measurements with regards to dry weight (Part II, page 25) would not be possible. The aleurone layers could not easily be removed from the PDMS pillars without residues of the adhesive clinging to the backside of the layers, which would affect dry weight measurements and therefore prevent normalisation of the redox data. Instead, normalisation of these data with regards to area could be achieved by using tissue punch-outs of whole aleurone layers. Barley aleurone layers are 2-3 cell layers thick [8, 23], and tissue punch-outs of identical diameter would therefore yield reasonably consistent and comparable weights with identical areas. A biopsy puncher with a diameter of 4 mm would work for all but the smallest barley grains and was therefore chosen to eliminate the need for sorting the grains according to size before sample preparations. This adaptation would allow the system to work well with both the cell viability assay, the transient expression studies, and the redox activity assay. Finally, having reduced both sample sizes and amounts, a 24-well plate was chosen instead of a 12-well plate to increase throughput of the system by allowing more samples to be run simultaneously.

I.6.3 The developed incubation system

With this design, the developed incubation system would enable simultaneous incubations of 24 immobilised aleurone layer punch-outs (Figure I.11), and due to the immobilisation of the aleurone layers the system would be compatible with time course studies using inverted microscopy.

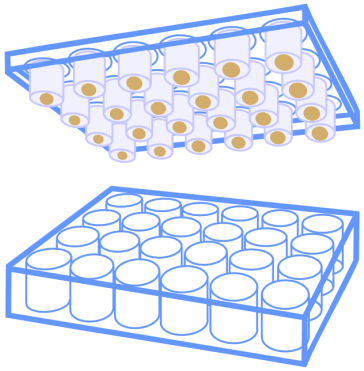

Figure I.11: Schematic representation of the novel incubation system for immobilised aleurone layers

PDMS-pillars are mounted in the lid of a 24-well multiwell plate with double-adhesive silicone tape, while aleurone layer punch-outs are immobilised at the end of the pillars with silicone tape, facing downwards towards the bottom of the wells during incubation. Lid-mounting facilitates easy movement of the aleurone punch-outs between assays as well as compatibility with an inverted microscope. See also Figures IV.1 and IV.2, pages 65 and 66.

It would also allow for time course experiments with assays on the aleurone layers performed in separate multiplates, as the lids with the aleurone layers could be moved, as well as for assays on the incubation buffer, as small volumes of this could be sampled at intervals for separate analyses.
Part IV: Article Manuscript #2 (page 61) presents results obtained with this novel incubation system for immobilised aleurone layers for both cell viability (12-well and 24-well), redox activity (24-well), and transient expression of target enzymes (24-well), as well as a schematic representation of the work flow used for combination of the different analyses.

I.7 Thesis outline

The remaining parts of this thesis describes the work performed:

- Part II: Article Manuscript #1 (page 25) presents the optimisation of and results obtained with the M-FiC redox activity assay, correlated to cell viability measured with the FDA-MM 4-64 assay. The effects of the NADPH oxidase-inhibitor DPI on the reducing capacity was also investigated with the M-FiC redox activity assay.
- Part III: Other results related to Article Manuscript #1 (page 43) presents other efforts conducted in relation to the work presented in Part II. The results described here all requires further work and optimisation before the methods described will yield publishable results. The work includes an alternative detection method for redox activity, and a description of a preliminary proteomics investigation performed by Assoc. Prof. Christine Finnie[4] and technician Birgit Andersen[4] on some of the samples produced in this project.
- Part IV: Article Manuscript #2 (page 61) describes the development of the incubation system for immobilised aleurone layers and the results obtained with this system in time course studies of cell viability, reducing capacity, and transient expression of the target proteins α-amylase and phytase. The developed incubation system is designed to enable high throughput analyses, which is demonstrated with six different treatments of aleurone layers.
- Part V: Other results related to Article Manuscript #2 (page 79) presents other efforts conducted in relation to the work presented in Part IV. The results described here all requires further work and optimisation before the methods described will yield publishable results. The work includes further use of the developed incubation system for screening of the effects of different compounds on cell viability of aleurone layers, and tests of two enzyme activity assays for use with the developed incubation system.
- Part VI: Summary and concluding remarks (page 89) summarises the findings and main conclusions obtained from the work described in Parts II-V.
- All references are listed numerically from page 95.
- The Appendices (page 107) contain a list of oral and poster presentations performed during the project (Appendix A), a list of all materials and methods used in this project (Appendix B), and a data disc with data and documents relevant to the proteomics investigation (Appendix C).

[4] Agricultural and Environmental Proteomics, Department of Systems Biology, Technical University of Denmark

Part II

Article Manuscript #1

Electrochemical measurement of the intra- and extracellular redox environment in intact plant tissue responding to phytohormones

Christina Mark[1#], Kinga Zór[2#], Arto Heiskanen[2], Martin Dufva[3], Jenny Emnéus[2], and Christine Finnie[1*]

[1]Agricultural and Environmental Proteomics, Department of Systems Biology, Technical University of Denmark, Kgs. Lyngby, Denmark
[2]Bioanalytics, Department of Micro- and Nanotechnology, Technical University of Denmark, Kgs. Lyngby, Denmark
[3]Fluidic Array Systems and Technology, Department of Micro- and Nanotechnology, Technical University of Denmark, Kgs. Lyngby, Denmark

*Corresponding Author. E-mail: csf@bio.dtu.dk (CF)
#These authors contributed equally to this work.

Submitted to Bioelectrochemistry

II.1 Abstract

The barley aleurone layer is an established model system for studying gibberellic acid induced enzyme secretion and programmed cell death during seed germination. Current methods applied to aleurone layers undergoing gibberellic acid-induced programmed cell death do not address redox homeostasis of intact cells. The electrochemical redox assay based on the menadione-ferricyanide double mediator system used in this paper enables probing of the reducing capacity and overall cellular redox environment in intact plant tissue without destroying cellular integrity. Redox changes were observed in intact barley (*Hordeum vulgare* cv. Himalaya) aleurone layers responding to gibberellic acid and abscisic acid. Remarkably, gibberellic acid caused an increase in the reducing capacity of barley aleurone layers, which occurred in parallel with a decrease in cell viability. The gibberellic acid-induced reducing capacity could be divided into an intracellular and an extracellular, i.e. plasma membrane-associated, component based on the dependence on menadione. Both intracellular and extracellular increases in reducing capacity were suppressed when aleurone layers were incubated with abscisic acid, or with the flavoenzyme inhibitor diphenyleneiodonium chloride suggesting involvement of the NADPH oxidase. The method provided new insight into the redox changes occurring in intact barley aleurone layers undergoing programmed cell death, showing that gibberellic acid induces an increase in reducing capacity in aleurone cells prior to cell death.

Highlights

- Reducing capacity increased with decreased cell viability over time.
- Gibberellic acid caused an increase in the reducing capacity in barley aleurone.
- Intra- and extracellular redox changes were measured in intact aleurone layers.
- Results support the existence of an 'oxidative window' during seed germination.

Keywords
Redox activity; Programmed cell death; Cell viability; Electrochemistry; Barley aleurone layer

Abbreviations
ABA, abscisic acid; DPI, diphenyleneiodonium chloride; FiC, ferricyanide; FoC, ferrocyanide; GA, gibberellic acid; M, menadione; PCD, programmed cell death; ROS, reactive oxygen species.

II.2 Introduction

Redox activity in plant cells plays a major role in a number of processes including abiotic stress, pathogen defence, tissue development, seed germination and programmed cell death (PCD) [36, 59, 60]. Plant cells contain five to ten times more genes encoding enzymes involved in regulation of redox homeostasis and protection of cells against oxidative stress than bacteria or mammalian cells [59, 60]. This is partially due to processes related to photosynthesis and to the constant need for adaptation to environmental changes, such as light conditions, water and nutrient availability as well temperature [59]. Regulation of the cellular redox environment is an important and dynamic process, since elevated levels of reactive oxygen species (ROS) can cause oxidative stress and lead to PCD [59,60,65,69]. PCD is an integral part of plant growth and survival, as it is involved in a range of processes such as seed germination, tissue development and defence against pathogens [6, 37–39]. Monitoring of the redox changes occurring during processes leading to PCD can therefore provide a better understanding of biological events occurring in plants.

In the barley (*Hordeum vulgare*) aleurone layer, the phytohormone gibberellic acid (GA) induces germination-related metabolism, enzyme secretion and subsequent PCD [13, 36]. Abscisic acid (ABA) counteracts GA, and in the presence of both phytohormones germination-related events of the aleurone layer are delayed, while ABA suppresses PCD entirely in the absence of GA [13,36]. The barley aleurone layer is an accepted model system for studying phytohormone signalling, enzyme secretion and PCD during seed germination [7–9] due to this well-known and widely studied tight hormonal regulation process. PCD in aleurone cells is not apoptotic [18, 19, 36] but a complex, multistep form of autolysis involving loss of plasma membrane integrity leading to cell shrinkage [18, 24].

Even though evidence shows that ROS play an important role in PCD during germination and that there are significant changes in activity of ROS-metabolising enzymes during GA-induced PCD [12], the exact mechanisms remain to be elucidated [4, 66]. Earlier studies demonstrated reduced amounts and activities of ROS-scavenging enzymes (e.g. superoxide dismutase, catalase, ascorbate peroxidase) in homogenates of GA-treated barley aleurone layers [12], whereas ABA-treated layers retained ROS scavenging ability and cell viability [12,32]. GA-induced production of ROS, such as H_2O_2, a major by-product of germination-induced metabolism, can be observed after only 3 h of incubation in the presence of GA [14], and this, in combination with decreased redox enzyme activities [12], is predicted to shift the overall redox balance towards conditions of oxidative stress, ultimately leading to PCD. The concept of an 'oxidative window' for germination has been defined as an optimal level of ROS, whereas either too low or too high levels of ROS inhibit germination [61].

The combined effects of cellular oxidative and reductive processes determine whether this window is open or closed. Recent evidence [14] supports the role of the membrane-bound flavoenzyme NADPH oxidase in providing pressure on the 'oxidative window' through production of

the superoxide radical ($O_2^{\bullet -}$), which dismutates to H_2O_2 (Figure II.1A). Inhibition of NADPH oxidase by the flavoenzyme inhibitor diphenyleneiodonium chloride (DPI) resulted in reduced ROS levels and delayed germination [14].

The current knowledge about aleurone layer redox environment, i.e. evaluation of reducing or oxidising capacity, is mainly based on colorimetric quantification of H_2O_2 [7, 9], measurement of selected enzyme activities, gene expression and protein appearance profiles in cell extracts [10, 12, 14], which do not give a complete understanding of cellular redox homeostasis. There is a lack of studies evaluating the overall redox environment in intact plant cells, comprising the sum of reductive and oxidative processes. Even though plant plasma membrane redox

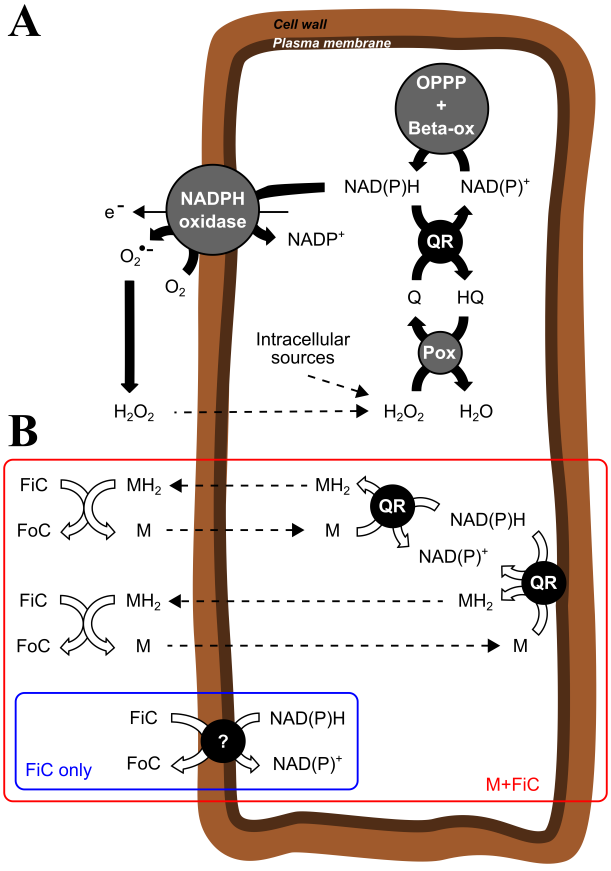

Figure II.1: Schematic representation of probing intra- and extracellular redox environment using the M-FiC double mediator system

A: Black arrows indicate major processes involving NAD(P)H and H_2O_2 metabolism in GA-induced aleurone layers. **B:** White arrows indicate potential mechanisms for reduction of M and FiC. FiC cannot pass the plasma membrane and measurements based on this mediator alone (blue box) will therefore only probe extracellularly. Measurements based on both mediators (red box) will probe the sum of intracellular, extracellular and membrane-related redox activity. GA: Gibberellic acid. M: Menadione. MH_2: Menadiol. FiC: Ferricyanide. FoC: Ferrocyanide. Q: Quinone. HQ: Hydroquinone. QR: Quinone reductase. Pox: Peroxidase. OPPP: Oxidative pentose phosphate pathway. $O_2^{\bullet -}$: Superoxide. Beta-ox: Beta oxidation of lipids.

reactions [49,73] and extracellular H_2O_2 concentrations [129] have been monitored electrochemically on living plant cells, to our knowledge there is no method reported which allows intra- and extracellular as well as membrane related redox activity measurements in intact plant tissues. Enabling detection in intact living tissues and cells could provide information closer to *in vivo* conditions than the more invasive, traditional methods.

Electrochemical techniques have been successfully used to evaluate intracellular redox activity in living intact mammalian [74–76], yeast [77, 80, 81] and bacterial [82, 83] cells. An amperometric detection method based on the menadione-ferricyanide (M-FiC) double mediator system has been developed for probing intracellular redox activity (NAD(P)H availability) in whole cells [78]. The principle of intracellular probing is based on the lipid-soluble quinone, M, which can pass through the cell membrane into the cytosol (Figure II.1B), where it is reduced by menadione reducing enzymes (MRE), such as quinone reductases (QR), to menadiol (MH_2) or possibly semiquinone radicals ($M^{\bullet -}$, not shown) [75]. The quantification of MH_2 or $M^{\bullet -}$ is enabled via their re-entrance to the extracellular environment, where they can reduce FiC (which is unable to pass the cell membrane) to ferrocyanide (FoC), while simultaneously being re-oxidised to M (Figure II.1B). The amount of FoC that is generated is therefore directly proportional to the overall reducing capacity of the cells and can be detected electrochemically by oxidation on an electrode [77–79].

Several studies describe the identification of MREs in *Saccharomyces cerevisiae* [79], whereas the knowledge about the identity and role of MREs in plant cells is more limited. Although QRs have not yet been characterised in the barley aleurone layer, the existence of cytosolic, mitochondrial and intracellularly active plasma membrane-bound QRs has been shown in several plants [70,72,85–88]. It has been demonstrated [89] that QRs can convert changes in H_2O_2 levels to changes in the NAD(P)H:NAD(P)$^+$ ratio (Figure II.1A), which enables probing of the cellular redox environment (the NAD(P)H:NAD(P)$^+$ ratio) of the aleurone layers through quinone reducing capability.

In this work, electrochemical redox probing was used for time dependent monitoring of reducing capacity, evaluation of intra- and extracellular as well as membrane related redox changes, and assessment of the effect of the NADPH oxidase inhibitor, DPI, on redox activity during GA-induced PCD in intact barley aleurone layers. In addition, the time dependence of changes in reducing capacity and cell death were compared using an established colorimetric assay.

II.3 Materials and Methods

II.3.1 Chemicals

Ethanol, ampicillin, nystatin, succinic acid, calcium dichloride, Trizma base, GA (gibberellin A3), ABA, DPI, fluorescein diacetate, M, and FiC were obtained from Sigma-Aldrich Co. (St. Louis, MO, USA), while MM 4-64 (N-(3-triethylammoniumpropyl)-4-(6-(4-(diethylamino)phenyl)hexatrienyl)pyridinium dibromide) was obtained from Biomol GmbH (Hamburg, Germany).

II.3.2 Plant material and incubation buffer

Barley seeds (*Hordeum vulgare* cv. Himalaya, 2003 harvest, Washington State University, Pullman, USA) from a batch previously used to study production of secreted hydrolases [7] were de-embryonated, surface sterilised with 70% ethanol, rinsed four times with sterile H_2O, and imbibed in sterile H_2O with 50 μg mL^{-1} ampicillin and 5 μg mL^{-1} nystatin for 4 days in the dark at 4°C. Aleurone layers were isolated by gently scraping away the starchy endosperm with the blunt side of a metal scalpel. Aliquots of approximately 50 mg (fresh weight) of aleurone layers were incubated in separate wells of 12-well multiplates in 1 mL of buffer at room temperature on a shaker at 150 rpm for the indicated time in incubation buffer (20 mM succinic acid, 20 mM $CaCl_2$, 20 mM Trizma base, 50 μg mL^{-1} ampicillin, 5 μg mL^{-1} nystatin, pH 5) with the relevant phytohormones or enzyme inhibitor. Concentrations of GA, ABA and DPI were 10 μM. For liquid N_2-treated samples, freshly isolated aleurone layers were immersed in liquid nitrogen for 1 min and allowed to thaw at room temperature, prior to assay of redox activity. All incubations were set up in at least triplicates.

II.3.3 Cell viability assay

Cell viability of intact aleurone layers was determined as previously described [12]. The incubation buffer was removed and aleurone layers were washed with 20 mM $CaCl_2$ before staining with fluorescein diacetate (2 μg mL^{-1} in 20 mM $CaCl_2$) and MM 4-64 (2 μM in 20 mM $CaCl_2$). Each staining step was followed by washing with 20 mM $CaCl_2$. The aleurone layers were observed with a microscope (AXIO OBSERVER.Z1 with EC Plan-Neofluar 10x/0.30 Ph 1 objective and AxioCamMR3 camera with the AxioVision LE 4.8.2.0 software, Carl Zeiss Microscopy GmbH, Jena, Germany) and digital images were taken of three different regions of three different aleurone layers for each sample. Percentages of dead cells were determined using the Colour Deconvolution plugin [130] for the ImageJ 1.45s software (National Institutes of Health, USA).

II.3.4 Redox activity assay

For redox activity measurements, after incubation of the intact aleurone layers in the presence or absence of phytohormones and/or DPI, the redox mediators M and/or FiC were added. The

procedure was based on the method described for yeast cells [79] with final concentrations of 20 mM FiC and 100 μM M in the incubation buffer. The aleurone layers were incubated in the presence of redox mediators for 1 h at room temperature on a shaker unless otherwise specified. The spent incubation buffer with the redox mediators was transferred to Eppendorf tubes and centrifuged (14800 rpm for 10 min; SIGMA 1-14, SIGMA Laborzentrifugen GmbH, Osterode am Harz, Germany). The clarified supernatant was transferred to new tubes, frozen in liquid nitrogen and stored at -80°C until electrochemical analysis. The aleurone layers were transferred to aluminium weighing boats, and dried for a minimum of 24 h at 80°C for determination of dry weight.

II.3.5 Electrochemical detection

The setup consisted of a peristaltic pump (Minipuls 2, Gilson, Inc., Middleton, WI, USA) providing a continuous flow (500 μL min^{-1}) of incubation buffer to define the baseline, an injection port (Model 7010, Rheodyne, Inc., Cotati, CA, USA) with a sample loop of 50 μL, an electrochemical cell designed and fabricated for commercial screen printed electrodes (DropSense) and a potentiostat (Model CHI 1010A, CH Instrument Inc., Austin, TX, USA). 50 μL of each sample was injected in carrier buffer flow through the injection port to the electrochemical cell containing a screen printed electrode (DS 250 AT, DropSense, Asturias, Spain). The FoC present in the samples was electrochemically oxidised on the Au working electrode at +400 mV vs. an Au reference electrode. Each of the three biological replicates was injected three times and peak currents were averaged. The FoC content was calculated using a linear calibration curve of FoC standard solutions and normalised by aleurone layer dry weight as follows:

$$c = \frac{I - b}{a} \cdot \frac{D}{m}$$

where c is the FoC concentration per dry weight, I the measured peak currents of the samples, a and b the slope and intercept, respectively, of the calibration curve, D the dilution factor, and m the measured dry weight of the aleurone layers.

II.3.6 Statistical analysis

All data was analysed using the GraphPad Prism 6.04 software (GraphPad Software, Inc., San Diego, CA, USA) by first subjecting datasets to the ROUT (Robust regression and Outlier removal) outlier analysis with a false discovery rate of 1%. Subsequently, outlier analysed data was then subjected to Fisher's LSD (Least Significant Difference) two-way ANOVA test at a confidence level of 95%.

II.4 Results and Discussion

II.4.1 Electrochemical assay for probing the redox environment of living barley aleurone layers

The electrochemically determined FoC content increased during incubation with the mediators from 15 min to 1 h (Figure II.2). After 1 h, a significant increase in reducing capacity of aleurone layers incubated with GA was observed, compared to all other samples. For GA+ABA treated samples, the signal was suppressed to a lower level than the untreated (UT) samples. The reducing capacity was lowest for aleurone layers treated with ABA alone, in agreement with the function of ABA to maintain the aleurone layers in a state of low metabolic activity [13, 36]. Therefore, in most studies of PCD in aleurone layers, ABA treated samples are used as controls [8, 12, 13, 16, 18, 19, 24, 36, 51]. In further experiments an incubation time of 1 h was chosen in order to maximise the sensitivity of the assay.
The biological relevance of the measurements is therefore supported, since we observed the well-documented antagonistic effect of the phytohormones GA and ABA [13,36] on redox activity. The observed increase in reducing capacity could support the existence of an 'oxidative window' [61], where the redox balance is shifted towards reducing processes enabling germination.
The buffer commonly used for incubation of aleurone layers has been $CaCl_2$, succinic acid, pH 4.2 [8], whereas for performing the electrochemical redox activity assay Trizma base, succinic acid, KCl, pH 5 [79] buffer was used. The buffer system compatible both with incubation of aleurone layers and subsequent redox assays was found to be 20 mM $CaCl_2$, 20 mM succinic acid, 20 mM Trizma base at pH 5. In order to be able to use the same buffer for both aleurone layer

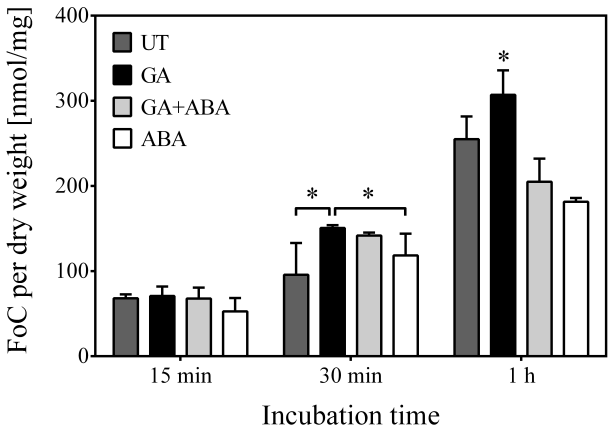

Figure II.2: Reducing capacity increases during incubation with the redox mediators

Aleurone layers were incubated for 24 h in the presence or absence of hormones before incubation with redox mediators (M+FiC) for 15 min^{-1} h. Error bars represent SD ($n \geq 6$), and asterisks indicate significant differences between indicated treatments (horizontal lines) or to all other treatments ($p<0.05$). UT: Untreated. GA: Gibberellic acid. ABA: Abscisic acid. M: Menadione. FiC: Ferricyanide. FoC: Ferrocyanide.

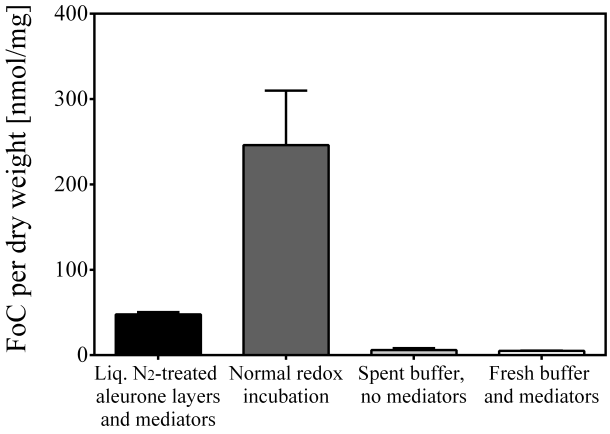

Figure II.3: No electrochemical interference from buffer components

Redox incubations (1 h, M+FiC) were performed on liquid N_2-killed aleurone layers, on aleurone layers with spent incubation buffer (24 h incubation with GA, then 1 h normal redox incubation) and on fresh incubation buffer without aleurone layers. A further electrochemical measurement was performed on spent incubation without addition of redox mediators. Error bars represent SD ($n \geq 4$). GA: Gibberellic acid. M: Menadione. FiC: Ferricyanide. FoC: Ferrocyanide.

incubation and redox activity assay, the buffer pH was kept at 5 to ensure chemical stability of FoC. Ca^{2+} ions are required for aleurone layer enzyme production and secretion [11, 15], and $CaCl_2$ was therefore chosen over KCl in the buffer composition.

In order to evaluate the accuracy of the electrochemical measurements, the effect of possible electrochemical interferences from the incubation buffer containing the phytohormones was quantified. We measured the reducing capacity of aleurone layers in incubation buffer containing the phytohormones with added mediators (redox incubation), on spent and centrifuged incubation buffer (from which the aleurone layers had been removed) without mediators, and on fresh incubation buffer (no contact with aleurone layers) with mediators added. No electrochemical interference was observed from the incubation buffer containing the phytohormones either in the presence or absence of the mediators (Figure II.3), and the redox changes were observed only in the presence of the aleurone layers. The negligible signal detected from spent incubation buffer in the absence of mediators was designated as background noise.

To verify that the measured activity was due to living aleurone cells and to determine the basal redox level, the redox assay was also carried out using freshly isolated aleurone layers that had been killed by submersion into liquid N_2 and allowed to thaw prior to incubation with redox mediators. A low level of FoC was detected (Figure II.3), indicating a small contribution from redox active components in the dead cells.

II.4.2 GA increases the reducing capacity of barley aleurone layers in parallel with a decrease in cell viability

The electrochemical redox assay was used to evaluate the time dependent effect of the phytohormones GA and ABA on reducing capacity of the aleurone layers. For all treatments, reducing capacity increased with incubation time from 0 to 48 h, which continued until 72 h for all other treatments than GA (Figure II.4A). A significant increase in the reducing capacity was observed from 24 h in GA-treated samples when compared with ABA-treated samples and from 36 h when compared with GA+ABA-treated samples. ABA suppressed the GA-induced increase in reducing capacity to a level below that of the untreated (UT) samples. The lowest reducing capacity was observed in samples treated with ABA alone. The reducing capacity at 0 h (Figure II.4A) was at the level of the signal measured from liquid N_2-killed cells (Figure II.3), and represents the basal level of redox activity that can be measured in the aleurone layers.
M is able to induce oxidative stress in different plant systems [42, 131] and could therefore affect both redox activity and cell viability. However, we observed no significant effect on cell viability after 1 h incubation with M alone or with M+FiC compared to aleurone layers that were not exposed to either mediator (Supplementary Figure II.S1).
To evaluate the progress of PCD, cell viability was monitored by fluorescence microscopy using a method previously established for barley aleurone layers [12] and quantified by image analysis (Figure II.4B-D). From a starting point of 9% dead cells at 0 h, cell death increased significantly in GA-treated aleurone layers from 36 h (9% at 12 h, 10% at 24 h, 20% at 36 h, 41% at 48 h and 88% at 72 h shown in Figure II.4B). Although the observed increase in cell death was slower, the trend was similar to previously published observations of approximately 60% dead cells at 36 h and 90% at 48 h [12]. The observed delay in the onset of PCD could be caused by the different seed batches, buffers, hormone concentrations and the method used for quantifying live/dead cells. The observations of cell death confirmed that the aleurone layers responded to GA and ABA as expected.
A significant increase in cell death was also observed in UT samples (53% dead cells at 72 h), although the rate was much slower than for GA-treated samples (Figure II.4B). This is supported by previous observations of increased H_2O_2 levels in both UT and GA-treated aleurone protoplasts [9] and small amounts of α-amylase produced in UT aleurone layers [7]. This supports the view that UT samples undergo germination-related processes and PCD, although the rate is slower than in the GA-treated samples. As expected, ABA delayed GA-induced cell death. After 72 h incubation, GA+ABA-treated samples contained 31% dead cells, while treatment with ABA alone maintained viability of the aleurone layers throughout the 72 h incubation period (approx. at the level of 11% dead cells).
The increase in reducing capacity between 0-48 h (Figure II.4A) correlates with the increase in the percentage of dead cells (Figure II.4B) for GA-treated samples, suggesting that the measured increase in reducing capacity in GA-treated aleurone layers was related to the GA-induced cell

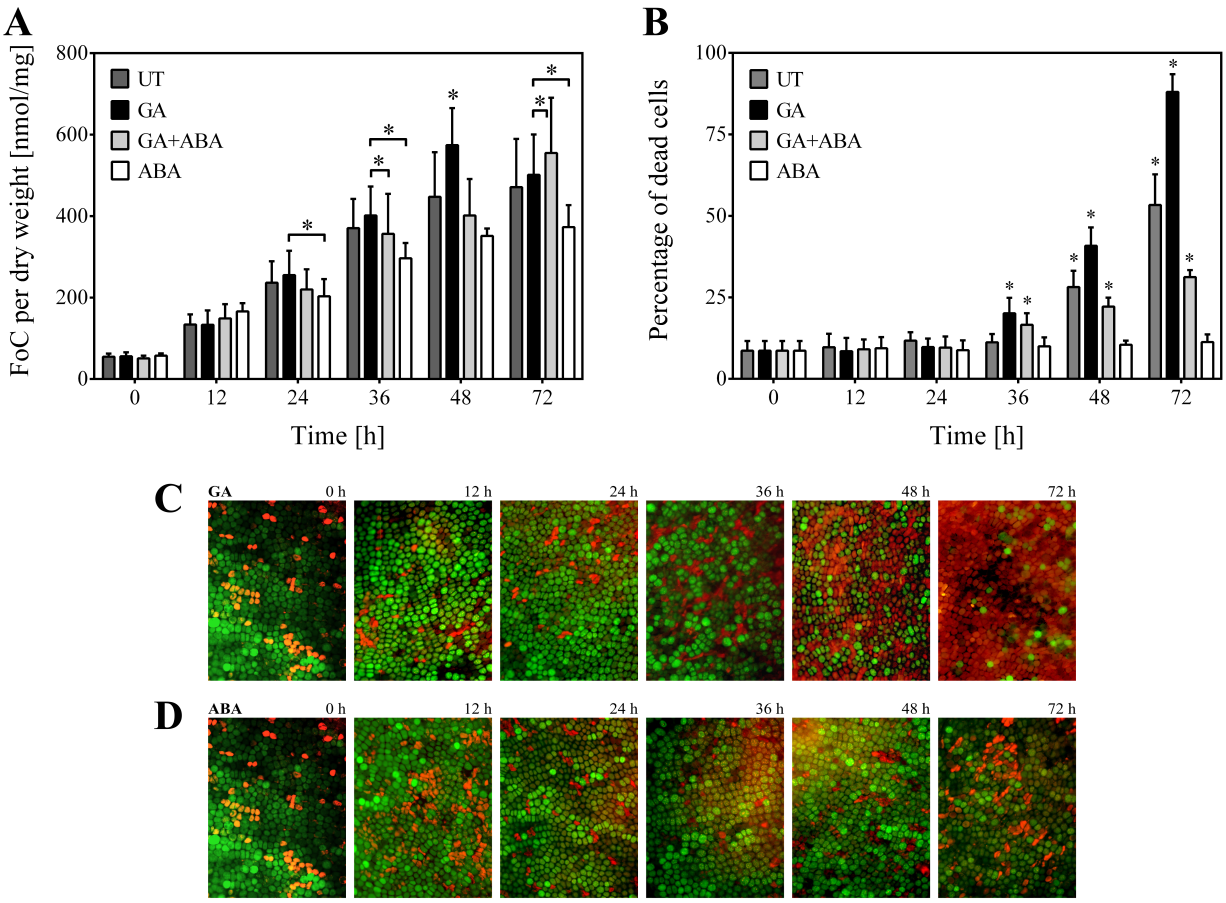

Figure II.4: Increased reducing capacity correlates with decreased cell viability over time

A: Aleurone layers were incubated for 0 to 72 h before 1 h incubation with redox mediators (M+FiC). Error bars represent SD ($n \geq 12$), and asterisks indicate significant differences between indicated treatments (horizontal lines) or to all other treatments ($p<0.05$). **B:** Aleurone layers were incubated for 0 to 72 h before being subjected to the cell viability assay. Error bars represent SD ($n \geq 9$), and asterisks indicate significant differences to 0 h samples. **C, D:** Fluorescence micrographs of aleurone layers treated with GA (C) or ABA (D) for 0 to 72 h. Live cells appear green, while dead cells appear orange-red. All images are 647x865 μm. UT: Untreated. GA: Gibberellic acid. ABA: Abscisic acid. M: Menadione. FiC: Ferricyanide. FoC: Ferrocyanide.

death. On the other hand, while the percentage of dead cells significantly increased until 72 h in GA-treated aleurone layers (Figure II.4B), the reducing capacity showed a slight decrease from 48 to 72 h as mentioned above (Figure II.4A). This probably reflected that only 12% of the cells in these aleurone layers remained alive and redox-active (Figure II.4B).

The measured reducing capacity was assumed to originate mainly from intact, viable cells, since the reducing capacity of ABA-treated aleurone layers increased over time with no increase in cell death, and the reducing capacity decreased in GA-treated aleurone layers during 48 to 72 h incubation, concurrent with a strong decrease in cell viability from 59% to 12%. This trend was

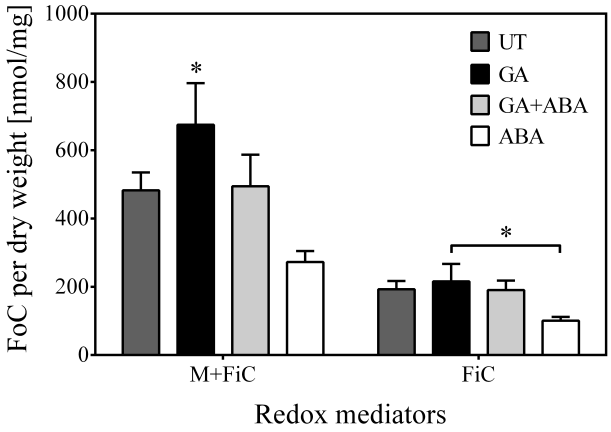

Figure II.5: Measured reducing capacity consists of an intracellular and an extracellular component

Redox assay performed for aleurone cells incubated for 48 h before 1 h incubation with either both redox mediators (M+FiC) or FiC only. Error bars represent SD ($n \geq 12$), and asterisks indicate significant differences between indicated treatments (horizontal lines) or to all other treatment types ($p<0.05$). UT: Untreated. GA: Gibberellic acid. ABA: Abscisic acid. M: Menadione. FiC: Ferricyanide. FoC: Ferrocyanide.

similar to results obtained by Palma and Kermode [16], demonstrating the ability of GA-treated aleurone layers to metabolise exogenous H_2O_2, at high cell viability, followed by a decrease in H_2O_2 metabolism with increasing rate of cell death [16]. The effect of GA on redox activity of the aleurone layers was suppressed by ABA, in agreement with the antagonistic effects of ABA and GA on germination [12, 18, 24].

II.4.3 The electrochemically measured reducing capacity has an intracellular and an extracellular component

The possibility of FiC reduction at the plasma membrane has previously been demonstrated in plant cells [49]. We investigated the contribution of the plasma membrane related reducing capacity in order to distinguish between intracellular and extracellular reducing capacity. We applied an incubation time of 48 h rather than 24 h, as the distinction between the samples was very clear at 48 h due to the high signal values (Figure II.4A). The reducing capacity detected using both redox mediators was compared with the capacity detected using FiC alone as schematically presented in Figure II.1. We found both M-dependent (intracellular) and M-independent (extracellular and plasma membrane-related) contributions to the overall GA-induced increase in the reducing capacity (Figure II.5). Furthermore, probing with FiC alone showed that approximately one third of the GA-induced reducing capacity could be attributed to M-independent reducing activity (Figure II.5).

II.4.4 The extracellular component of the reducing capacity is plasma membrane associated

Although Figure II.1 depicts only aleurone layer associated extracellular reducing capacity, enzymes and/or redox-active compounds (e.g. flavonoids) released into the incubation buffer might also contribute to this part of the measured signal. Such sources of reducing capacity can be related to active secretion by the aleurone layers [8, 24, 69], release of cell wall components, or release due to loss of plasma membrane integrity during PCD [24]. To evaluate the source of the reducing capacity, the aleurone layers were removed from the incubation buffer after incubation with phytohormones, and the redox assay was performed separately for the aleurone layers and the spent and centrifuged incubation buffer. The redox assays were performed with both redox mediators and with FiC alone, enabling M-dependent and M-independent events to be distinguished (Figure II.6).
We observed that 73% of the overall reducing capacity determined when adding both redox mediators directly to the aleurone layers in the spent incubation buffer (Figure II.6A, GA) was associated with the aleurone layers alone (Figure II.6B, GA). The spent and centrifuged incubation buffer yielded no redox signal with either M+FiC or FiC alone (Figure II.6C), indicating that the extracellular reducing capacity was not caused by enzymes or compounds secreted or released into the buffer. Rather, the remaining 27% of the overall signal (Figure II.6A, GA) was caused by components associated with cell debris, accounting for the difference between GA-samples in

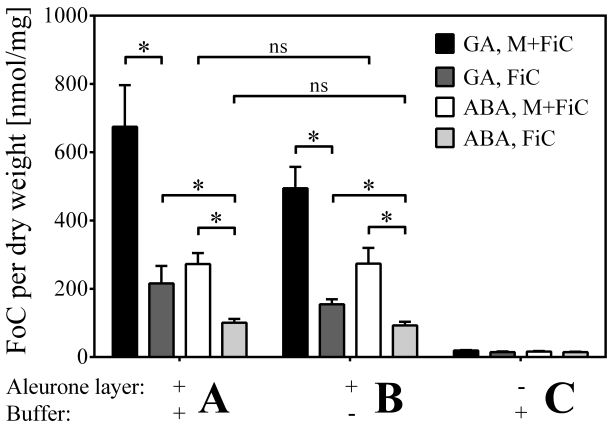

Figure II.6: Extracellular reducing capacity of aleurone layers is associated with the plasma membrane

Extracellular reducing capacity is aleurone layer is associated to the plasma membrane. Two batches of aleurone layers were incubated for 48 h before 1 h incubation with either both redox mediators (M+FiC) or FiC only. One batch was subjected to incubation with redox mediators immediately after phytohormone incubation (**A**). The second batch was split in two (aleurone layers (**B**) and spent, centrifuged incubation buffer (**C**)) and subjected separately to incubations with redox mediators. Error bars represent SD ($n \geq 12$), and asterisks indicate significant differences between indicated treatments (horizontal lines, $p<0.05$), while ns indicates non-significant changes between indicated treatments ($p<0.05$). GA: Gibberellic acid. ABA: Abscisic acid. M: Menadione. FiC: Ferricyanide. FoC: Ferrocyanide.

Figure II.6A and II.6B.
A contribution to the overall reducing capacity from cell debris was also observed when cells were treated with liquid N_2-treatment (Figure II.3). This was further supported by the lack of difference for ABA-treated samples when comparing the complete incubation system (aleurone layer and incubation buffer, Figure II.6A) with the aleurone layer alone (Figure II.6B), since ABA suppresses PCD and therefore also cell degradation.
Analysis of the aleurone layer associated reducing capacity (Figure II.6B, M+FiC) revealed that approximately two thirds of the reducing capacity was M-dependent (69% and 67% for GA and ABA-treated samples, respectively). This part of the reducing capacity was most likely due to cytosolic and/or intracellularly active plasma membrane-bound QRs [86–88]. The remaining reducing capacity (Figure II.6B, FiC) was M-independent and therefore extracellular, since FiC was unable to pass the plasma membrane. The FiC-related reducing capacity was therefore likely to be localised to the plasma membrane [49], although a cell wall location cannot be ruled out. Furthermore, this extracellular component was significantly higher in GA-treated compared to ABA-treated samples (Figure II.6B).

II.4.5 The GA-induced increase in reducing capacity is dependent on a DPI-sensitive enzyme

Given the involvement of NADPH oxidase in the redox environment [61], we investigated the effect of the unspecific flavoenzyme inhibitor, DPI, on the redox activity and cell viability of the

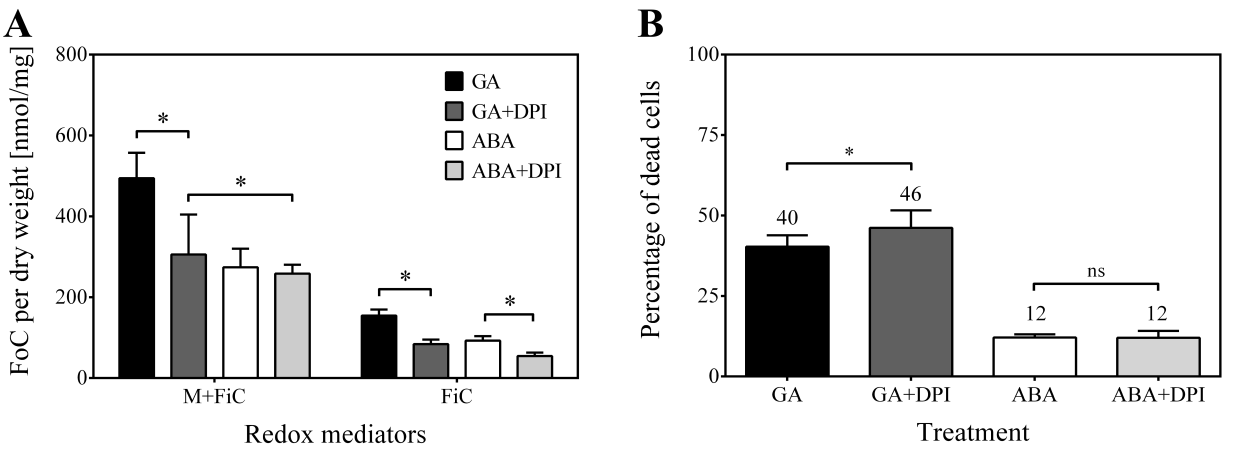

Figure II.7: DPI suppresses the GA-induced reducing capacity and increases GA-induced cell death

A: Aleurone cells were incubated for 48 h before being transferred to clean incubation buffer and subjected to 1 h incubation with either both redox mediators (M+FiC) or FiC only. **B:** Aleurone cells were incubated for 48 h before being subjected to the cell viability assay. Error bars represent SD ($n \geq 9$), and asterisks indicate significant differences between indicated treatments (horizontal lines, $p<0.05$), while ns indicate non-significant differences ($p>0.05$). GA: Gibberellic acid. ABA: Abscisic acid. M: Menadione. FiC: Ferricyanide. FoC: Ferrocyanide. DPI: Diphenyleneiodonium chloride.

aleurone layer. The concentration of 10 μM DPI applied in this work was expected to mainly inhibit the membrane-bound NADPH oxidase, since the K_i of DPI with respect to NADPH oxidase activity is less than 15 μM, whereas other flavoenzymes are inhibited much more weakly [68]. DPI significantly decreased the reducing capacity of GA-treated aleurone layers to the level of ABA-treated samples (Figure II.7A, M+FiC), suggesting that the NADPH oxidase might be involved in the reducing capacity that was induced by GA. DPI did not have a significant effect on the ABA-treated aleurone layers, indicating that the overall reducing capacity measured in ABA-treated aleurone layers was not determined by the NADPH oxidase (Figure II.7A, M+FiC). When FiC was used alone (Figure II.7A, FiC), the reducing capacity of GA-treated samples was again decreased by DPI to the level of the ABA-treated samples, indicating that the extracellular GA-induced reducing capacity was also dependent on the activity of a DPI-sensitive enzyme such as NADPH oxidase. DPI also slightly decreased the amount of FiC reduction in ABA-treated aleurone layers, suggesting that the ABA-treated aleurone layers do exhibit some NADPH oxidase activity (Figure II.7A, FiC). Whereas DPI counteracted the GA-induced increase in reducing capacity, it slightly increased the level of cell death in GA- but not ABA-treated aleurone layers (Figure 7B), possibly as a result of increased oxidative stress.

II.4.6 A model for regulation of the cellular redox environment during seed germination

The reducing capacity of GA-treated aleurone layers increased between 24 and 48 h (Figure II.4A), in parallel with a dramatic decrease in the number of live cells between 36 and 48 h (Figure II.4B), suggesting that GA induces a major increase in cellular reducing capacity. This finding contrasts with previous reports predicting increased oxidative capacity in the form of oxidative stress and reduced activity of redox active enzymes [12, 14, 16, 32]. At the same time, this might support the existence of the proposed 'oxidative window' for germination [61], since the measured increase in reducing capacity could be a mechanism by which the aleurone cells may counteract oxidative stress, thus holding the 'oxidative window' open long enough to complete the synthesis and release of hydrolytic enzymes required to facilitate seedling growth. This is also supported by the observation of decreased reducing capacity simultaneously with increased cell death for GA-treated aleurone layers in the presence of DPI (Figure 7). The increase in reducing capacity is probably due to the GA-induced enhanced metabolic activity [16] through e.g. the NADPH-producing pentose phosphate pathway [132] and NADH-producing beta-oxidation of lipids (Figure II.1A) [32]. As stored lipids constitute up to 25-30% of the aleurone cell volume, beta-oxidation contributes significantly to the reducing capacity [13, 133]. Increased beta-oxidation of lipids also leads to generation of intracellular H_2O_2 as a metabolic by-product [16]. The redox homeostasis of the cells is also doubly influenced by the NADPH oxidase, which is fuelled by NADPH produced during metabolism [89]. Thus, it both affects the NADPH:NADP+ ratio and produces superoxide that dismutates to H_2O_2 [14, 69], which can diffuse freely into the

cells (Figure II.1A) [134]. Via peroxidases and quinone reductases, this triggers additional production of NAD(P)H, which could lead to further activation of the NADPH oxidase in a positive feedback mechanism (Figure II.1A). The significant role of the NADPH oxidase in the redox environment is further underlined by the observed ability of DPI to block the GA-induced increase in reducing capacity (Figure II.7A). Additionally, the superoxide generated by the NADPH oxidase (Figure II.1A) may reduce FiC, which would directly affect the measured reducing capacity.

II.5 Conclusions

The application of electrochemical techniques is scarcely explored in plant biology [49,135], and with the presented method we open up new possibilities for monitoring the cellular redox environment in plant cells. We successfully applied the electrochemical redox assay to monitor redox state changes in living aleurone layers in response to hormones without destroying cellular integrity. It was demonstrated that the redox assay could be used for measuring PCD-related redox changes from 0 to 72 h, and that these changes occur in parallel with a decrease in cell viability. We also demonstrated that the method allows dissection of the redox measurements into an intracellular and an extracellular component. Finally, we provide evidence that a GA-induced increase in reducing capacity is dependent on the NADPH oxidase.

The electrochemical redox assay is not proposed as a replacement for the commonly used redox assays but rather as a complementary technique in plant redox biology, facilitating parallel probing of intra- and extracellular (including membrane-associated, cell wall-associated and secreted) redox activity providing new, otherwise unrevealed, information about the cellular redox environment of intact cells. Although the aleurone layer is a model system for studying PCD, germination, enzyme secretion and hormone signalling, the method also has potential for addressing different biological problems in other plant tissues, such as responses to abiotic or biotic stress in leaf tissues or germinating embryos. Knowledge of redox changes occurring during e.g. PCD, which has an important role in seed germination, tissue development and pathogen defence, could help to improve yield and quality of crops.

An advantage of the method is elimination of the need for cell lysis or other sample pre-treatment steps making real-time intracellular redox probing possible, and opening up possibilities for future online detection. Given the advantages of electrochemical detection techniques, such as possibilities for miniaturisation, multiplexing and automation [136,137], development of electrochemical methods, as demonstrated here, has great potential in the area of plant biology.

II.6 Acknowledgements

We are grateful to Prof. Birte Svensson (Enzyme and Protein Chemistry, Dept. of Systems Biology, Technical University of Denmark) for critical revision of the manuscript, to Gregorio Barba-Espín, PhD (Agricultural and Environmental Proteomics Dept. of Systems Biology, Technical University of Denmark) for stimulating discussions, to Birgit Andersen (Agricultural and Environmental Proteomics, Dept. of Systems Biology, Technical University of Denmark) for technical assistance with aleurone layer sample preparations, and to Mette Hemmingsen, PhD (Fluidic Array Systems and Technology, Dept. of Micro- and Nanotechnology, Technical University of Denmark) for technical assistance with fluorescence microscopy.

II.7 Author Contributions

The project was conceived by CF, JE and MD. CM and KZ de-signed the experiments and wrote the manuscript. CM performed sample preparation, tissue and redox incubation, cell viability and statistical analysis. KZ performed electrochemical detection and data analysis. AH helped with design of the redox assay and critically revised the manuscript. MD and JE critically revised the manuscript. CF supervised the research, helped with interpretation of results and revised the manuscript. All authors read and approved the final manuscript.

II.8 Supplementary Information

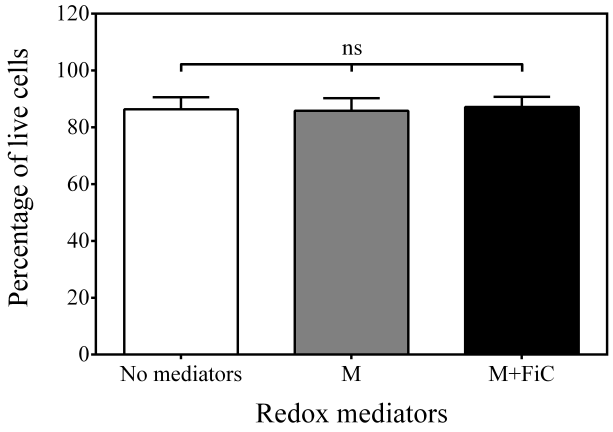

Figure II.S1: M and FiC do not affect cell viability

Freshly isolated aleurone layers were incubated without redox mediators, with M only or with M+FiC for 1 h before being subjected to the cell viability assay. Error bars represent SD (n≥12), and ns indicates non-significant changes between indicated treatments (p<0.05). M: Menadione. FiC: Ferricyanide.

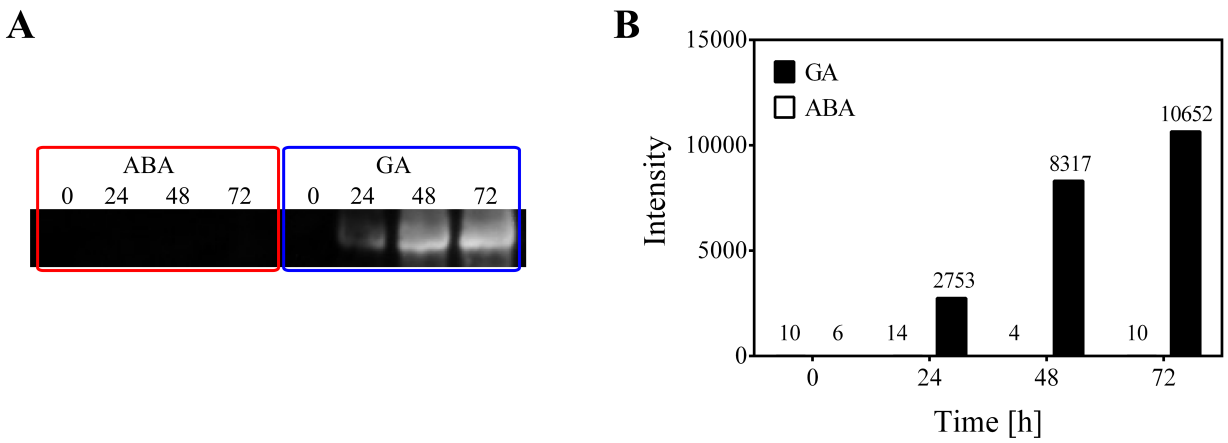

Figure II.S2: α-amylase secretion over time in response to GA or ABA

Incubation buffer from aleurone layers incubated for 48 h with GA or ABA was collected, centrifuged to remove debris, and analysed by Western blotting with an antibody raised against barley α-amylase. **A:** The α-amylase band at approximately 45 kDa is indicated. Red: Abscisic acid (ABA). Blue: Gibberellic acid (GA). **B:** Bar-plot of band intensities (analysed by ImageJ). Numbers indicate exact intensity values with the background intensity being 14.

Part III

Other results related to Article Manuscript #1

This part describes other work conducted in continuation of the results presented in Part II: Article Manuscript #1 (page 25).

III.1 Spectrophotometric redox activity assay

The redox activity assay presented in Part II (page 25) measures the concentration of ferrocyanide (FoC) by passing the fluid with the mediators over an electrode. The fluid enters the detection setup via an injection port with a sample loop of 50 μL, but injection of three times this volume is necessary to ensure the removal of washing fluid, air bubbles, and remnants from previous samples. With three measurements of each biological replicate, the sample volume needs to be at least 450 μL. Approximately 15 times fewer cells (Part IV, page 68) would be present in the new incubation system due to the use of aleurone layer punch-outs instead of whole aleurone layers, which would expectedly result in lower levels of FoC. The applicability and practicality of a spectrophotometric assay for quantification of FoC [138] using much smaller sample volumes was therefore investigated.

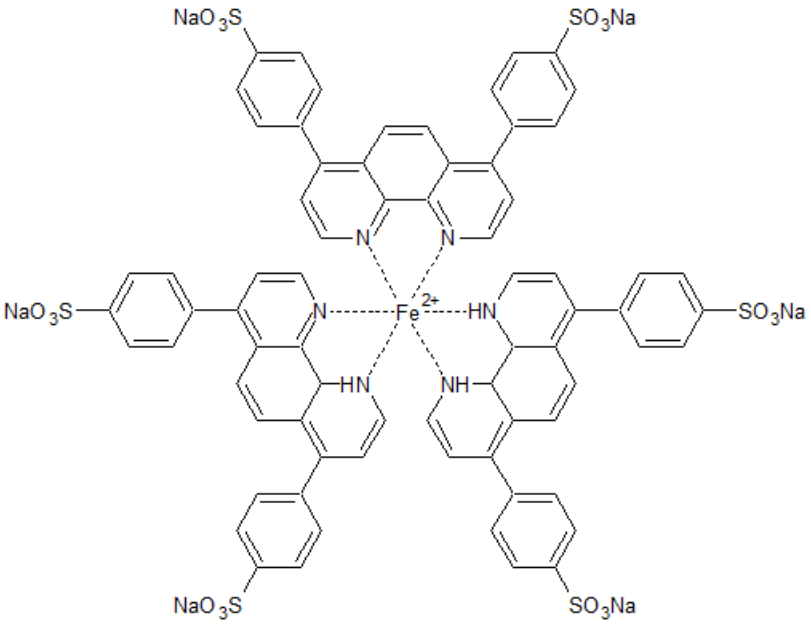

Figure III.1: Coloured complex of bathophenanthroline disulfonate and ferrous ion

Bathophenanthroline disulfonate (BPDS) forms the stable complex Fe^{2+}-$(BPDS)_3$ with the ferrous ion (Fe^{2+}) from ferrocyanide (FoC) but not with the ferric ion (Fe^{3+}) from ferricyanide (FiC). See Figure I.9 (page 14) for chemical structures of FiC and FoC.

With no previous experience with the assay, the first tests were performed with the traditional setup to enable comparison with the results obtained in Part II (page 25), i.e. incubations of aleurone layers with phytohormones and subsequently with redox mediators (M and FiC) were performed as previously described. The only difference was the use of the spectrophotometric assay for determination of FoC concentrations instead of the electrochemical detection setup. The assay measured the concentration of FoC through the formation of a coloured complex (Figure III.1) of the ferrous ion (Fe^{2+}) with the chelator bathophenanthroline disulfonate (BPDS) [138–141]. After incubation with the redox mediators, the incubation buffer with the mediators was mixed with the BPDS reaction mix, and the Fe^{2+}-$(BPDS)_3$ complex was allowed to form for a short period of time (5 min) before being subjected to spectrophotometry [138]. The concentration (c) of the complex was then determined by Lambert Beers law:

$$c = \frac{A_{sample} - A_{background}}{\epsilon \cdot l} \cdot D$$

using the difference in absorbance between the sample and the background ($A_{sample} - A_{background}$), the molar extinction coefficient of BPDS ($\epsilon = 20.500$ M^{-1} cm^{-1} [138, 141]), the length of the spectrophotometer cuvette ($l = 1$ cm), and the dilution factor (D). The assay required 100 μL diluted sample per measurement [138] and hence a total sample volume of 300 μL for triplicate measurements of all samples if no dilution was necessary. Surprisingly, a dilution factor D of 20 was necessary, lowering the required volume to just $5 \cdot 3 = 15$ μL, corresponding to 30 times less than the previously required 450 μL. Unfortunately, this low required sample volume seemed to be the only improvement to the practical side of determining the FoC concentration. The assay proved very time-consuming due to the pipetting involved in extracting triplicate volumes from each sample for dilution and subsequent transfer to individual cuvettes and finally addition of the BPDS reaction mix. In addition to this, triplicate volumes also had to be extracted (again by pipetting) from all samples prior to the addition of the redox mediators, as these volumes would act as background absorbance measurements that would be subtracted from the actual sample absorbance measurements, resulting in a duplication of the measurements to be performed. Finally, the assay was also highly resource-consuming due to the use of individual cuvettes for every measurement.

As for the results obtained with the spectrophotometric assay, reproducibility was an issue as identically treated samples rarely yielded similar results (Figure III.2A,B), resulting in high standard deviations when averaging experiments (Figure III.2C). This was possibly an effect of the very high dilution factor required. The effect of DPI on the reducing capacity was also tested with the spectrophotometrical assays, again with disappointingly high standard deviations (Figure III.3). A comparison of the coefficients of variation, i.e. the standard deviations normalised by the reducing capacity, for the electrochemical and spectrophotometrical assays showed higher coefficients of variation for the spectrophotometrical assay in most cases (Table III.1). This was a result of both lower levels of reducing capacity and higher standard deviations for the spec-

trophotometrical assay (Figures III.2C and III.2) compared to the electrochemical assay (Figures II.6, page 37, and II.7, page 38).
Despite the spectrophotometrical assay yielding high coefficients of variation for all treatments, the general tendencies remained the same when comparing with the electrochemical assay:

- GA-treated aleurone layers exhibited higher reducing capacity than ABA-treated aleurone layers.
- Only negligible reducing capacities were detected from the spent and centrifuged incubation buffer.
- Most of the reducing capacity for GA-treated aleurone layers was aleurone layer dependent (Figure III.2C (X compared to Y)).
- The remaining part of the reducing capacity for GA-treated aleurone layers was concluded to originate from cell debris (Figure III.2C (X compared to Y)).
- A large part of the reducing capacity was M-dependent and hence most likely intracellular (Figure III.2C (M+FiC compared to FiC)).
- The remaining part of the reducing capacity was M-independent and therefore extracellular, since FiC was unable to pass the plasma membrane (Figure III.2C (M+FiC compared to FiC)).
- DPI decreased the aleurone layer-dependent reducing capacity of GA-treated aleurone layers to the level of ABA-treated samples whether both redox mediators or only FiC were used (Figure III.3).
- DPI slightly decreased the amount of FiC reduction in ABA-treated aleurone layers (not significantly), suggesting that ABA-treated aleurone layers exhibit some NADPH oxidase activity (Figure III.3 (FiC)).

However, some discrepancies were discovered for the spectrophotometrical assay, as the aleurone layer-dependent part of the reducing capacity for GA-treated aleurone layers had dropped from the previous 73% to 59% (Figure III.2C (X,Y, GA, M+FiC)), while a sudden difference in reducing capacity for ABA-treated aleurone layers could be discerned (Figure III.2C (X,Y, ABA, M+FiC)), which had not been the case with the electrochemical assay. Similarly, the intracellular, M-dependent part of the reducing capacity had dropped from 69% to 58% for GA-treated aleurone layers and from 67% to 30% for ABA-treated aleurone layers (Figure III.2C (Y)). A in difference in the extracellular reducing capacity (FiC only) could no longer be discerned for neither GA- nor ABA-treated aleurone layers (Figure III.2C (X,Y, FiC)), which had been possible with the electrochemical assay (Figure II.6, page 37). Lastly, an increase was observed for ABA+DPI-treated aleurone layers compared to ABA-treated aleurone layers (Figure III.3), which had not

been observed with the electrochemical assay (Figure II.6, page 37). As this increase contradicts both previously obtained results and logic (inhibition of NADPH oxidase should result in a decrease in the reducing capacity), it was most probably caused by errors in the incubation or assay procedures. This would of course have to be confirmed by a repetition of the experiment.
Although the spectrophotometrical assay was indeed applicable to the biological system, the electrochemical assay was concluded to be a more precise method for detection of changes in the reducing capacity due to the high standard deviations obtained with the spectrophotometrical

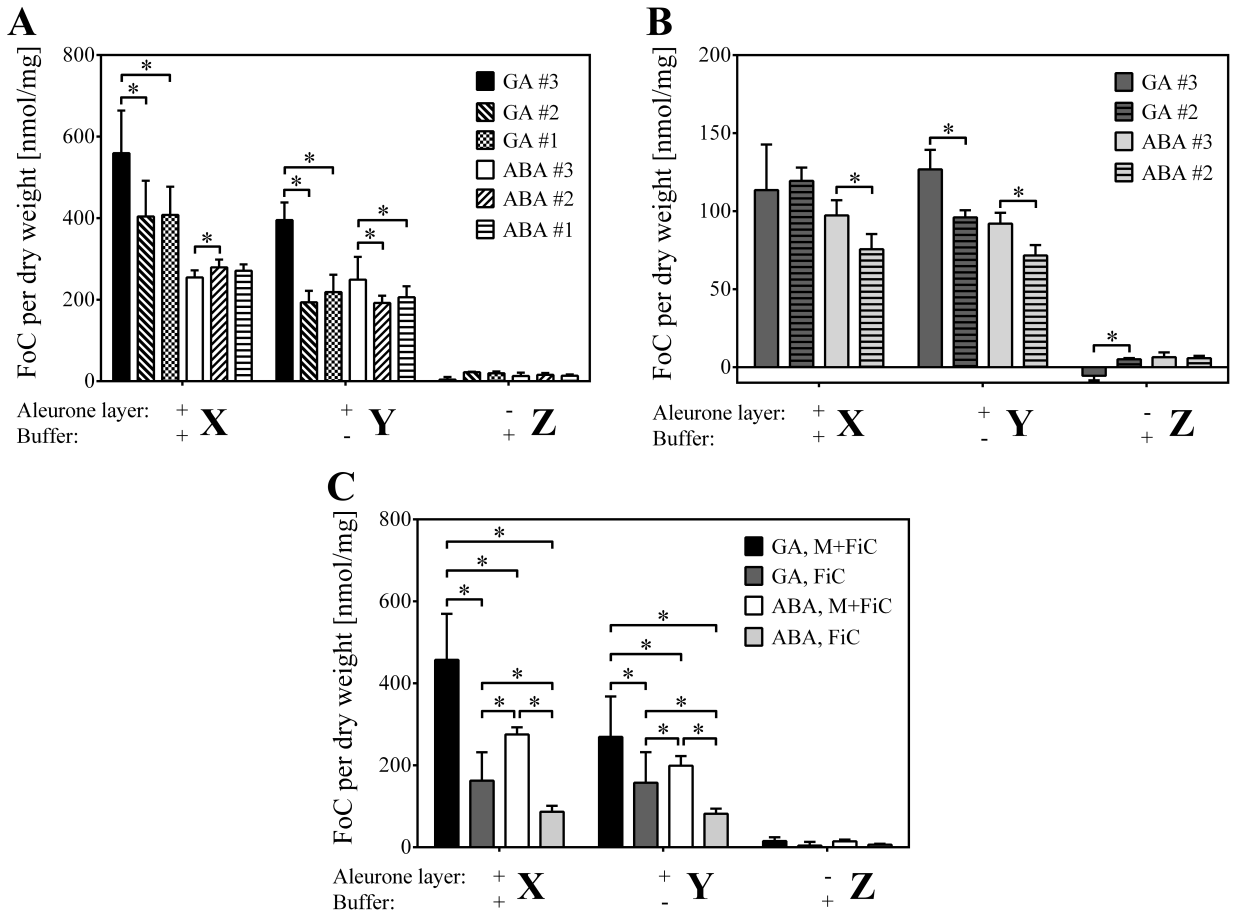

Figure III.2: Reducing capacity measured with the spectrophotometric ferrocyanide assay

Aleurone layers were incubated for 48 h before 1 h incubation with either both redox mediators (A: M+FiC) or FiC only (B). **A,B:** Individual values of up to 3 identical experiments. **C:** Average values of up to 3 identical experiments. A-C: Two batches of aleurone layers were used for each experimental condition, and one batch was subjected to incubation with redox mediators immediately after phytohormone incubation (X). The second batch was split in two (aleurone layers transferred to clean incubation buffer (Y) and spent, centrifuged incubation buffer (Z)) and subjected separately to incubations with redox mediators. Error bars represent SD (A,B: n=9. C: n=27), and asterisks indicate significant differences between indicated treatments ($p<0.05$). GA: Gibberellic acid. ABA: Abscisic acid. DPI: Diphenyleneiodonium chloride. M: Menadione. FiC: Ferricyanide. FoC: Ferrocyanide.

assay. In addition to the high standard deviations, the only practical advantage of the spectrophotometrical assay compared to the electrochemical assay, both with the traditional incubation setup, were the decreased required sample volumes. Enabling the use of the spectrophotometrical assay with the developed incubation system would first of all require decreased sample volumes to correct for the lower amount of aleurone cells present in the immobilised punch-outs. However, the volume of the mediator mix into which the lid with the immobilised punch-outs would be lowered would still have to be large enough to ensure that all cells were exposed to the mix, and thereby contributing to the measurements, and to ensure that no cells were allowed to dry, as this could result in increased cell viability affecting the reducing capacity. Lower sample volumes might also allow for direct addition of the BPDS reaction mix to the multiplate in which the redox activity assay had been performed, which would allow for easier spectrophotometrical measurements through the use of a multiplate spectrophotometer. This would also decrease the amount of pipetting and cuvettes necessary, resulting in a less time- and resource-consuming assay. As time became a limiting factor for this project, testing of such a setup with the developed incubation system was not possible.

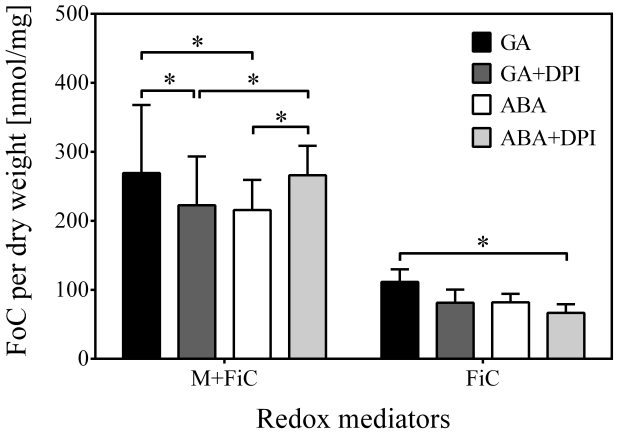

Figure III.3: Effect of DPI on reducing capacity measured with the spectrophotometric ferrocyanide assay

Aleurone cells were incubated for 48 h before being transferred to clean incubation buffer and subjected to 1 h incubation with either both redox mediators (M+FiC) or FiC only. Error bars represent SD (n=27), and asterisks indicate significant differences between indicated treatments ($p<0.05$). GA: Gibberellic acid. ABA: Abscisic acid. M: Menadione. FiC: Ferricyanide. FoC: Ferrocyanide. DPI: Diphenyleneiodonium chloride.

Table III.1: Comparison of two assays for measuring reducing capacity

Mediators	Treatment	Conditions		Electrochemical assay			Spectrophotometrical assay		
		Aleurone layer	Buffer	Reducing activity [nmol mg^{-1}]	Standard deviation [nmol mg^{-1}]	Coefficient of variation [%]	Reducing activity [nmol mg^{-1}]	Standard deviation [nmol mg^{-1}]	Coefficient of variation [%]
M+FiC	GA	+	+	675	122	18	457	112	**25**
		+	−	494	63	13	269	99	**37**
		−	+	19	1	8	15	9	**60**
	ABA	+	+	273	32	12	**275**	17	6
		+	−	274	46	17	269	23	12
		−	+	16	1	9	15	4	**27**
	GA+DPI	+	+	643	43	7	276	91	**33**
		+	-	334	22	7	223	71	**32**
		−	+				74	64	87
	ABA+DPI	+	+	379	24	6	278	83	**36**
		+	−	258	22	8	**266**	43	**16**
		−	+				41	33	80
FiC	GA	+	+	216	51	24	162	69	**43**
		+	−	155	15	10	**157**	75	**47**
		−	+	15	2	12	4	9	**222**
	ABA	+	+	101	11	12	86	15	**16**
		+	−	93	11	12	82	12	**15**
		−	+	14	1	9	6	2	**39**
	GA+DPI	+	+	120	9	8	84	13	**15**
		+	−	84	11	13	81	19	**23**
		−	+				5	9	208
	ABA+DPI	+	+	88	5	6	63	14	**22**
		+	−	55	9	16	**67**	13	**19**
		−	+				1	8	744

Coefficient of variation: Standard deviation normalised by reducing capacity. All values are rounded to the nearest whole number. Higher values of both reducing capacity and coefficient of variation for the spectrophotometrical assay are marked in bold. +: Present during incubation with redox mediator(s). −: Not present during incubation with redox mediator(s). See Figure IV.3 for details; ++ corresponds to X, +− to Y, and −+ to Z.

III.2 Proteomics analysis of protein abundance levels

The NADPH oxidase-inhibitor DPI had been shown to lower the increased reducing capacity induced by GA in parallel to increasing the level of cell death induced by GA (Part II, Figure II.7, page 38). However, DPI is not specific to NADPH oxidase but is a general flavoenzyme inhibitor and might therefore affect other flavoenzymes as well, although a low concentration of DPI had been used to minimise the risk of this. As a sidetrack to the main project, mass spectrometry (MS)-based proteomics using tandem mass tags (TMTs) was therefore applied to investigate the effect of the DPI on the protein abundance profiles of barley aleurone layer extracts. The effect of DPI on the extracellular fraction (i.e. proteins secreted into the incubation buffer) was not investigated due to time constraints.
A total of 452 peptides were identified by MS-based proteomics, of which 114 peptides were unique, leading to the identification and relative quantification of 67 proteins. Table III.3 (page 55) lists the findings with blank spaces, where lack or errors of identifications of the relevant TMT-reagent resulted in incalculable levels of the protein in question. 67 identified proteins was an unexpectedly low amount, corresponding to about one fourth of the expected amount (Christine Finnie, personal communication). This low amount was most likely caused by the sample preparations, as the usual equipment used for drying the samples were out of order (Appendix B.13, page 118). Instead, samples were air-dried which could have resulted in the samples becoming too dry or in inadequate evaporation of urea, both factors that could result in only partial resuspension of the samples. A repetition of the experiment was therefore necessary to obtain a full analysis of the effect of DPI on the protein abundance profiles of barley aleurone layers, but as time became a limiting factor for this project, such a repetition was not a possibility.
Due to the incomplete results of the proteomics experiment, the following is not an extensive and in-depth analysis of the existing data, but merely a short overview of the effect of DPI on the up- and downregulation of certain proteins.

Of the 67 identified proteins, only the abundance levels of 12 proteins were up- or downregulated by at least 2-fold ($\pm$ 10%) for at least one treatment compared to abundance levels for GA- or ABA-treatment (Table III.3, page 55, and Figure III.4). Two of these were the α-amylase isozymes A and B that were both highly upregulated for GA compared to ABA (4.2- and 2.3-fold, respectively), confirming the basic biological response of the aleurone layers to these phytohormones and the assumption of an error in the MS-preparations rather than in the aleurone layer incubations. The abundance of both isozymes were slightly reduced for GA+DPI compared to GA (0.7- and 0.6-fold, respectively) but still expressed at a higher level compared to ABA (2.8- and 1.4-fold, respectively), while ABA+DPI yielded levels of the isozymes very close to those for ABA (1.2- and 0.8-fold changes, respectively). The decreased GA-induced reducing capacity observed in the presence of DPI (Part II, Figure II.7A, page 38) thereby also affects the production of α-amylase.

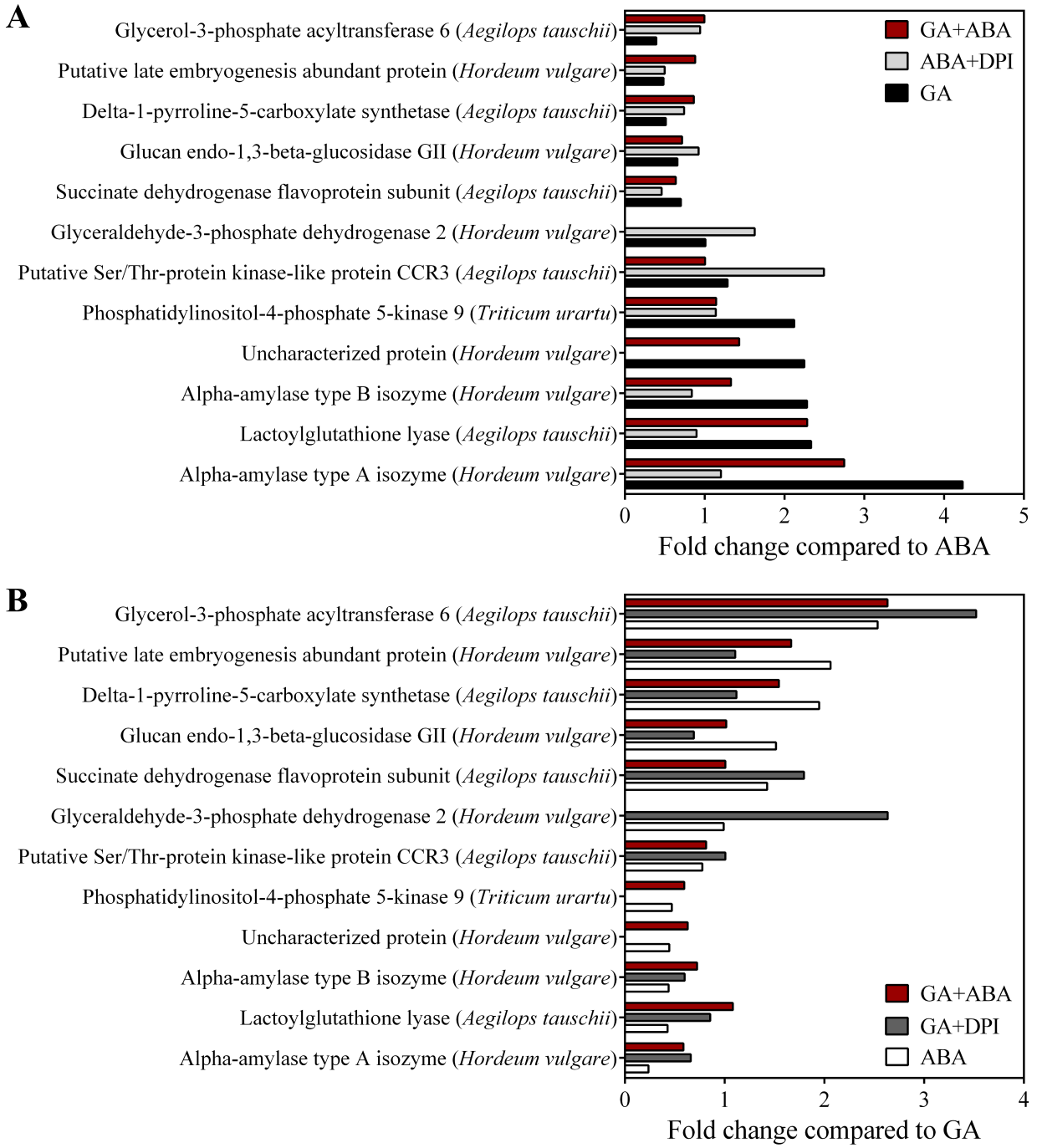

Figure III.4: Protein abundance profiles obtained by LC-MS-proteomics analysis

Five aleurone layers per well were incubated for 48 h with GA, GA+DPI, ABA, ABA+DPI, or GA+ABA before extraction of total protein content. Protein extracts were labelled with TMT reagents to allow relative quantification of identified proteins. Abundance levels are compared to levels induced by ABA (**A**) or GA (**B**). Protein names and functions are from UniProt and EnsemblPlants. *Aegilops tauschii*: Goatgrass, progenitor of wheat. *Hordeum vulgare*: Barley. *Triticum urartu*: Wild einkorn, progenitor of wheat. ABA: Abscisic acid. GA: Gibberellic acid. DPI: Diphenyleneiodonium chloride.

Another highly upregulated protein in the presence of GA compared to ABA was a homologue of the *Aegilops tauschii* lactoylglutathione lyase (2.3-fold), which detoxifies methylglyoxal, a by-product of glycolysis [142]. An increased abundance level of this enzyme corresponds with metabolism and hence also glycolysis being increased by GA but not ABA. DPI did not have a significant effect on the abundance level of lactoylglutathione lyase, neither in the presence of GA (0.9-fold change compared to GA only) nor ABA (0.9-fold change compared to ABA only), again hinting to the significance of this protein in ensuring cell survival.
A homologue of the *Triticum urartu* phosphatidylinositol-4-phosphate 5-kinase 9, was upregulated in the presence of GA (2.1-fold compared to ABA), while the effect of GA+DPI on the abundance of phosphatidylinositol-4-phosphate 5-kinase 9 homologue was undetectable. In *Arabidopsis thaliana*, phosphatidylinositol-4-phosphate 5-kinase 9 (*PIP5K9*) negatively regulates root cell elongation [143], and a similar role in prevention of germination might be envisioned in barley. A homologue of the *Aegilops tauschii* putative, mitochondrial Ser/Thr-protein kinase-like protein CCR3, was upregulated in the presence of ABA+DPI (2.5-fold compared to ABA), but treatment with GA+DPI did not increase the abundance of the Ser/Thr-protein kinase-like protein homologue compared to GA. Being only putative, not much is known about the Ser/Thr-protein kinase-like protein homologue, and the importance of its upregulation in the presence of ABA+DPI compared to ABA can therefore not be determined.
Possibly the most exciting result of the proteomics experiment was the upregulation of the oxidoreductase glyceraldehyde-3-phosphate dehydrogenase 2 (GAPDH2) in the presence of GA+DPI (2.6-fold) and ABA+DPI (1.6-fold) compared to GA and ABA, respectively, while no difference in abundance levels was detected between GA and ABA alone. DPI probably did not induce increased abundance levels of this enzyme directly. More likely, DPI affected the redox status of the aleurone cells through its inhibitory effect on NADPH oxidase and possibly also other flavoenzymes, leading to reduced levels of $NADP^+$ and NAD^+ (Part II, Figure II.1A, page 28), the last of which is essential to the action of GAPDH2 [143]. The activity of the enzyme may thereby have been lowered indirectly by DPI, which could have prompted the cells to increase abundance levels in an attempt to maintain their carbohydrate metabolism. Should a repetition of the proteomics experiment confirm the upregulation of GAPDH2 in the presence of DPI, this enzyme would be an obvious candidate for further studies of the effect of DPI in ROS signalling and PCD.
Interestingly, glyceraldehyde-3-phosphate dehydrogenase 1 (GAPDH1), a paralogue of GAPDH2, was not upregulated in the presence of GA+DPI compared to GA (1.1-fold change, Table III.3, page 55). Sequence alignment shows that GAPDH1 and both splice variants of GAPDH2 are highly similar and that the active site is preserved (Figure III.5) [143]. Both enzymes are expected to be located in the cytoplasm [143, 144], but a TargetP analysis shows increased probability for a mitochondrial location for GAPDH1 compared to both splice variants of GAPDH2, though a mitochondrial location is still less probable than a cytoplasmic location (Table III.2) [145]. Only minute amounts of DPI should diffuse into the mitochondria with the low concentration of DPI

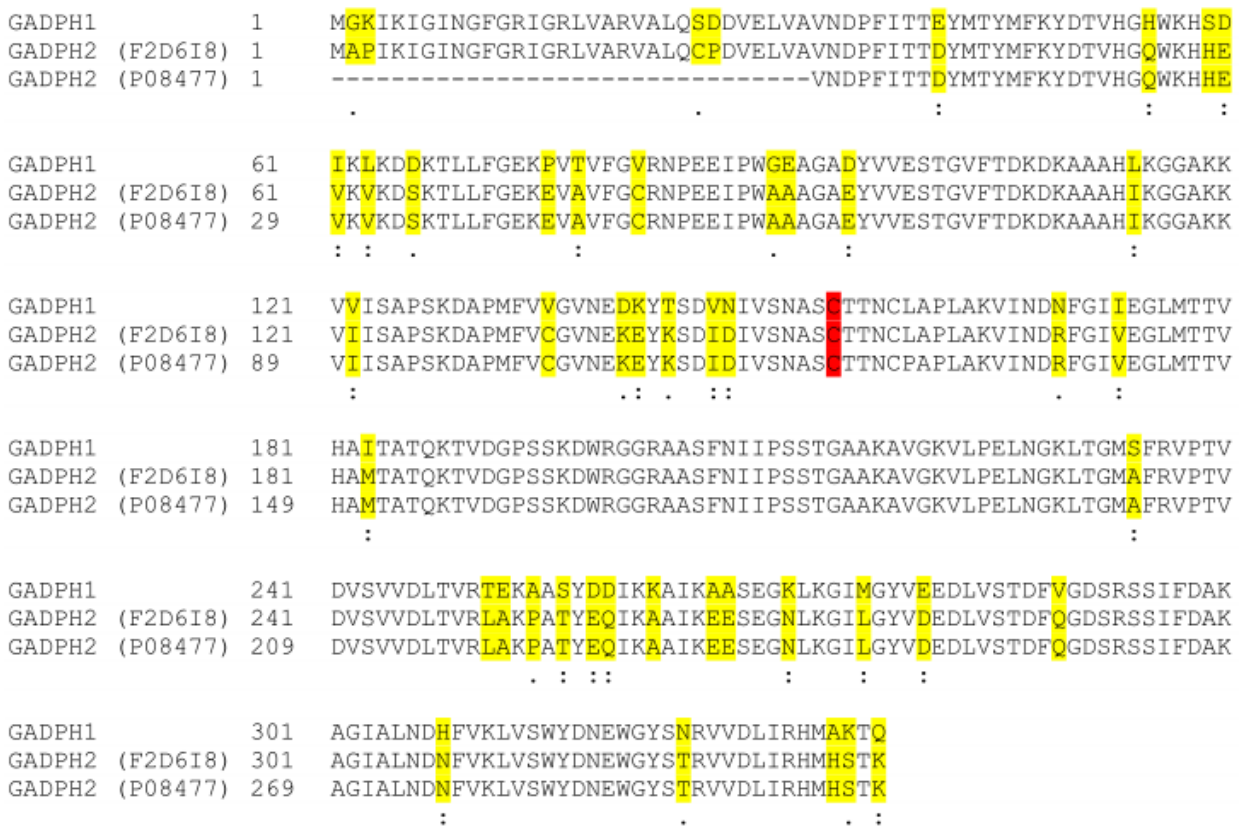

Figure III.5: Sequence alignment of glyceraldehyde-3-phosphate dehydrogenase 1 and 2

Sequence alignment and active site (marked in red) identification performed with UniProt Align [143]. Non-identical residues are marked in yellow. ':' indicates strongly similar properties, while '.' indicates weakly similar properties. UniProt accession numbers for GAPDH2 splice variants are listed in parentheses. GADPH1: Glyceraldehyde-3-phosphate dehydrogenase 1. GADPH2: Glyceraldehyde-3-phosphate dehydrogenase 2.

present in the extracellular environment during the experiment, and a mitochondrial location of GAPDH1 could therefore explain the observed non-existent effect of DPI on this enzyme. As the enzymes are highly similar, further investigations are needed to determine if this is the case, and if not, how and why DPI affects only GAPDH2 and not GAPDH1.

Another oxidoreductase, a homologue of the *Aegilops tauschii* succinate dehydrogenase flavoprotein subunit, was also upregulated in the presence of GA+DPI compared to GA (1.8-fold), while the abundance in the presence of ABA+DPI was downregulated compared to ABA (0.5-fold). The increased abundance of the succinate dehydrogenase flavoprotein subunit observed in the presence of GA+DPI compared to GA could be a direct consequence of the flavoenzyme-inhibitory effects of DPI, resulting in decreased activity of the subunit, to which the cells responded by increasing abundance levels. Another possibility was that reduced throughput of glycolysis caused by lower activity of GAPDH2 (as mentioned above) would result in reduced

throughput of the tricarboxylic acid cycle, which would severely affect the energy levels and carbohydrate metabolism of the cells. Upregulation of abundance levels of the succinate dehydrogenase flavoprotein subunit may therefore have been an attempt to counter both these effects in the presence of GA+DPI, but would not explain the downregulation observed in the presence of ABA+DPI.

A third oxidoreductase, a homologue of the *Aegilops tauschii* delta-1-pyrroline-5-carboxylate synthetase, was downregulated in all treatments compared to ABA with no significant difference induced by GA+DPI compared to GA (1.1-fold change). This enzymes is a key factor in osmoregulation and in the synthesis of the amino acid proline [143] and has been shown to induce osmotolerance under drought stress [146]. The downregulation of delta-1-pyrroline-5-carboxylate synthetase compared to the dormant state of the aleurone layers is thereby in agreement with its protective role in the desiccated (dormant) state. Furthermore, the enzyme utilises NAD^+ like GADPH2, which could again explain the downregulation of the enzyme in the presence of ABA+DPI compared ABA (0.7-fold), as mentioned above.

In general, an effect of DPI on oxidoreductive enzymes was expected due to its effect on the reducing capacity, and one possibility was the induction of the oxidative effect of dehydrogenases, but the effects observed here are unfortunately somewhat inconsistent.

Another hydrolase, glucan endo-1,3-beta-glucosidase GII, which degrades fungal cell wall polysaccharides as part of the defence against pathogen attacks [143], was slightly decreased for GA+DPI compared to GA (0.7-fold) and significantly decreased compared to ABA (0.5-fold), while ABA+DPI again did not induce a change compared to ABA (0.9-fold change). Similarly, a homologue of the glycerol-3-phosphate acyltransferase 6 was severely downregulated in the presence of GA compared to ABA (0.4-fold change). GA+DPI resulted in a high upregulation compared to GA (3.5-fold), whereas no effect was seen from ABA+DPI compared to ABA (0.9-fold change). The transferase is involved synthesis of the lipid cutin, which covers the cell walls of cells exposed to air and protects against water loss and pathogen attacks [147]. Treatment

Table III.2: TargetP analysis of glyceraldehyde-3-phosphate dehydrogenase 1 and 2

Enzyme	Prediction scores			Predicted	Reliability
	Mitochondria	Secretory pathway	Other location	location	class
GAPDH1	0.335	0.250	0.391	A	5
GAPDH2 (F2D6I8)	0.292	0.295	0.381	A	5
GAPDH2 (P08477)	0.085	0.162	0.921	A	2

Prediction scores: Final scores on which the final prediction of location is based. Scores are not probabilities, but the location with the highest score is the most likely according to TargetP, and the relationship between the scores (the reliability class) may be an indication of how certain the prediction is. A: Any other location than mitochondria or secretory pathway. Reliability class: Ranges from 1 to 5, where 1 indicates the strongest prediction. Reliability class is a measure of the size of the difference between the highest and the second highest prediction scores. UniProt accession numbers for GAPDH2 splice variants are listed in parentheses. Text adapted from [145].

with GA thereby seems to reduce the ability to the aleurone layers to combat pathogen attacks. The NADPH oxidase is also part of the cellular protection against pathogen attack through its involvement in the oxidative burst [46], and the acyltransferase may therefore be upregulated in the presence of GA+DPI to compensate for the inhibited NADPH oxidase.
A putative late embryogenesis abundant protein was upregulated in the presence of ABA compared to GA (2.1-fold change), which was to be expected as ABA is known to induce this protein to maintain dormancy and protect living cells against desiccation [99, 148]. This upregulation was, however, cancelled by the presence of ABA+DPI (0.5-fold change compared to ABA), similar to the effects of treatment with GA or GA+DPI (both 0.5-fold changes compared to ABA). DPI thereby has no effect in the presence of GA, but severely lowers the abundance level of this dormancy-maintaining protein in the presence of ABA. Finally, an uncharacterised protein was the fourth most upregulated protein in the presence of GA compared to ABA (2.3-fold change), whereas changes induced by DPI were not detectable.

All experimental procedures were performed by Birgit Andersen[5] and Christine Finnie[5] on aleurone layers that had been frozen in liquid nitrogen and stored at $-80°C$ immediately after 48 h incubation. Procedures for preparation of aleurone layers for MS can be found in Appendix B.13, page 115, while documents concerning the setup up for the LC-MS-analysis and the full data sets can be found on the enclosed data disc (Appendix C, page 119). MultiNotch MS3 was used for analysis of the TMT-tagged samples [149].

[5] Agricultural and Environmental Proteomics, Department of Systems Biology, Technical University of Denmark

Table III.3: Protein identifications and relative abundance levels

Accession number[a]	Organism	Protein[c]	Function	Sequence coverage[b]	No. of peptides		Protein abundance levels Compared to ABA				Compared to GA		
					Unique	Total	GA	GA+ DPI	GA+ ABA	ABA+ DPI	GA+ DPI	GA+ ABA	ABA
MLOC_19148.1 (M0V697) (R7VZ99*)	*Aegilops tauschii**	**Glycerol-3-phosphate acyltransferase 6***	Acyltransferase	3.91	1	2	0.395	1.390	0.996	0.943	3.522	2.634	2.535
AK358709 (M0Y3K8, F2D4A0) (B6TWM4*)	*Zea mays**	JD1*	Acyltransferase	37.01	1	7			1.032				
MLOC_67202.1 (F2DVB3) (C0P4F3*)	*Zea mays**	DAG protein isoform 1*	Aromatic amino acid family biosynthetic process	36.40	1	3							
AK376513 (F2EK36) (P11955)*	*Hordeum vulgare**	26 kDa endochitinase 1*	Chitinase, defence response	28.84	3	9	0.743	0.649	0.816	0.911	0.874	1.115	1.347
MLOC_6801.1 (P23951, M0YD01)	*Hordeum vulgare*	26 kDa endochitinase 2	Chitinase, defence response	33.46	2	5	0.700	0.605	0.710	0.820	0.863	1.103	1.428
AK362464 (F2DEZ7) (M8BES6*)	*Aegilops tauschii**	Disease resistance protein RPM1*	Defence response	14.10	1	12	1.396	1.483	1.347	1.214	1.062	1.067	0.716
MLOC_76783.1 (M0Z4D8) (Q84KC7*)	*Hordeum vulgare**	NBS-LRR disease resistance protein homologue*	Defence response	15.30	1	8							
AK369971 (M0UFF8, F2E1F0)	*Hordeum vulgare*	Uncharacterised protein	Defence response	17.65	1	10						0.800	
MLOC_11707.1 (M0UK71) (F6M1S0*)	*Triticum aestivum**	5-methylcytosine DNA glycosylase*	Endonuclease, DNA repair	10.12	1	12							
AK362498 (F2DF31)	*Hordeum vulgare*	Uncharacterised protein	GTPase	8.43	1	6							
MLOC_76265.1 (M0Z371) (D0EX74*)	*Oryza sativa* subsp. *japonica**	DEAD/DEAH box helicase domain-containing protein PIE1*	Helicase	7.69	1	7							

Table continued on next page

Table III.3 – continued from previous page

Accession number[a]	Organism	Protein[c]	Function	Sequence coverage[b]	No. of peptides		Protein abundance levels Compared to ABA				Compared to GA		
					Unique	Total	GA	GA+ DPI	GA+ ABA	ABA+ DPI	GA+ DPI	GA+ ABA	ABA
MLOC_71318.1 (M0YP02) (M8BM42*)	*Aegilops tauschii**	Putative SWI/SNF-related matrix-associated actin-dependent regulator of chromatin subfamily A member 3-like protein 3*	Helicase, DNA repair	19.14	1	9	1.187	1.023	0.815	1.038	0.863	0.760	0.843
MLOC_55142.1 (P00693, C3W8M8)	*Hordeum vulgare*	**Alpha-amylase type A isozyme**	Hydrolase	29.68	3	10	4.233	2.793	2.748	1.203	0.660	0.587	0.236
AK372405 (C3W8N0) (P04063*)	*Hordeum vulgare**	**Alpha-amylase type B isozyme***	Hydrolase	17.80	3	7	2.284	1.368	1.330	0.839	0.599	0.724	0.438
AK368873 (M0Y0Q4, F2DYA5) (Q53MQ1*)	*Oryza sativa* subsp. *japonica**	Beta-D-xylosidase*	Hydrolase	10.63	1	3	0.635		0.660	1.012		1.027	1.574
MLOC_73077.1 (P15737, M0YUE3)	*Hordeum vulgare*	**Glucan endo-1,3-beta-glucosidase GII**	Hydrolase, defence response	34.02	3	7	0.660	0.456	0.717	0.925	0.692	1.017	1.515
AK365205 (F2DMT7, M0UE88) (Q7X9R7*)	*Hordeum vulgare**	Putative cyclic nucleotide and calmodulin-regulated ion channel protein*	Ion transmembrane transport	8.54	1	5							
MLOC_63120.1 (M0XUD7) (M7ZJ33*)	*Triticum urartu**	Solute carrier family 12 member 6*	Ion transmembrane transport	11.24	1	2	1.040	1.238	0.788	1.000	1.191	0.749	0.962
MLOC_351.5 (P80284, F2D284)	*Hordeum vulgare*	Protein disulfide-isomerase	Isomerase, electron carrier, cell redox homeostasis	12.28	1	5							
MLOC_78807.1 (M0Z870)	*Hordeum vulgare*	DNA ligase	Ligase, DNA repair	27.00	1	13	0.970	1.412	1.418	1.348	1.457	1.618	1.031
MLOC_63401.3 (M0XVE2) (N1R068*)	*Aegilops tauschii**	Putative E3 ubiquitin-protein ligase HERC2*	Ligase	17.66	1	12							

Table continued on next page

Table III.3 – continued from previous page

Accession number[a]	Organism	Protein[c]	Function	Sequence coverage[b]	No. of peptides		Protein abundance levels Compared to ABA				Compared to GA		
					Unique	Total	GA	GA+ DPI	GA+ ABA	ABA+ DPI	GA+ DPI	GA+ ABA	ABA
AK356020 (M0WH63, F2CWL7)	*Hordeum vulgare*	Oleosin	Lipid particle membrane component	37.50	2	4	0.995	1.246	0.975	1.035	1.253	1.011	1.005
MLOC_73299.1 (F2CXT7)	*Hordeum vulgare*	Fructose-bisphosphate aldolase	Lyase, glycolysis	23.46	5	7	1.100	1.625	1.201	1.158	1.477	1.086	0.909
MLOC_3462.1 (M0VN24)	*Hordeum vulgare*	Isocitrate lyase	Lyase	4.56	1	2	1.541	1.805	1.155	0.714	1.171	0.786	0.649
MLOC_12359.2 (F2CQP8) (M8B1Z5*)	*Aegilops tauschii**	**Lactoylglutathione lyase***	Lyase	21.99	1	6	2.335	1.997	2.286	0.898	0.855	1.083	0.428
MLOC_56464.2 (M0X2B4) (M8AEI6*)	*Triticum urartu**	**Phosphatidylinositol-4-phosphate 5-kinase 9***	Kinase	7.64	1	5	2.123		1.144	1.139		0.596	0.471
MLOC_64769.1 (M0Y0W8) (R7WF87*)	*Aegilops tauschii**	**Putative Ser/Thr-protein kinase-like protein CCR3, mitochondrial***	Kinase	11.66	1	3	1.287	1.297	1.005	2.494	1.008	0.815	0.777
MLOC_53068.9 (M0WMX9) (M7ZBB6*)	*Triticum urartu**	Receptor-like Ser/Thr-protein kinase ALE2*	Kinase	12.13	1	4				0.625			
MLOC_55033.1 (M0WVM9) (M8CV18*)	*Aegilops tauschii**	Armadillo repeat-containing kinesin-like protein 2*	Microtubule-based movement	14.51	1	8	0.801	0.911	0.751	1.550	1.138	0.938	1.248
MLOC_61996.2 (M0XPX6) (Q93XF2*)	*Zea mays**	Kinesin heavy chain*	Microtubule-based movement	8.44	1	7	0.823						1.216
MLOC_46003.1 (P06470, M0WA02)	*Hordeum vulgare*	B1-hordein	Nutrient reservoir activity	15.94	1	2	0.854	0.635	0.895	0.956	0.744	0.996	1.170
MLOC_59994.1 (M0XH58) (Q03678*)	*Hordeum vulgare**	Embryo globulin*	Nutrient reservoir activity	35.84	7	14	0.846	0.963	0.809	1.531	1.137	0.972	1.182
MLOC_63227.1 (M0XUU4) (M7ZQM3*)	*Triticum urartu**	Globulin-1 S allele*	Nutrient reservoir activity	36.41	7	15	0.855	0.883	0.939	1.049	1.032	1.097	1.169

Table continued on next page

Table III.3 – continued from previous page

Accession number[a]	Organism	Protein[c]	Function	Sequence coverage[b]	No. of peptides		Protein abundance levels Compared to ABA				Compared to GA		
					Unique	Total	GA	GA+ DPI	GA+ ABA	ABA+ DPI	GA+ DPI	GA+ ABA	ABA
MLOC_10176.1 (P06293, M0UEE6)	*Hordeum vulgare*	Serpin-Z4	Nutrient reservoir activity, defence response	25.50	3	9	1.080	0.770	1.291	1.037	0.713	1.050	0.926
AK373549 (F2EBM4)	*Hordeum vulgare*	Uncharacterised protein	Nutrient reservoir activity	17.73	6	9	1.008	1.023	1.133	0.914	1.014	1.020	0.992
MLOC_57363.1 (F2CYL7) (M8C814*)	*Aegilops tauschii**	Vicilin-like antimicrobial peptides 2-2*	Nutrient reservoir activity	25.73	1	8	0.721	0.758	0.862	0.935	1.051	1.184	1.388
MLOC_37763.1 (M0VW03) (N1QZD4*)	*Aegilops tauschii**	**Delta-1-pyrroline-5-carboxylate synthetase***	Oxidoreductase, transferase	13.70	1	7	0.513	0.574	0.864	0.743	1.119	1.545	1.948
MLOC_65694.1 (P52572, M0Y4T3)	*Hordeum vulgare*	1-Cys peroxiredoxin PER1	Oxidoreductase, maintenance of seed dormancy	57.34	6	11	0.959	1.193	1.107	0.878	1.243	1.174	1.042
MLOC_18586.2 (F2CSK4) (M8C904*)	*Aegilops tauschii**	Glucose and ribitol dehydrogenase-like protein	Oxidoreductase	29.39	7	9	1.082	1.399	1.053	1.048	1.293	0.999	0.924
MLOC_18233.1 (P26517, F2CUE9)	*Hordeum vulgare*	Glyceraldehyde-3-phosphate dehydrogenase 1	Oxidoreductase, glycolysis	19.58	1	7	0.960	1.072	1.079	0.719	1.116	1.024	1.041
MLOC_72170.1 (P08477, F2D6I8)	*Hordeum vulgare*	**Glyceraldehyde-3-phosphate dehydrogenase 2**	Oxidoreductase, glycolysis	7.42	1	3	1.009	2.660		1.627	2.635		0.991
MLOC_63302.1 (F2EL27) (M8C1D6*)	*Aegilops tauschii**	**Succinate dehydrogenase (ubiquinone) flavoprotein subunit, mitochondrial***	Oxidoreductase, tricarboxylic acid cycle	12.12	1	4	0.701	1.257	0.638	0.460	1.795	1.008	1.427
MLOC_5179.2 (M0WIB7) (Q6UFY8*)	*Hordeum vulgare**	Caleosin 1*	Oil-body protein	25.58	1	6	1.157	1.103	1.025	1.288	0.954	0.877	0.865
MLOC_64926.1 (F2EAF7)	*Hordeum vulgare*	Uncharacterised protein	Phosphatase	30.73	1	7						1.300	
MLOC_10834.2 (M0UGW6) (Q7XUW5*)	*Oryza sativa* subsp. *japonica**	23.2 kDa heat shock protein*	Stress response	22.22	1	3							
AK376662 (F2EKI5) (M8AYS8*)	*Aegilops tauschii**	Heat shock cognate 70 kDa protein*	Stress response	20.91	2	12	1.052	1.001	1.023	1.116	0.952	0.958	0.950

Table continued on next page

Table III.3 – continued from previous page

Accession number[a]	Organism	Protein[c]	Function	Sequence coverage[b]	No. of peptides		Protein abundance levels Compared to ABA				Compared to GA		
					Unique	Total	GA	GA+ DPI	GA+ ABA	ABA+ DPI	GA+ DPI	GA+ ABA	ABA
MLOC_66541.2 (F2DYL9) (C5MKK0*)	*Pennisetum americanum**	Heat shock protein 17.9*	Stress response	29.81	2	5	0.604	1.005	0.703	0.808	1.662	1.116	1.654
AK355146 (F2CU44) (Q94KM0*)	*Triticum aestivum**	HSP17 (heat shock protein)*	Stress response	21.60	1	3							
MLOC_54721.2 (M0WU86) (M7Z406*)	*Triticum urartu**	Callose synthase 10*	Transferase	11.59	1	12							
MLOC_17477.1 (M0V2Z3) (M8BSC5*)	*Aegilops tauschii**	Cellulose synthase-like protein D4*	Transferase	12.58	1	8	0.771	0.798	0.637	0.914	1.035	1.495	1.297
MLOC_69019.1 (M0YG96) (N1QQI7*)	*Aegilops tauschii**	40S ribosomal protein S18*	Translational initiation	25.00	1	3	1.254	1.471	0.983	1.176	1.173	0.867	0.797
MLOC_64085.2 (M0XY03)	*Hordeum vulgare*	Cytoplasmic tRNA 2-thiolation protein 1	tRNA processing	23.68	1	7							
MLOC_62398.2 (F2E349) (M8AAJ6*)	*Triticum urartu**	Cullin-3A*	Ubiquitin-protein ligase binding	15.44	1	9							
AK375075 (M0Z4D1, F2EFZ8) (R7VZC9*)	*Aegilops tauschii**	Protein BREAST CANCER SUSCEPTIBILITY 1-like protein*	Ubiquitin-protein transferase, DNA repair	15.74	1	10							
MLOC_7183.1 (M0YQP0)	*Hordeum vulgare*	Coatomer subunit beta	Vesicle-mediated protein transport	13.26	1	6							
AK376810 (M0ZDL8, F2EKY2) (A9Q2Q5*)	*Hordeum vulgare*	**Putative late embryogenesis abundant protein***		6.96	1	4	0.485	0.536	0.881	0.499	1.106	1.667	2.062
MLOC_22521.1 (F2CUL7) (B6U3W6*)	*Zea mays**	Remorin*		29.14	1	6							
MLOC_58247.1 (M0X9Y8)	*Hordeum vulgare*	**Uncharacterised protein**		11.68	1	5	2.248		1.433			0.630	0.455
MLOC_58037.1 (M0X956)	*Hordeum vulgare*	Uncharacterised protein		8.02	1	3	1.788	1.642	1.499	1.525	0.918	0.829	0.559
MLOC_72722.1 (F2E8N5)	*Hordeum vulgare*	Uncharacterised protein		46.38	2	5	1.242	0.954	1.663	1.391	0.769	1.066	0.805

Table continued on next page

Table III.3 – continued from previous page

Accession number[a]	Organism	Protein[c]	Function	Sequence coverage[b]	No. of peptides		Protein abundance levels Compared to ABA				Compared to GA		
					Unique	Total	GA	GA+ DPI	GA+ ABA	ABA+ DPI	GA+ DPI	GA+ ABA	ABA
MLOC_71550.1 (M0YPT8)	*Hordeum vulgare*	Uncharacterised protein		26.09	1	3	1.023	1.282	1.199	1.236	1.253	1.013	0.977
AK371534 (M0V4P0, F2E5W0)	*Hordeum vulgare*	Uncharacterised protein		25.56	1	12							
AK355929 (M0X628, F2CWC6)	*Hordeum vulgare*	Uncharacterised protein		17.31	1	10							
AK360671 (M0WCY0, F2D9V8)	*Hordeum vulgare*	Uncharacterised protein		13.81	1	7							
AK252410.1	*Hordeum vulgare*			24.52	2	4	1.173	1.483	1.092	1.039	1.264	0.995	0.853
AK252796.1	*Hordeum vulgare*			8.60	1	4							

Identified proteins are sorted with regards to their function. Changes in abundance levels of at least 2-fold (± 10%) are marked with red for downregulation and blue for upregulation and affected proteins are marked in bold. Sum of peptides: 452. Sum of unique peptides: 114. Sum of proteins: 67. [a]EnsemblPlants [144], UniProt in parenthesis [143]. [b]Average of four replicates. * Result of UniProt blast [143].

Part IV

Article Manuscript #2

Easy immobilisation of living plant tissue, enabling higher throughput and parallelisation of assays: Time course analysis of programmed cell death in barley aleurone layers

Kinga Zór[1#], Christina Mark[2#], Arto Heiskanen[1], Claus Krogh Madsen[3], Martin Dufva[4], Jenny Emnéus[1], Henrik Brinch-Pedersen[3], and Christine Finnie[2*]

[1]Bioanalytics, Department of Micro- and Nanotechnology, Technical University of Denmark, 2800 Kgs. Lyngby, Denmark
[2]Agricultural and Environmental Proteomics, Department of Systems Biology, Technical University of Denmark, 2800 Kgs. Lyngby, Denmark
[3]Department of Molecular Biology and Genetics, Research Center Flakkebjerg, Aarhus University, 4200 Slagelse, Denmark
[4]Fluidic Array Systems and Technology, Department of Micro- and Nanotechnology, Technical University of Denmark, 2800 Kgs. Lyngby, Denmark

*Corresponding Author. E-mail: csf@bio.dtu.dk (CF)
#These authors contributed equally to this work.

Intended for submission to Plant Methods

IV.1 Abstract

Background

The barley aleurone layer is an established model system for studying phytohormone signalling, enzyme secretion and programmed cell death during seed germination. Most analyses performed on the aleurone layer are end-point assays based on cell extracts, which are limited by the fact that each analysis is performed on a different pool of samples, as each tissue sample or population of cells can only be analysed at a single time point. Time course experiments on the same tissue or population of cells can be enabled by the use of assays that do not destroy cellular integrity, which could also facilitate the performance of multiple assays.

Results

We present a method for immobilisation of barley aleurone layers on polydimethylsiloxane pillars in the lid of a multiwell plate, which enables monitoring of multiple parameters over time in the same tissue sample, without destroying cellular integrity. The system is amenable to transient gene expression analysis by particle bombardment, and allows individual transformed cells to be followed over time. Cell viability, intracellular reducing capacity and transient expression profiles of α-amylase and phytase were monitored in parallel in the immobilised tissue, under multiple incubation conditions.

Conclusions

The cell death profile was slower for immobilised tissues than in free aleurone layers, probably due to mass transfer, however the same trends were observed. A clear effect could be observed on both the rate of cell death and reducing capacity of living cells by compounds inducing protein unfolding (T), increased (SNP) or decreased (cPTIO) NO levels. The system enabled single transformed cells to be followed over time in parallel with cell viability determinations, and provided an insight into the cell-to-cell variability of the actual transformation event.

The experimental setup developed here enabled simple, user-friendly handling of plant tissue incubations and has potential for time course studies using any plant tissue that can be immobilised, for example leaves or epidermal peels. Advantages include parallelisation and higher throughput, which would be valuable e.g. for screening of bioactive compounds; and the ability to follow the same tissue sample and/or individual cells over a time course.

IV.2 Background

The barley (*Hordeum vulgare*) aleurone layer is an established model system for studying phytohormone signalling, enzyme secretion and programmed cell death (PCD) during grain germination [7–9], which is tightly regulated by the phytohormones gibberellic acid (GA) and abscisic acid (ABA) [13, 36]. GA induces germination-related metabolism, enzyme secretion and subsequent PCD in the aleurone layer, whereas ABA as an antagonist of GA delays germination-related events and suppresses PCD entirely in the absence of GA [13, 36]. Traditionally, aleurone layers are dissected from mature grains and incubated in buffer containing the relevant phytohormones for one to two days [9, 18, 19, 47]. Most of the post-incubation analyses commonly used to study germination-related events in barley aleurone layers are based on extracted proteins, RNA, or small molecules. Protein extracts are used for determinations of enzyme activities and quantities [9,11–17], SDS-PAGE and Western blotting [9,13,15–17,19], two-dimensional electrophoresis [7,8,34], and proteomics investigations by mass spectrometry [7,8]. Gene expression profiling by quantitative RT-PCR [9,14] or Northern blotting [9,12,13,16] is performed on RNA extracts, while cell lysates are used for determination of intracellular H_2O_2 concentrations by absorbance measurements of coloured complexes [7,9]. Gene expression can also be investigated by transforming aleurone layers with the promoter of a target protein fused to a reporter gene like β-glucuronidase. Expression of the reporter gene is then determined by enzymatic activity in cell extracts [28,29,97,99–102,104,107] or by histochemical staining of fixated tissue [103,110–115].
End-point assays based on cell lysates are limited by the fact that each analysis is performed on a different pool of samples, as each tissue sample or population of cells can only be analysed at a single time point. Therefore, time course experiments can be affected by the biological diversity between independent samples, which could distort the interpretation of the results. Time course experiments on the same tissue or population of cells can be enabled by the use of assays that do not destroy cellular integrity, which could also facilitate the performance of multiple assays.
Techniques enabling analysis of barley aleurone layers without destroying cellular integrity do exist and are mostly based on optical detection, such as fluorescent staining for evaluation of cell viability [7,12,13,36], visualization of cellular structures [19], detection of intracellular levels of ions such as Ca^{2+} [17], electrochemical measurements of intra- and extracellular redox activity [150], as well as determinations of intracellular H_2O_2 levels of intact cells by fluorescent staining [13,36] or chemiluminescence [14,16]. Fluorescence microscopy can also be used for detection of transient expression when aleurone layers are transformed with e.g. the green fluorescent protein (GFP) as the reporter gene [29, 107–109, 112, 113]. Using GFP instead of β-glucuronidase as the reporter gene has the distinct advantage that detection is performed on living cells. To study enzymes released by the aleurone layer during germination, the same techniques are used as for the cell extracts for determination of enzymatic activities and quantities [7, 11, 15, 17, 18], SDS-PAGE [8, 15], Western blotting [8, 15], as well as two-dimensional electrophoresis [7] and proteomics investigations by mass spectrometry [7]. Even though such non-destructive methods

exist, they are still mainly used as end-point analyses.
Time course studies on the same cell sample without destroying cellular integrity can be achieved by e.g. analysing proteins released into the incubation media by determinations of activities and protein quantities [7, 11, 18], or mass spectrometry-based proteomics [7] in samples taken from the incubation media at different time points. Non-destructive techniques based on fluorescence microscopy can also be used in time course studies to evaluate intracellular changes through e.g. monitoring cell viability [7, 12, 13, 36, 150], determining H_2O_2 levels [13, 36], or observing transient expression in cells transformed with a fluorescent protein conjugate [151]. However, using microscopic techniques to follow the same population of cells throughout a time course study requires immobilisation of the aleurone layers.
Immobilisation strategies and subsequent cultivation of single plant cells or plant tissues have been used extensively in the industry [117–119], and although single barley aleurone protoplasts have been immobilised [120, 121], nothing similar has yet been implemented for whole barley aleurone layers, to the best of our knowledge. In established methods, immobilisation of cells is achieved by attachment to carrier surfaces, or by entrapment in porous polymer gels or in membranes [117–119]. The attachment of plant cells to carrier surfaces has the distinct advantage compared to entrapment strategies of improved mass transfer of nutrients and products to and from the cells, respectively, as the immobilisation matrix does not surround the cells [117]. Another advantage of attachment is that growth of cells immobilised in a matrix can lead to disintegration of the immobilisation matrix and possibly release of the cells into the incubation media [118]. The latter consideration is not a concern in connection with incubation of the aleurone layer, as these cells do not divide [7, 9, 13, 36, 152], but may be of concern for other types of plant tissue. Other examples of immobilised plant tissues are leaves, shoots, embryos and especially roots [117–119, 122, 123] but these are much less frequently used than single cell immobilisation methods.
Time course studies with analysis of multiple parameters using different detection techniques are still a challenge due to two major concerns. Firstly, the different assays under consideration may be incompatible. Secondly, some assays may affect the plant tissue and therefore influence the outcome of simultaneous or subsequent analyses.
In this work, a multiwell plate setup for immobilised plant tissue was implemented and used for a time course study of barley aleurone layers in which cell viability, intracellular reducing capacity, and transient expression profiles of α-amylase and phytase were monitored. The setup enabled the combination of several established detection techniques and multiple incubation conditions as well as parallelisation enabling higher throughput.

IV.3 Results and discussion

IV.3.1 Multiwell plate setup for immobilised aleurone layers

The plate setup (Figure IV.1) for incubation of immobilised punch-outs of barley aleurone layers consisted of a regular 24-well plate with a cylindrical polydimethylsiloxane (PDMS) pillar (diameter 12 mm, height 16 mm) attached to the lid by double-sided adhesive silicone tape above the centre of each well. The height of the pillars was extended with a 0.5 mm polymethyl methacrylate (PMMA) disc using silicone tape to adjust the gap between the end of the pillar and the bottom of the well to 1 mm to enable compatibility with an inverted microscope used for cell viability detection.
An aleurone layer punch-out (4 mm diameter), made with a biopsy punch as described in Methods, was immobilised on the end of each PDMS pillar with silicone tape on the external face such that the endosperm side faced towards the bottom of the wells during incubation (Figure IV.1). The decision to use tissue punch-outs instead of entire dissected aleurone layers was based on our goal to ensure uniform sample size to circumvent the need for normalisation of the experimental data by sample dry weight [150]. Barley aleurone layers are 2-3 cell layers thick [23, 152], resulting in consistent weights when using an identical tissue area.
Immobilisation of the samples in the lid of the multiwell plate facilitated the combination of

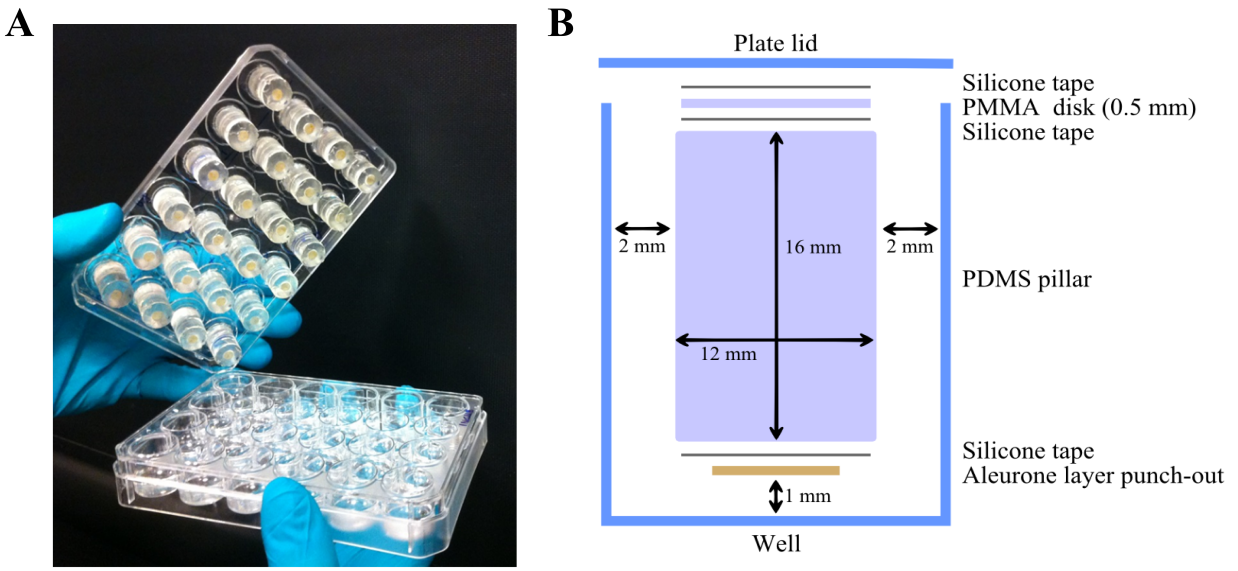

Figure IV.1: Multiwell plate setup for immobilised aleurone layer punch-outs

PDMS pillars were mounted in the lid of a 24-well multiwell plate with double-adhesive silicone tape, and aleurone layer punch-outs were immobilised at the end of the pillars with silicone tape, facing downwards towards the bottom of the wells during incubation. Lid-mounting facilitated easy movement of the punch-outs between assays as well as compatibility with an inverted microscope. **A:** Photograph of multiwell plate setup. **B:** Schematic showing the dimensions of a pillar in a well.

multiple assays since the aleurone layers could simply be transferred from one multiwell plate to another as depicted in the experimental overview (Figure IV.2). Another advantage of the new setup was the lessened workload; a time course study with five time points and two conditions (e.g. ABA and GA) in triplicates of five aleurone layers incubated per well had previously required 30 samples, corresponding to a total of 150 dissected aleurone layers, while the same study using the new setup would only require six samples and hence only six dissected aleurone layers. Apart from decreasing the amount of samples fivefold and the amount of aleurone layers to be dissected 25-fold, the new setup also enables a higher throughput, as a total of eight conditions can be studied over time in one experiment with the 24-well plate setup against only four conditions per time point with the traditional 12-well plate incubation setup.

IV.3.2 Immobilisation results in slower rate of cell death

To test the effect of immobilisation on the punch-out used in the multiwell plate setup, cell viability was compared for the non-immobilised setup applied previously (using five aleurone layers per incubation well [150]), immobilised entire aleurone layers (one per well), and immobilised punch-outs (one per well). ABA-treated samples were used as the control, since ABA suppresses PCD [13, 36], while GA was used for induction of PCD. As expected, treatment with ABA main-

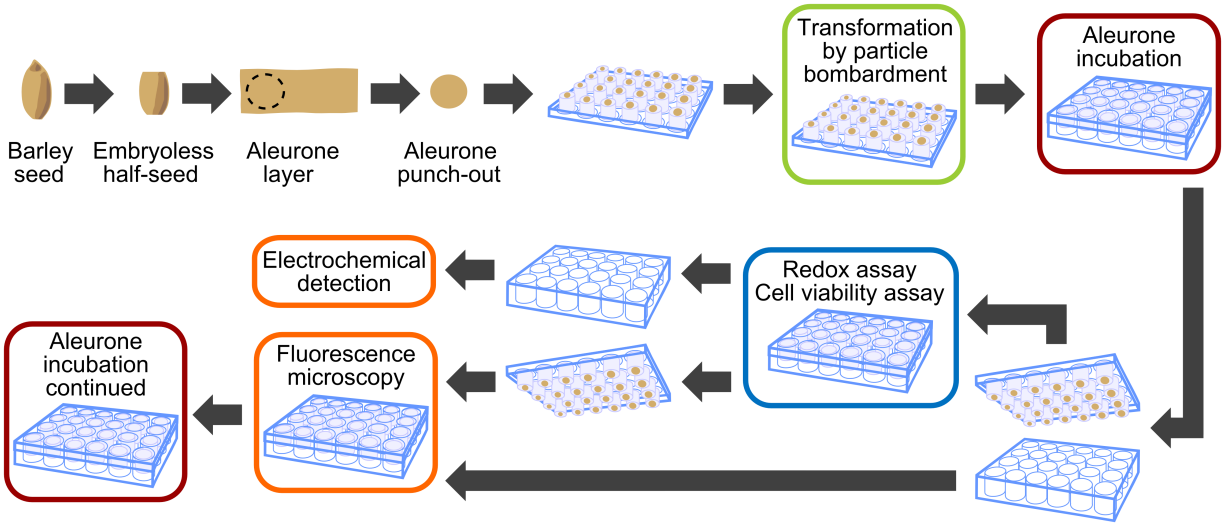

Figure IV.2: Workflow / Experimental overview

Transformation by particle bombardment was performed immediately after isolation, punching and immobilisation, after which incubation of the aleurone layer punch-outs (red) was started. Assays on aleurone punch-outs (blue) were conducted in sequence by moving lids with immobilised aleurone punch-outs between incubation plates with washing between each step. Assay analyses (orange) were conducted either using incubation media (electrochemical detection) or directly on the aleurone punch-outs (fluorescence microscopy), before after transferral of aleurone punch-outs back to original incubation plate. Finally, incubation of the punch-outs was continued as before until next time point for the analyses.

tained viability of the immobilised aleurone layers and punch-outs throughout the incubation period at approx. 22% and 31% dead cells, respectively (Figure IV.3A). In both cases the basal level of dead cells was higher than the previously reported level of 11% dead cells for ABA-treated non-immobilised samples [150] and was probably caused by additional stress induced by the immobilisation and punching-out of tissue. Treatment with GA resulted in increased death of immobilised cells at the start of the incubation period; this was 22% and 30% for the immobilised full layers and punch-outs, respectively, after which cell death increased from 24 h (Figure III.3B). The trend was similar to the decrease in cell viability observed previously in non-immobilised aleurone layers [150], although the rate of cell death was slower for both immobilised setups, reaching levels of 59% and 68% dead cells, respectively, at 96 h, whereas 88% of the non-immobilised cells were dead by 72 h [150]. Linear regression analysis (Figure IV.3B) of the data from 24 to 96 h resulted in almost identical slopes of 0.49% h^{-1} (R^2 = 0.95) and 0.48% h^{-1} (R^2 = 0.98) for the immobilised full layers and punch-outs, respectively, which was significantly different from the slope of 1.68% h^{-1} (R^2 = 0.98) achieved for the non-immobilised setup.
The immobilisation procedure in itself therefore resulted in a higher proportion of dead cells at the beginning of the incubation than in the traditional non-immobilised setup [150], however this level remained stable throughout the incubation in the presence of ABA. In addition, GA-induced cell death occurred more slowly in the immobilised layers, maybe due to lower exposure of the immobilised samples to incubation buffer compared to non-immobilised aleurone layers. This lower exposure is expected because (i) non-immobilised aleurone layers are exposed to the incubation buffer from all sides, whereas immobilised punch-outs were only exposed to the buffer

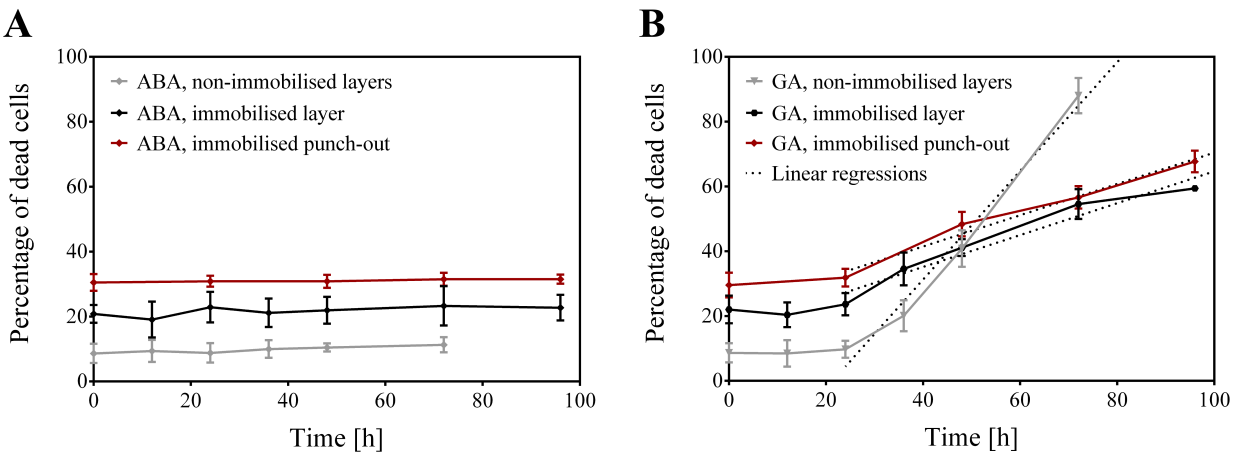

Figure IV.3: Cell viability over time

Aleurone layers were incubated for 0 to 72 or 96 h and subjected to the cell viability assay at the indicated times. **A:** Cell viability for ABA-treated samples from three setups, five non-immobilised layers per well, one single immobilised layer per well and one immobilised punch-out per well. **B:** Cell viability for GA-treated samples, same setup as for A. Linear regressions from 24 h for all treatments. Error bars represent SD (n≥4). ABA: Abscisic acid. GA: Gibberellic acid.

on the endosperm side of the aleurone layer; and (ii) the hydrophobicity of the silicone tape used for immobilisation could create a zone of stationary or less mobile volume of incubation buffer close to the tape. This, combined with the narrow space between the aleurone layer and the base of the well, would result in lower mass transfer between the main body of the incubation buffer and this less mobile buffer volume, resulting in reduced exposure of the aleurone punch-outs to the phytohormones.

IV.3.3 Comparison of reducing capacity in immobilised and non-immobilised aleurone layers

Previously [150], we observed that the GA-induced cell death was accompanied by an increase in reducing capacity of the aleurone layers, which was dependent on a diphenyleneiodonium chloride (DPI)-sensitive component, probably the NADPH oxidase. Changes in reducing capacity of immobilised aleurone layer punch-outs were therefore followed for up to 96 h in a time course experiment. We compared the reducing capacity as a function of the percentage of live cells for ABA- and GA-treatment with the results previously obtained with non-immobilised aleurone layers (Figure IV.4) [150]. The reducing capacity was normalised by the percentage of living cells at each time point to facilitate comparison between the two experiments. A lower reducing capacity was observed for the immobilised punch-outs compared to the non-immobilised layers (Figure IV.4), which was expected due to the smaller sample size in the punch-outs, which we estimated to contain approximately 15 times fewer cells than the 5 non-immobilised aleurone layers. Despite this, similar tendencies were observed in both cases, with ABA-treatment resulting

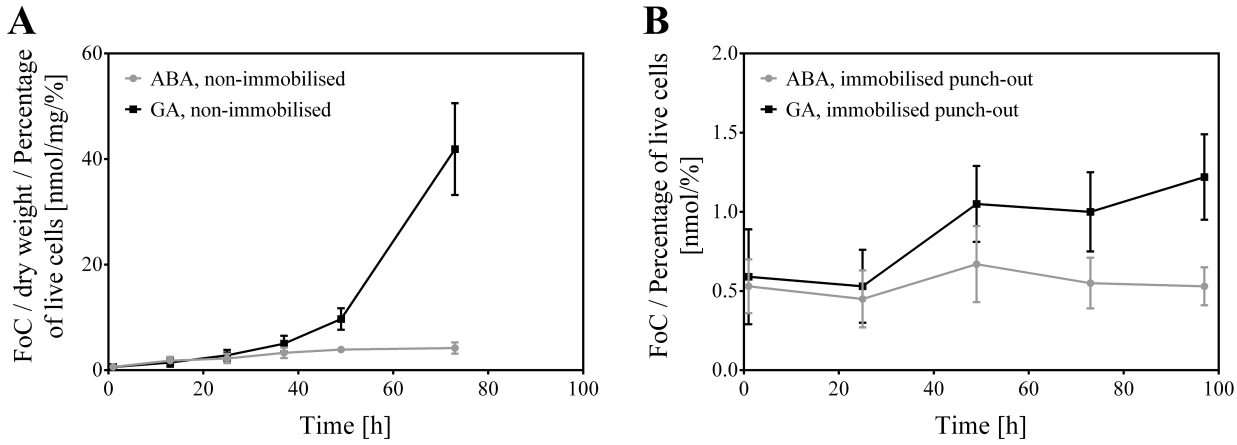

Figure IV.4: Redox activity over time

Aleurone layers were incubated for 0 to 72 or 96 h and subjected to the redox assay at the indicated times. **A:** Reducing capacity normalised by percentage of living cells for five non-immobilised aleurone layers per well. **B:** Reducing capacity normalised by percentage of living cells for one immobilised punch-out per well. Error bars represent SD (n≥4). ABA: Abscisic acid. GA: Gibberellic acid. FoC: Ferrocyanide.

in a very slight increase in reducing capacity/live cells over time, and GA-treatment inducing a steeper increase starting at 24 h, although this was less pronounced in the immobilised tissue punch-outs.

IV.3.4 The immobilised setup allows monitoring cell viability and reducing capacity in response to different effectors

Six different treatments were applied to immobilised aleurone layer punch-outs to monitor the effect on cell viability (Figure IV.5A). Tunicamycin (T), an inhibitor of protein N-glycosylation, induces ER stress and can result in cell death at a concentration of just 20 μg mL^{-1} [7]. Addition of T increased the level of GA-induced cell death already from 24 h, which is in agreement with previous results showing that T caused an increased level of GA-induced cell death in aleurone layers after 24 h of incubation [7]. The NO donor sodium nitroprusside (SNP) prevented the GA-induced increase of cell death, maintaining the number of dead cells at the same level as the ABA-treated samples throughout the time course, corresponding to the known ability of NO donors to delay PCD in aleurone layers [47]. The effect of SNP was reversed by the addition of the NO scavenger 2-(4-carboxyphenyl)-4,4,5,5-tetramethylimidazoline-1-oxyl-3 oxide (cPTIO), as cell death in GA+SNP+cPTIO-treated samples was indistinguishable from GA-treated samples.

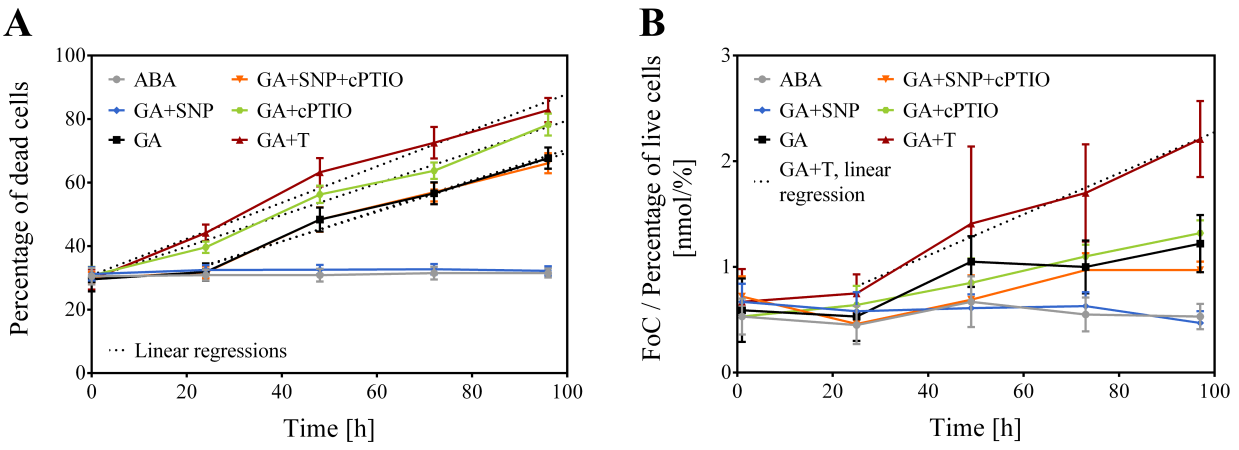

Figure IV.5: Effects of six different treatments on cell viability and reducing capacity for immobilised aleurone layer punch-outs

Immobilised aleurone layer punch-outs were incubated for 0 to 96 h and subjected to the redox assay at the indicated times. **A:** Effect of different treatments on cell viability for one immobilised punch-out per well. Dotted lines indicate linear regressions from 0 h for GA+T and GA+cPTIO and from 24 h for GA and GA+SNP+cPTIO. **B:** Effect of different treatments on reducing capacity normalised by percentage of living cells for one immobilised punch-out per well. Dotted line indicates linear regression from 24 h for GA+T. Error bars represent SD (n≥4). ABA: Abscisic acid. GA: Gibberellic acid. SNP: Sodium nitroprusside. cPTIO: 2-4-carboxyphenyl-4,4,5,5-tetramethylimidazoline-1-oxyl-3-oxide. T: Tunicamycin. FoC: Ferrocyanide.

An increase in GA-induced PCD by cPTIO [47,48] was also confirmed in GA+cPTIO-treated samples from 24 h.
Linear regression analysis of samples treated with GA+T and GA+cPTIO from 0 to 96 h and of samples treated with GA and GA+SNP+cPTIO from 24 to 96 h showed that the rate of cell death for GA+T-treated samples (0.57% h^{-1}, R^2 = 0.95) was significantly higher than the others. The rates of cell death were not significantly different for GA (0.48% h^{-1}, R^2 = 0.92), GA+cPTIO (0.50% h^{-1}, R^2 = 0.97) and GA+SNP+cPTIO (0.47% h^{-1}, R^2 = 0.93). Interestingly, cell death started earlier in the GA+T- and GA+cPTIO-treated samples than in the GA- and GA+SNP+cPTIO-treated samples. As the rate of cell death for GA+cPTIO is not higher than the rate for GA, this earlier induction of cell death is the cause of the higher level of cell death at 96 h, while the higher level of cell death at 96 h for GA+T is a combination of earlier induction of cell death and a higher rate of cell death compared to GA.
The effect of these treatments on the reducing capacity of the immobilised aleurone layers was also analysed (Figure IV.5B). Treatment with GA+T caused the steepest increase in reducing capacity, differing significantly from the rest with a reducing capacity increase of $19.5 \cdot 10^{-3}$ nmol $\%^{-1}$ h^{-1} (R^2 = 0.98), which may reflect the stress induced by T. SNP did not induce a detectable increase in GA-induced reducing capacity, in agreement with its ability to suppress PCD (Figure IV.5A) [47,48]. Conversely, incubation with GA+SNP+cPTIO resulted in an increase in reducing capacity over time, although at a lower level than for GA-treatment alone (Figure IV.5B). The same tendency was observed for GA+cPTIO-treatment in the absence of SNP, although the levels of reducing capacity for GA+cPTIO were consistently higher than those for GA+SNP+cPTIO, underlining the PCD-suppressing capabilities of SNP. However, significant differences between GA, GA+cPTIO and GA+SNP+cPTIO could not be detected. For all treatments except GA+SNP, significant differences from the ABA control could be detected only from 72 h, although GA, GA+T and GA+cPTIO-treated samples had visibly higher values than the ABA-treated samples by already at 48 h.

IV.3.5 Transient expression profile of α-amylase and phytase in time course study

The applicability of the multiwell plate setup was tested for performing transient expression and following expression profiles in individual cells over time, while monitoring PCD in the same cells in parallel (Figure IV.6). Green Fluorescent Protein (GFP) was used as a reporter, under the control of either ubiquitin (positive control [151]), an α-amylase (*AMY1*), or phytase (*PAPhy*_b [153]) promoters. Both the α-amylase and phytase genes are controlled by GA and are expressed in the aleurone layer during germination [154], while ubiquitin expression is constitutive [155,156] and therefore not expected to be influenced by GA. Additionally, in the construct controlled by the alpha amylase promoter, the alpha amylase signal peptide, directing secretion of the protein product, was fused to the GFP reporter. The multiwell plate setup with immobilised aleurone layer punch-outs proved useful for performing transient expression by particle

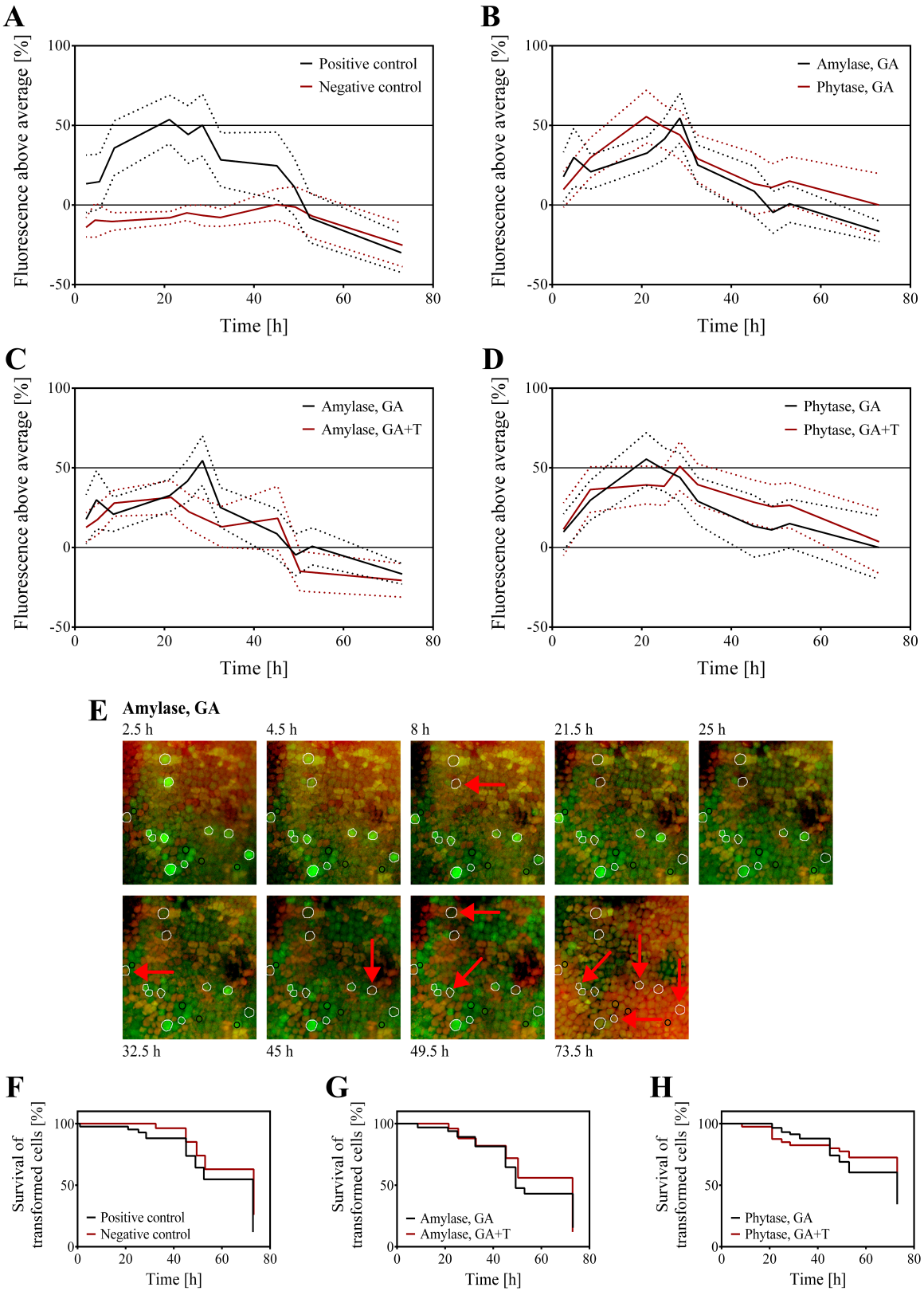

Figure IV.6: Transient expression of α-amylase and phytase over time

Figure caption continued on following page.

Figure IV.6: Transient expression of α-amylase and phytase over time − continued

Aleurone layers were transformed with the ubiquitin-GFP, α-amylase-GFP or phytase-GFP construct, incubated for 0 to 73.5 h and subjected to the cell viability assay (MM 4-64 only) at the indicated times. **A:** Averages (full lines) and 95% confidence intervals (dotted lines) for fluorescence levels of GFP-fluorescing cells (positive control) and randomly chosen non-GFP-fluorescing cells (negative control), both treated with GA. **B-D:** Averages (full lines) and 95% confidence intervals (dotted lines) for fluorescence levels of GFP-fluorescing cells for indicated constructs and treatments. All fluorescence levels are shown as percentage above average background/autofluorescence. Error bars represent SD (A: positive control, n=42; negative control, n=27. C: GA, n=65; GA+T, n=50. D: GA, n=58; GA+T, n=40). **E:** Example of fluorescence micrographs of aleurone layers bombarded with the α-amylase-GFP-construct and treated with GA from 2.5 to 73.5 h. GFP-fluorescing cells appear bright green and are ringed in white, while live cells appear green, and dead cells appear orange-red. Non-GFP-fluorescing cells used for determination of background fluorescence are ringed in black. Red arrows indicate observed death of a transformed cell. All images are 600x600 μm. **F-H:** Survival plots of transformed cells. GA: Gibberellic acid. T: Tunicamycin.

bombardment, since the aleurone layers were well aligned during the procedure. Using immobilised tissue, after gene bombardment it was possible to transfer the immobilised tissue to the cell viability stain and then monitor the punch-outs under the microscope. This unique setup enabled parallel analysis of GFP production in individual transformed cells and staining for cell death. Expression profiles were obtained for the a-amylase- and phytase- promoter-controlled reporters, which to the best of our knowledge has not previously been achieved with transient expression in barley aleurone layers.

For all three constructs (ubiquitin, α-amylase and phytase), GFP-fluorescence was observed in the earliest images taken 2.5-3.5 h after transformation, and fluorescence reached levels of approximately 50% above the average auto-fluorescence (Figure IV.6A-D). The negative control (uncoated gold particles) behaved as expected, as no cells with higher than background fluorescence were detected (Figure IV.6A). With GA-treatment, the α-amylase-controlled GFP was detected from the first time point until approximately 50 h, whereas the phytase-controlled GFP could be detected until the end of the time course experiment at 73 h (Figure IV.6B). The difference is likely to be due to the fact that the α-amylase-controlled GFP is fused to a signal peptide and is expected to be secreted from the aleurone cells. The phytase-controlled GFP will not be directed to the secretory system and will remain within the cells until it is turned over by cellular degradation mechanisms or until cell death, which should result in its release into the extracellular environment. For both promoters, GFP-fluorescence increased from the initial time point and peaked between approximately 20 and 30 h, which were consistent with the expected expression of both promoters during GA-induced germination. GA+T-treatment, on the other hand, had quite different effects on the fluorescence profiles of the two constructs. For the α-amylase construct (Figure IV.6C), the peak fluorescence did not reach the same level for GA+T-treated samples (approx. 30% above average) as for GA-treated samples (approx. 50% above average), which could indicate a dampening effect of T on the α-amylase promoter, or degradation of the reporter protein due to T-induced ER-stress, corresponding to earlier findings of reduced levels of both intra- and extracellular α-amylase in the presence of T [7]. Peak fluorescence was

not affected by GA+T-treatment for the phytase construct (Figure IV.6D), which is in agreement with the lack of an ER-targeting signal peptide in the phytase construct. However, the entire fluorescence profile was shifted slightly towards later time points, indicating a delaying effect of T on phytase gene expression. The effect of T on expression of especially the α-amylase construct could be further investigated by co-transformation of the aleurone layers with other genes that affect the production of α-amylase or the secretory pathway, such as the transcription factor GAMyb that induces expression of α-amylase [35].
In parallel with detection of GFP-fluorescence, staining with the fluorescent probe MM 4-64 allowed for detection of cell death of individual transformed cells (Figure IV.6E-H). Cell death was detected earlier for all three constructs compared to the negative control, but the rates of cell death was similar for the positive and negative controls (Figure IV.6F). Cells transformed with the α-amylase construct died earlier and at a faster rate than cells transformed with the phytase construct (Figure IV.6G,H). Treatment with GA+T did not induce earlier cell death compared to GA-treated samples for neither the α-amylase nor the phytase construct, which may be an effect of the smaller amount of cells investigated compared to previous determination of the effect of T on cell death (Figure IV.5A). Visual investigation of the micrographs showed that for cells transformed with the α-amylase construct GFP-fluorescence typically subsided to the background level at one time point, and cell death then followed in either the first or second time point after that (Figure IV.6E). In contrast to this, cells transformed with the phytase construct fluoresced until just before cell death, as fluorescence could be detected at one time point and cell death at the next time point. As mentioned above, the α-amylase-controlled GFP is secreted, whereas the phytase-controlled GFP remains in the cells, which could account for this difference. α-amylase-controlled GFP-production thereby seems to stop prior to cell death, but no similar conclusion can be made for phytase-controlled GFP-production due to the accumulation of GFP in the cells. Transformation of cells with a phytase-controlled GFP gene fused to a signal peptide targeting it for secretion would most probably allow for distinction between the timing of GFP-production in relation to the time of cell death.
The application of the developed 24-well system for transient expression provided a more detailed picture compared to the traditional approach of enzyme activity determinations in cell extracts at single time points: The system enabled single transformed cells to be followed over time and provided an insight into the cell-to-cell variability of the actual transformation event.

IV.4 Conclusions

Immobilisation of barley aleurone layers on PDMS cylinders fixed to the lid of a multiwell plate facilitated use of multiple incubation conditions and the combination of a cell viability and a reducing capacity assay on the same tissue. A clear effect could be observed on the rate of cell death and reducing capacity of living cells by compounds inducing protein unfolding (T), increased (SNP) or decreased (cPTIO) NO levels. The setup enabled simple, user-friendly handling

of plant tissue incubations, and facilitated easy transient expression studies in plant tissues by particle bombardment as well as time course studies on the same population of cells combining multiple non-destructive assays. We envision the application of this type of setup for other types of plant tissues such as leaves or germinating embryos for studying the effects of e.g. biotic and abiotic stresses or for screening of compounds for biological effects. Due to the ease of use and many possibilities of assay combinations, we believe the setup has great potential in the area of plant science.

IV.5 Methods

IV.5.1 Chemicals

Ethanol, ampicillin, nystatin, succinic acid, calcium dichloride, Trizma base, GA (gibberellin A3), ABA, T, SNP, cPTIO, fluorescein diacetate, M, and FiC were obtained from Sigma-Aldrich Co. (St. Louis, MO, USA), while MM 4-64 (N-(3-triethylammoniumpropyl)-4-(6-(4-(diethylamino) phenyl)hexatrienyl)pyridinium dibromide) was obtained from Biomol GmbH (Hamburg, Germany).

IV.5.2 Multiwell plate setup

The 24 cylindrical pillars (diameter 12 mm, height 16 mm) were fabricated by casting PDMS in a 48-well multiwell flat-bottomed plate (Nunc, Nunclon Delta Surface, Thermo Scientific, Waltham, MA, USA) and cured at 50°C overnight. After removal, the cylinders were immobilised on the inside of the lid of a 24-well multiwell flat-bottomed culture plate (Nunc, Nunclon Delta Surface, Thermo Scientific, Waltham, MA, USA) with cut-outs of double-sided adhesive silicone tape (INT TA106, Intertronics, Oxfordshire, UK) cut using laser ablation (48-5S Duo Lase carbon dioxide laser from Synrad Inc., Mukilteo, WA, USA). The pillars were immobilised on the lid to have one pillar in each well, and the height of the pillars was extended with a 0.5 mm polymethyl methacrylate (PMMA) disc using silicone tape to adjust the gap between the end of the pillar and the bottom of the well to 1 mm to enable compatibility with an inverted microscope used for cell viability detection. Double-sided adhesive silicone tape was also placed at the bottom of the pillars (facing the bottom of the wells) for aleurone layer immobilisation. PMMA discs were also cut using laser ablation (48-5S Duo Lase carbon dioxide laser from Synrad Inc., Mukilteo, WA, USA).

IV.5.3 Plant material and incubation buffer

Barley grains (*Hordeum vulgare* cv. Himalaya, 2003 harvest, Washington State University, Pullman, USA) from a batch previously used to study production of secreted hydrolases [7] were

de-embryonated, surface sterilised with 70% ethanol, rinsed four times with sterile H_2O, and imbibed in sterile H_2O with 50 μg mL^{-1} ampicillin and 5 μg mL^{-1} nystatin for 4 days in the dark at 4°C. Aleurone layers were isolated by gently scraping away the starchy endosperm with the blunt side of a metal scalpel. The external face of the aleurone layers (facing outwards in the grains) were briefly dried by placing them on filter paper for 5 seconds, before 4 mm circular punch-outs were made with a biopsy puncher (Disposable Biopsy Punch, 4.0 mm w/Plunger, Miltex, Integra LifeSciences, Plainsboro, NJ, USA). The aleurone layer punch-outs were immobilised on the pillars of the multiwell by lightly pressing the outside of the aleurone layer punch-outs onto the silicone tape, so that the internal face of the aleurone layer (endosperm side in the grains) was oriented towards the bottom of the wells. To prevent drying of already immobilised punch-outs during immobilisation of the remaining punch-outs, a drop of sterile H_2O was applied on top of each punch-out immediately after immobilisation. Immobilising all 24 aleurone layer punch-outs lasted approximately 15-20 min. For immobilisation of full aleurone layers, the same procedure was applied with the exception of the biopsy puncher. The procedure for the non-immobilised setup was described by Mark et al. [150].
Incubation was started immediately after immobilisation (for immobilised entire aleurone layers) or immediately after transformation (for immobilised punch-outs) by placing the lid with the immobilised aleurone layers or punch-outs in a 24-well multiwell plate and placing the plate at room temperature on a shaker at 150 rpm for the indicated time. Each well held 0.5 mL incubation buffer (20 mM succinic acid, 20 mM $CaCl_2$, 20 mM Trizma base, 50 μg mL^{-1} ampicillin, 5 μg mL^{-1} nystatin, pH 5) with phytohormones or effector compounds as indicated elsewhere. Concentrations of phytohormones and effector compounds: ABA, 10 μM; GA, 10 μM; T, 20 mg mL^{-1} [7]; SNP, 100 μM [47, 48]; cPTIO, 100 μM. All incubations were set up in four replicates within each multiwell plate lid, and two identical plate lids were set up.

IV.5.4 Cell viability assay

Cell viability determination was based on a previously described method [12]. The lids with the immobilised aleurone layers or punch-outs were transferred to new multiwell plates for washing in 20 mM $CaCl_2$ before being transferred to a second set of plates for staining with fluorescein diacetate (2 μg mL^{-1} in 20 mM $CaCl_2$, 0.5 mL, 15 min) and to a third set of plates for staining with MM 4-64 (2 μM in 20 mM $CaCl_2$, 0.5 mL, 3 min). Each staining step was followed by washing with 20 mM $CaCl_2$ in a new multiwell plate each time. After staining and a last washing step, the lids were transferred back to the original multiwell plates with the incubation buffer. The aleurone layers were then observed with a microscope (AXIO OBSERVER.Z1 with EC Plan-Neofluar (10x or 5x)/0.16 Ph 1 M27 objective and AxioCamMR3 camera with the AxioVision LE 4.8.2.0 software, Carl Zeiss Microscopy GmbH, Jena, Germany) and digital images were taken of three separate regions of each aleurone layer (10x optical zoom) or of the middle of each punch-out (5x optical zoom). The position of each region was saved with the microscope software to

enable imaging of the same region for each aleurone layer throughout the time course study. The size of the photographed regions were 872x655 μm for 10x zoom and 1784x1310 μm for 5x zoom. Percentages of dead cells were determined using the Colour Deconvolution plugin [130] for the ImageJ 1.45s software (National Institutes of Health, USA).

IV.5.5 Redox activity assay

The procedure was based on the method previously applied by the authors for non-immobilised aleurone layers [150]. The lids with the immobilised aleurone layer punch-outs were transferred to new multiwell plates for washing in sterile H_2O before being transferred to two identical new plates containing 0.5 mL redox mediator mix (20 mM FiC and 100 μM M in incubation buffer) in each well. After 1 h incubation at room temperature on a shaker at 150 rpm, both lids were washed in sterile H_2O in separate new plates and then transferred back to the original plates with the incubation buffer. The redox mediator mix was transferred to separate Eppendorf tubes, frozen in liquid nitrogen and stored at $-80°C$ until electrochemical analysis.

IV.5.6 Electrochemical detection

The setup consisted of a peristaltic pump (Minipuls 2, Gilson, Inc., Middleton, WI, USA) providing a continuous flow (500 μL min^{-1}) of incubation buffer to define the baseline, an injection port (Model 7010, Rheodyne, Inc., Cotati, CA, USA) with a sample loop of 50 μL, an electrochemical cell designed and fabricated for commercial screen printed electrodes (Dropsense) and a potentiostat (Model CHI 1010A, CH Instrument Inc., Austin, TX, USA). 50 μL of each sample was injected in carrier buffer flow through the injection port to the electrochemical cell containing a screen printed electrode (DS 250 AT, DropSense, Asturias, Spain). The FoC present in the samples was electrochemically oxidised on the Au working electrode at +400 mV vs. an Au reference electrode. Each of the biological replicates was injected three times and peak currents were averaged. The FoC content was calculated using a calibration curve of FoC standard solutions.

IV.5.7 Transient expression

Transformation of aleurone layer punch-outs were performed immediately after immobilisation by bombardment in a DuPont Biolistic PDS-1000/He Particle Delivery System (Bio-Rad, USA) using 650 psi rupture discs and 0.6 μm gold particles coated with plasmid DNA as detailed by the supplier. Three or four PDMS pillars were placed in the bombardment area per shot, and the pillars were placed at the lowest level of the bombardment system to increase the chance of the plasmid-coated gold particles penetrating the cell walls of the aleurone cells and decrease the risk of the particles ricocheting off of the cell walls. To prevent drying of already transformed aleurone layer punch-outs during transformation of the remaining punch-outs, a drop of sterile H_2O was applied on top of each punch-out immediately after re-mounting of the PDMS pillars in the

lid of the multiwell plate system. Aleurone layers were transformed with naked gold particles (negative control) or with particles coated with one of three constructs. The amylase construct (pAMY-αGFP-N) comprises an α-amylase promoter (*AMY1*) fused to the α-amylase signal peptide [157] and a synthetic GFP-sequence, the phytase construct (pScPAPb-pro-GFP-N) a phytase promoter (*ScPAPhy*_b [153]) fused to a synthetic GFP-sequence, and the positive control construct (pU-hGFP-C3-N [151]) the maize ubiquitin 1 gene (*Ubi-1*) fused to a synthetic GFP-sequence. pAMY-αGFP-N and pScPAPb-pro-GFP-N were constructed by replacing the PstI-EcoRI ubiquitin promoter of pU-hGFP-C3-N with a 745 bp or 2687 bp PstI-EcoRI fragment of the α-amylase and rye *PAPhy*_b promoter, respectively. For pAMY-αGFP-N the α-amylase signal peptide from pUSPPhyN [157] was ligated into the PstI site downstream the α-amylase promoter.
Observations of GFP-fluorescence was performed similarly to the cell viability assay, as cells were stained with MM 4-64 (see staining procedure above) at the first imaging session and then every 24 h to ease identification of dead cells. After staining and washing, the transformed aleurone layers were observed with a microscope (AXIO OBSERVER.Z1 with EC Plan-Neofluar 5x/0.16 Ph 1 M27 objective and AxioCamMR3 camera with the AxioVision LE 4.8.2.0 software, Carl Zeiss Microscopy GmbH, Jena, Germany) and digital, two-channel (red, green) images were taken of the middle of each punch-out (5x optical zoom). The position of each region was saved with the microscope software to enable imaging of the same region for each aleurone layer throughout the time course study. For digital image analysis, 600x600 μm regions containing visually identified GFP-fluorescing cells were excised. To ensure correct determination of fluorescence levels for GFP-fluorescing cells and non-GFP-fluorescing autofluorescent (green [116]) cells without interference from dead cells (orange-red), only the green channel of the images were used for the subsequent analysis. Using the ImageJ 1.45s software (National Institutes of Health, USA), fluorescence levels of GFP-fluorescing cells in the excised 600x600 μm regions were determined by measuring intensity per area for GFP-fluorescing cells and comparing to the average of four non-GFP-fluorescing cells per image. Cells were only accepted as truly GFP-fluorescing cells, if their fluorescence level exceeded 115% of the average of the non-GFP-fluorescing cells at minimum one time point throughout the time course study. No GFP-fluorescing cells were identified for the negative control. For data analysis the average of the background/autofluorescence was subtracted from GFP-fluorescence values.

IV.5.8 Statistical analysis

All data was analysed using the GraphPad Prism 6.04 software (GraphPad Software, Inc., San Diego, CA, USA) by first subjecting datasets to the ROUT (Robust regression and Outlier removal) outlier analysis with a false discovery rate of 1%. Subsequently, outlier analysed data was then subjected to Fisher's LSD (Least Significant Difference) two-way ANOVA test at a confidence level of 95%.

IV.6 Competing interests

The authors declare they have no competing interests.

IV.7 Authors' contributions

The project was conceived by CF, JE and MD. CM and KZ designed the multiwell plate setup and the experiments, and prepared the manuscript. CM performed sample preparation, tissue and redox incubation, cell viability detection, transient expression, fluorescence microscopy, data analysis, and statistical analysis. KZ constructed the multiwell plate setup for aleurone layer immobilisation, including preparation of the PDMS pillars and silicone tape, performed electrochemical detection and data analysis. CKM and HBP supervised and assisted with the transformation by particle bombardment, provided the constructs used for the transient expression, and revised the paper. MD, AH and JE critically revised the manuscript. CF supervised the research and revised the manuscript. All authors read and approved the final manuscript.

IV.8 Acknowledgements

We are grateful to Christina Rønn Ingvardsen, Lis Bagnkop Holte and Inger Holme (Department of Molecular Biology and Genetics, Research Center Flakkebjerg, Aarhus University) for technical assistance and guidance in connection with the transformation of aleurone layers by particle bombardment. This work was supported by the Danish Council for Independent Research | Natural Sciences (to CM, KZ and CF) and the Lundbeck Foundation (to AH).

Part V
Other results related to Article Manuscript #2

This part describes other work conducted in continuation of the results presented in Part IV: Article Manuscript #2 (page 61).

V.1 Cell viability measurements with the developed incubation system

Having used the immobilised setup to investigate the effect of T (an inducer of protein unfolding in the endoplasmic reticulum), SNP (an $NO^{\bullet}$ donor), and cPTIO (an $NO^{\bullet}$ scavenger) on cell viability, we used the setup for further investigations of T, SNP, dicoumarol, a QR inhibitor [62, 72, 87, 158]), DPI, ascorbic acid (AsA, a ROS scavenger [10, 60]), and sodium azide (NaN_3, a cytochrome *c* oxidase inhibitor).
For ABA-treated aleurone layers, we investigated the effect of T, SNP, dicoumarol, DPI, AsA, and NaN_3 (Figure V.1). Despite the increasing effect of T on cell death for GA-treated aleurone layers (Part IV, Figure IV.5A, page 69), the compound had no effect on viability of ABA-treated aleurone layers, as the amount of dead cells did not increase throughout the time course study from the initial 31-34% (Figure V.1). ABA prevents enzyme production in aleurone layers [8], which explains the non-existent effect of T, as this compound is a known inducer of protein unfolding in the endoplasmic reticulum [7]. SNP has previously been shown to delay PCD in aleurone layers [47], and also prevented an increase in cell death for GA-treated layers (Part IV, Figure IV.5,

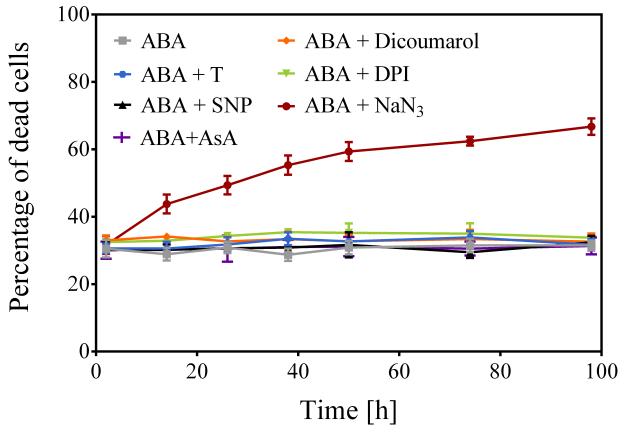

Figure V.1: Effect of different treatments on cell viability of immobilised ABA-treated aleurone layer punch-outs

One immobilised aleurone layer punch-out per well was incubated for 0 to 98 h and subjected to the cell viability assay at the indicated times. Error bars represent SD (n≥4). ABA: Abscisic acid. T: Tunicamycin. SNP: Sodium nitroprusside. DPI: Diphenyleneiodonium chloride. AsA: Ascorbic acid.

page 69), which corresponds with ABA-treatment maintaining the level of cell viability at 31-34% dead cells throughout the time course study (Figure V.1). Similarly, neither the QR inhibitor dicoumarol, the NAPDH oxidase (flavoenzyme) inhibitor DPI, nor the ROS scavenger AsA induced an increase in cell death but maintained the amount of dead cells at 32-34%, 32-35%, and 30-32%, respectively, throughout the incubation period (Figure V.1). As both dicoumarol and DPI inhibit redox-active enzymes and AsA is an antioxidant, a non-existent effect of these compounds agrees with our previous findings that ABA limits the level of reducing capacity (Part II, Figures II.2 and II.4-II.7, pages 32-38). Furthermore, the non-existent effect of DPI on immobilised aleurone layer punch-outs is in accordance with the lack of effect on both redox activity and cell viability obtained for this compound with ABA-treatment of non-immobilised aleurone layers (Part II, Figure II.7, page 38). The only compound with an effect on cell viability of ABA-treated aleurone layers was the cytochrome *c* oxidase inhibitor NaN_3, which resulted in a significant increase in the amount of dead cells already from 14 h (Figure V.1). Increased cell death with decreased activity of cytochrome *c* oxidase, even for ABA-treated cells, corresponds with the role of this enzyme in the mitochondrial respiratory pathway [52, 159]. Interestingly, [52] did not detect an effect of 30 min incubation with NaN_3 on cell viability of aleurone layers pre-treated with ABA for 12 or 23 h, which could indicate that such treatment before the addition of NaN_3 induces a certain level of resistance towards the compound. However, a more likely explanation is that NaN_3 does not affect cell viability of ABA-treated aleurone layers after only 30 min of incubation with the compound, as used by [52], but rather after several hours, as indicated by our results.
Linear regression analysis (Table V.1) on the entire incubation period for all treatments underlined the effects mentioned here, as only NaN_3 resulted in a significantly ($p<0.0001$) increased rate of cell death of 0.333% h^{-1} compared to 0.013% h^{-1} for ABA. For ABA+NaN_3-treatment, the low R^2-value of 0.83 was caused by the curve being most steep before and less steep after

Table V.1: Linear regression analysis of cell viability of immobilised ABA-treated aleurone layer punch-outs

Treatment	Time period	Slope: Rate of cell death [% h^{-1}]	Goodness of fit: R^2-value	Slope significantly different from ABA?	Initial level of cell death [%]	Level significantly different from ABA?
ABA	2 – 98 h	0.013	0.05	–	30.5	–
ABA+T	2 – 98 h	0.026	0.19	No (p = 0.29)	30.6	No (p = 0.89)
ABA+SNP	2 – 98 h	0.015	0.05	No (p = 0.92)	30.1	No (p = 0.60)
ABA+Dic.	2 – 98 h	−0.006	0.02	No (p = 0.16)	33.0	Yes (p = 0.0267)
ABA+DPI	2 – 98 h	0.029	0.15	No (p = 0.35)	32.5	No (p = 0.08)
ABA+AsA	2 – 98 h	0.010	0.02	No (p = 0.80)	30.1	No (p = 0.59)
ABA+NaN_3	2 – 98 h	0.333	0.83	Yes (p < 0.0001)	31.6	No (p = 0.33)
ABA+NaN_3	2 – 50 h	0.559	0.90	Yes (p < 0.0001)	31.6	No (p = 0.33)

Time period: Data used for analysis. ABA: Abscisic acid. T: Tunicamycin. SNP: Sodium nitroprusside. DPI: Diphenyleneiodonium chloride. Dic.: Dicoumarol. AsA: Ascorbic acid.

50 h. For regression analysis from 2 to 50 h only for ABA+NaN_3 (the steep part of the curve), the rate of cell death increases to 0.559% h^{-1}, indicating that the effect of NaN_3 subsides after a certain incubation time, possibly due to degradation or evaporation of the compound. For ABA-treatment, the very low R^2-value of 0.05 was caused by the flat nature of the curve along with the rate of cell death (0.013% h^{-1}) not being significantly different from 0. The rate of cell death for the remaining treatments were not significantly different from ABA-treatment (all p-values were above 0.16) and all suffered from similarly low R^2-values for the same reasons as mentioned above for ABA. Initial levels of cell death varied slightly from 30.1 to 33.0% with only the level for dicoumarol (33.0%) being significantly different from that of ABA alone (30.5%). As these values are actually quite similar, the statistically significant difference is most likely caused by low standard deviations of 2.6 and 1.4% for ABA and ABA+Dicoumarol, respectively.
For GA-treated aleurone layers, we investigated the effect of NaN_3, dicoumarol, AsA, and DPI (Figure V.2). Again, treatment with GA+NaN_3 induced the highest increase in cell death with a significant difference to GA-treatment already at the first time point of 2 h, which is in agreement with the results obtained by [52], showing extensive cell death of aleurone layers pre-treated with GA after only 30 min incubation with NaN_3. Both dicoumarol and DPI induced a slightly earlier increase in cell death compared to treatment with GA only. This effect of DPI on cell viability had previously been shown with GA-treatment of non-immobilised aleurone layers in parallel with a decrease in reducing capacity (Part II, Figure II.7, page 38). Such decreased reducing capacity caused by inhibition of NADPH oxidase may lead to increased oxidative stress causing earlier induction of cell death in agreement with the proposed 'oxidative window' (Part I, Figure I.8, page 13). A similar mechanism could be proposed for the earlier increase in cell death observed in the presence of dicoumarol, as this compound inhibits QRs, which are involved in ROS pro-

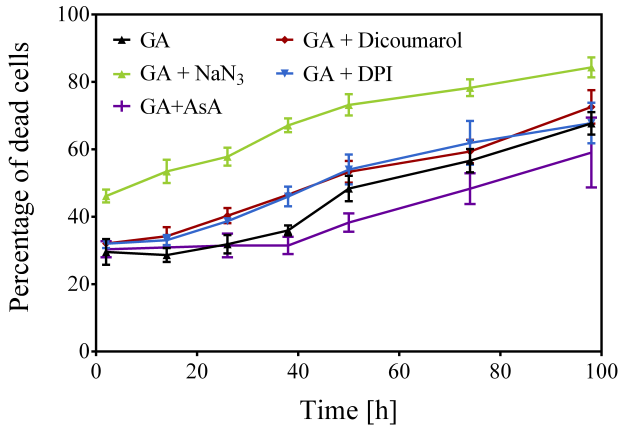

Figure V.2: Effect of different treatments on cell viability of immobilised GA-treated aleurone layer punch-outs

One immobilised aleurone layer punch-out per well was incubated for 0 to 98 h and subjected to the cell viability assay at the indicated times. Error bars represent SD (n≥4). GA: Gibberellic acid. Diphenyleneiodonium chloride. AsA: Ascorbic acid.

duction [70–72]. However, investigations of the reducing capacity in the presence of dicoumarol would be needed to determine if this inhibitor elicits a similar effect to DPI on reducing capacity. Finally, the delay in induction of cell death generated by the addition of AsA is consistent with its role as an antioxidant and hence a scavenger of ROS [10, 60].

Linear regression analysis (Table V.2) was performed on the entire incubation period for GA+NaN_3, from 14 to 98 h for GA+DPI and GA+Dicoumarol, and from 26 to 98 h for GA and GA+AsA. As expected, both the rate of cell death and the initial level of cell death for GA+NaN_3-treatment differed significantly from treatment with GA only. However, as the curve for GA+NaN_3 is most steep before and less steep after 50 h as for ABA+NaN_3, the overall rate of cell death of 0.400% h^{-1} is lower than that for GA-treatment of 0.491% h^{-1}. Re-analysis from 2 to 50 h for GA+NaN_3 (the steep part of the curve) shows an increase in the rate of cell death to 0.565% h^{-1}, again indicating that the effect of NaN_3 subsides after a certain incubation time, as shown for ABA+NaN_3. Consistent with cell death being detectable already after 30 min of incubation with NaN_3 [52], treatment with GA+NaN_3 also showed a significantly higher initial amount of dead cells with 46.2% after 2 h incubation compared to only 29.6% for treatment with GA only. Interestingly, the rates of cell death for GA+NaN_3 (0.565% h^{-1}) and ABA+NaN_3 (0.559% h^{-1}) are not significantly different, indicating that mechanism of action of NaN_3 is the same, regardless of whether germination-related processes has been induced by GA or inhibited by ABA. The initial levels of cell death for GA+NaN_3 (46.2%) and ABA+NaN_3 (31.6%) are significantly different, which points to NaN_3 not affecting cell viability of ABA-treated aleurone layers after only a shorter incubation period (up to 2 h at least) but rather needs several hours, as mentioned above. GA-treatment on the other hand seems to shorten the incubation time needed for manifestation of the NaN_3 effect. Despite the rate of cell death for both dicoumarol and DPI being lower (0.439 and 0.431% h^{-1}, respectively) than the rate of cell death for treatment with GA alone (0.491% h^{-1}), these rates were not significantly different from GA, and neither were the initial levels of

Table V.2: Linear regression analysis of cell viability of immobilised GA-treated aleurone layer punch-outs

Treatment	Time period	Slope: Rate of cell death [% h^{-1}]	Goodness of fit: R^2-value	Slope significantly different from GA?	Initial level of cell death [%]	Level significantly different from GA?
GA	26 – 98 h	0.491	0.93	–	29.6	–
GA+Dic.	14 – 98 h	0.439	0.94	No (p = 0.11)	32.1	No (p = 0.16)
GA+DPI	14 – 98 h	0.431	0.89	No (p = 0.10)	32.0	No (p = 0.17)
GA+AsA	26 – 98 h	0.452	0.77	No (p = 0.29)	30.4	Yes (p = 0.56)
GA+NaN_3	2 – 98 h	0.400	0.92	Yes (p = 0.0034)	46.2	Yes (p < 0.0001)
GA+NaN_3	2 – 50 h	0.565	0.94	Yes (p = 0.0077)	46.2	Yes (p < 0.0001)

Time period: Data used for analysis. GA: Gibberellic acid. DPI: Diphenyleneiodonium chloride. Dic.: Dicoumarol. AsA: Ascorbic acid.

cell death (32.1 and 32.0%, respectively). For DPI, this again indicates the involvement of decreased reducing capacity in the induction of earlier cell death. The rate of cell death was also decreased slightly by the presence of AsA (0.452% h^{-1}), again insignificantly, with the only effect of AsA on cell viability seemingly being a delay in induction of cell death compared to treatment with GA only.

V.2 α-amylase activity measurements with the developed incubation system

As the immobilised incubation system was designed for easy combination of a range of assays by moving the lid with the immobilised aleurone layers between multiwell plates with different assay components (Section I.6.3, page 22), we tested the compatibility of the system with a commercially available kit for determination of amylase activity (Amylase Activity Assay Kit, Sigma-Aldrich Co., St. Louis, MO, USA). This assays measures the activity of amylases by their conversion of a substrate (ethylidene-pNP-G7) into a coloured product (*p*-nitrophenol), which can be quantified by spectrophotometry. Information from the manufacturer does not state whether the assay is specific for α-amylases [160], but a kit from a different manufacturer using the same substrate (ethylidene-pNP-G7) is listed as specific for α-amylase activity [161]. Detection of activity from β-amylase from the small amounts of starchy endosperm that may have remained with the dissected aleurone layers [8] is therefore unlikely.
As α-amylases are secreted into the incubation buffer by the aleurone layers, the assay was performed by transferring aliquots of the incubation buffer from the incubation plate to a 96-well plate for mixing with the kit components. Unfortunately, initial tests with the commercial kit had revealed undetectable levels of α-amylase activity in the incubation buffer, and increased incubation time (up to 135 min) did not yield increased activities, as maximum activity was achieved at 60 min (data not shown). Spiked samples were therefore employed to allow true determination of α-amylase activity in unspiked samples by comparison, as the presence of unknown substrate amounts (in the form of starch residues from the small amounts of starchy endosperm that could have remained with the dissected aleurone layers [8]) would result in apparent activity difference between samples. Spiking was done by transferring two aliquots of 24 μL incubation buffer to separate wells of a 96-well plate, and adding 1 μL fresh buffer to one replicate, while spiking the other replicate with 1 μL pure α-amylase solution to obtain a final concentration of 1 U mL^{-1} α-amylase in the spiked sample. To evaluate the activity of the pure α-amylase, 1 μL α-amylase solution was transferred to a separate well and 24 μL fresh buffer was added. A total sample volume of 25 μL was used instead of the 50 μL specified in the kit protocol to avoid removing too much incubation buffer from the incubation system throughout the incubation period of 98 h, and the volume of the kit reaction mix added to the samples was therefore also lowered from 100 μL to 50 μL. Samples and reaction mix were then incubated for 1 h at room temperature before

spectrophotometric analysis. A standard curve was used to calculate the actual activity of the pure spike (1 μL α-amylase and 24 μL buffer) using a blank of pure buffer as follows:

$$\Delta nitrophenol = \frac{(Abs_{pure\ spike} - Abs_{blank}) - intercept_{std.\ curve}}{slope_{std.\ curve}}$$

$$Activity\ in\ pure\ spike = \frac{\Delta nitrophenol \cdot Dilution\ Factor}{Reaction\ Time \cdot Volume}$$

This calculation results in the unit nmol min^{-1} mL^{-1} for α-amylase activity, which is converted to mU mL^{-1}, as one unit of α-amylase is defined as the amount of α-amylase that cleaves ethylidene-pNP-G7 to generate 1.0 μmol of *p*-nitrophenol per minute at 25°C [160]. Along with absorbance measurements on both samples and spiked samples, this activity was then used to calculate the actual activity in the samples as follows (Christine Finnie, personal communication):

$$Activity\ in\ sample = \frac{Activity\ in\ pure\ spike \cdot (Abs_{sample} - Abs_{blank})}{(Abs_{spiked\ sample} - Abs_{blank}) - (Abs_{sample} - Abs_{blank})}$$

As shown in Figure V.3, the standard deviations obtained with this analysis were very high, especially for GA+T-treatment, while the measured levels of activity are low. This indicates that the levels of α-amylase in the samples are very close to the detection level of the commercial kit, rendering confident analysis of the data almost impossible.
Despite the low levels of activity and high standard deviations, linear regression analysis was performed for the entire incubation period (Table V.3). As is also visible in Figure V.3, treatment

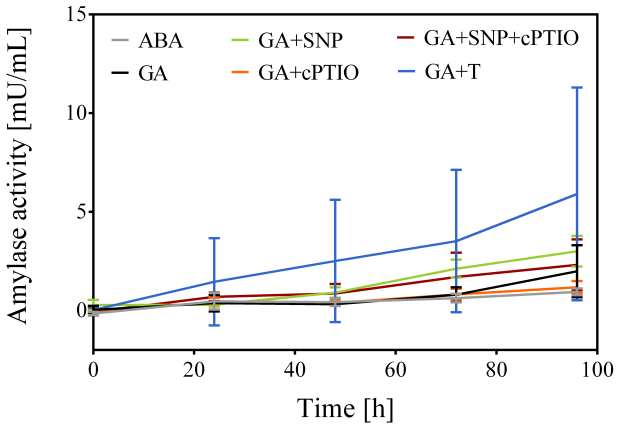

Figure V.3: Test of immobilised setup with commercial α-amylase activity assay

One immobilised aleurone layer punch-out per well was incubated for 0 to 98 h, and 24 μL incubation buffer was transferred to a 96-well plate and subjected to the α-amylase activity assay at the indicated times after spiking with buffer or pure α-amylase. 1 U is the amount of α-amylase that cleaves 1.0 μmole of ethylidene-pNP-G7 to *p*-nitrophenol per minute at 25°C [160]. Error bars represent SD (n≥4). ABA: Abscisic acid. GA: Gibberellic acid. T: Tunicamycin. SNP: Sodium nitroprusside. cPTIO: 2-(4-carboxyphenyl)-4,4,5,5-tetramethylimidazoline-1-oxyl-3-oxide.

with T, SNP, or SNP+cPTIO in addition to GA resulted in a significant increase in the rate of activity increase compared to ABA from 0.0098 mU mL^{-1} h^{-1} for ABA to 0.0240 mU mL^{-1} h^{-1} for GA+SNP+cPTIO, 0.0303 mU mL^{-1} h^{-1} for GA+SNP, and 0.0576 mU mL^{-1} h^{-1} for GA+T. Statistical analysis also showed that the final levels of activity after 96 h incubation for GA+T and GA+SNP were significantly higher than for ABA, but this was not the case for GA+SNP+cPTIO. However, in comparison to treatment with GA alone (not shown), only GA+T-treatment resulted in significant differences in both the rate of activity increase ($p = 0.0023$) and the final level of activity ($p = 0.0003$). Again, large deviations and low levels of activity are the cause of these disappointing results.

From a practical point of view, the use of the commercial amylase activity assay was easily incorporated into an ongoing incubation in the new incubation system for immobilised aleurone layer punch-outs: The lid with the punch-outs were simply removed from the incubation plate shortly, while aliquots of incubation buffer from each well were transferred to a 96-well plate for the activity assay, after which the lid was placed back in the incubation plate. However, the obtained measurements suffer from both low levels of activity and high deviations, as mentioned above. Enabling activity measurements with the immobilised setup will therefore require further optimisation of the incubation buffer to reaction mix ratio and possibly also pooling of samples prior to addition of the reaction mix to obtain measurable levels of α-amylase activity in the samples. Another possibility, should this not prove to be enough, is upconcentration of pooled samples prior to addition of reaction mix by e.g. dialysis or through the use of centrifugal filter devices. Unfortunately, both pooling and upconcentration of samples will increase the work load required for activity measurements, which is in sharp contrast to the intentions with the new incubation system (Section I.6, page 17). A final possibility is to use larger amounts of plant material, e.g. intact aleurone layers instead of punch-outs, which should result in higher activities of α-amylases. However, this will lead back to the problem with normalisation of data by dry weight, which was solved by the use of punch-outs, as mentioned in Section I.6 (page 17).

Table V.3: Linear regression analysis of α-amylase activity of immobilised aleurone layer punch-outs

Treatment	Slope: Rate of activity increase [mU mL^{-1} h^{-1}]	Goodness of fit: R^2-value	Slope significantly different from ABA?	Final level of activity [mU mL^{-1}]	Slope significantly different from ABA?
ABA	0.0098	0.87	–	0.95	–
GA	0.0181	0.80	No ($p = 0.20$)	2.00	No ($p = 0.31$)
GA+SNP	0 0303	0.92	Yes ($p = 0.0115$)	3.00	Yes ($p = 0.0490$)
GA+cPTIO	0.0120	0.93	No ($p = 0.47$)	1.18	No ($p = 0.82$)
GA+SNP +cPTIO	0.0240	0.97	Yes ($p = 0.0041$)	2.31	No ($p = 0.19$)
GA+T	0.0576	0.97	Yes ($p = 0.0002$)	5.91	Yes ($p < 0.0001$)

ABA: Abscisic acid. GA: Gibberellic acid. T: Tunicamycin. SNP: Sodium nitroprusside. cPTIO: 2-(4-carboxyphenyl)-4,4,5,5-tetramethylimidazoline-1-oxyl-3-oxide.

V.3 Phytase activity measurements with the developed incubation system

In connection with the α-amylase activity measurements described above (Section V.2, page 83), we also tested the compatibility of the phytase assay described by [162] and [163] with the new incubation system. The assay measures the activity of the enzyme by its liberation of *ortho*-phosphate from phytic acid. *Ortho*-phosphate binds to a commercially available vanadate-molybdate reagent (Sigma-Aldrich Co., St. Louis, MO, USA), forming a coloured complex that can be quantified by spectrophotometry. The assay measures overall phytase activity and does not distinguish between types of phytases [162, 163].
As active phytases are likely not secreted into the incubation buffer by the aleurone layers [8] but rather occupy either a cell wall-associated (Henrik Brinch-Pedersen, personal communication, and [164]) or intracellular location [8, 154, 165], the assay was performed on the immobilised aleurone layer punch-outs: The lid with the immobilised punch-outs was transferred to a new plate containing a solution with the substrate, phytic acid, for the incubation time of 1 h and then transferred back to the incubation plate after completion of the assay. Standard dilutions were made with dibasic potassium phosphate in a separate plate that was incubated along with the assay plate for 1 h at 37°C before spectrophotometric analysis. Based on a polynomial standard curve [162], measured absorbances were translated to activities and expressed in phytase activity units (FTU). One FTU is defined as the amount of phytase that liberates 1.0 μmol of *ortho*-phosphate per minute at 37°C [165, 166].

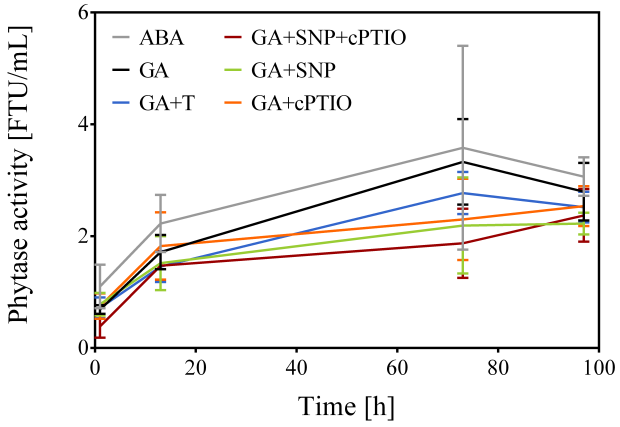

Figure V.4: Test of immobilised setup with phytase activity assay

One immobilised aleurone layer punch-out per well was incubated for 0 to 96 h, and the lid with the immobilised punch-outs was transferred to a new plate and subjected to the phytase activity assay at the indicated times. The lid was transferred back to the incubation plate after completion of the assay. 1 FTU is the amount of phytase that liberates 1.0 μmol of *ortho*-phosphate per minute at 37°C [166]. Error bars represent SD (n$\geq$4). ABA: Abscisic acid. GA: Gibberellic acid. T: Tunicamycin. SNP: Sodium nitroprusside. cPTIO: 2-(4-carboxyphenyl)-4,4,5,5-tetramethylimidazoline-1-oxyl-3-oxide.

Similar to the commercial α-amylase activity assay (Section V.2, page 83), the standard deviations obtained with this analysis were very high, while the measured levels of activity are low (Figure V.4). This again indicates enzyme levels very close to the detection level of the assay, rendering confident analysis of the data almost impossible, although a definite increase in phytase activity over the entire time course experiment can be discerned.
Despite the low levels of activity and high standard deviations, linear regression analysis was performed for the entire incubation period (Table V.4), which did not reveal significant differences in the rates of activity increase for any of the treatments compared to treatment with either ABA or GA only, reflecting the visual representation of Figure V.4. With regards to initial levels of activity, only GA+SNP-samples were significantly different from ABA-samples and then only slightly (p = 0.0427). As one type of phytase (*PAPhy*_a) is produced in aleurone layers already during grain filling [167], any differences in initial levels of activity would simply indicate biological differences between the samples and not an effect induced by any of the treatments. Even though a definite increase in phytase activity over time can be seen for all treatments, the data does not allow for conclusive determination as to whether certain treatments generate a higher production of a second type of phytase (*PAPhy*_b), which is induced by GA during germination [24, 32, 167, 168] due to the lack of significant differences between the rates of activity increase.
Another issue with this analysis is to what degree the substrate is actually exposed to the phytases produced by the aleurone layers. Some sources list phytases as being located in the endoplasmic reticulum or the protein storage vacuoles along with their substrates [8, 154, 165], while others mention an extracellular, cell wall-associated location (Henrik Brinch-Pedersen, personal communication, and [164]). A location in the cell wall is supported by a TargetP analysis of the two *PAPhy*_b phytases identified in barley [153, 167] showing a strong probability of secretion

Table V.4: Linear regression analysis of phytase activity of immobilised aleurone layer punch-outs

Treatment	Slope: Rate of activity increase [FTU mL^{-1} h^{-1}]	Goodness of fit: R^2-value	Slope significantly different from ABA?	Slope significantly different from GA?	Initial* / final** level of activity [FTU mL^{-1}]
ABA	0.020	0.74	–	No (p = 0.85)	1.10 / 3.07
GA	0.025	0.79	No (p = 0.85)	–	0.69 / 2.80
GA+SNP	0 014	0.85	No (p = 0.51)	No (p = 0.38)	0.78 / 2.23
GA+cPTIO	0.015	0.78	No (p = 0.64)	No (p = 0.50)	0.75 / 2.54
GA+SNP +cPTIO	0.016	0.72	No (p = 0.89)	No (p = 0.57)	0.39 / 2.37
GA+T	0.019	0.86	No (p = 0.98)	No (p = 0.75)	0.72 / 2.52

*: No initial activity levels are significantly different from either ABA or GA. **: Only the final activity level of GA+SNP is significantly different from ABA, while no final activity levels are significantly different from GA. ABA: Abscisic acid. GA: Gibberellic acid. T: Tunicamycin. SNP: Sodium nitroprusside. cPTIO: 2-(4-carboxyphenyl)-4,4,5,5-tetramethylimidazoline-1-oxyl-3-oxide.

(Table V.5). Hydrolysis of phytic acid by phytase has previously been shown to result in secretion of *ortho*-phosphate into the incubation medium of barley aleurone layers [154, 169], but the question is if endogenous phytases are able to liberate phosphate from exogenous phytic acid sources. This requires either the presence of phytases in the cell wall or the exterior of the plasma membrane, or the transport of phytic acid into the cells to make it available for phytases located in the endoplasmic reticulum or the protein storage vacuoles. Based on the increases in phytase activity observed for all treatments over the time course study, at least one of these options holds true, but further investigations are needed to determine the exact location of the measured phytase activity.

From a practical point of view, the use of the phytase activity assay was just as easily incorporated into an ongoing incubation in the new incubation system for immobilised aleurone layer punch-outs as the commercial amylase activity assay: The lid with the punch-outs were simply moved from the incubation plate to the assay plate containing the substrate, the assay was performed, and then the lid was placed back in the incubation plate. However, the obtained measurements suffer from both low levels of activity and high deviations, as was the case for the amylase activity assay. Enabling activity measurements with the immobilised setup will therefore require further optimisation of the substrate solution (concentration, pH, buffer composition), optimisation of the incubation time, and possibly also pooling of samples prior to addition of the vanadate-molybdate reagent to obtain measurable levels of phytase activity in the samples. Unfortunately, as for the amylase activity assay, pooling of samples will increase the work load required for activity measurements, which is in contrast to the intentions with the new incubation system (Section I.6, page 17). Finally, as mentioned for the amylase activity assay, a last possibility will be to use larger amounts of plant material, which should result in higher activities of phytase. However, using intact aleurone layers will lead back to the problem with normalisation of data by dry weight, which was solved by the use of punch-outs (Section I.6, page 17).

Table V.5: TargetP analysis of barley phytases (*PAPhy*_b)

Enzyme	Prediction scores			Predicted	Reliability
	Mitochondria	Secretory pathway	Other location	location	class
HvPAPhy_b1 (ACR23332)	0.086	0.843	0.030	S	2
HvPAPhy_b2 (ACR23333)	0.043	0.876	0.042	S	1

Prediction scores: Final scores on which the final prediction of location is based. Scores are not probabilities, but the location with the highest score is the most likely according to TargetP, and the relationship between the scores (the reliability class) may be an indication of how certain the prediction is. S: Secretory pathway. Reliability class: Ranges from 1 to 5, where 1 indicates the strongest prediction. Reliability class is a measure of the size of the difference between the highest and the second highest prediction scores. GenBank accession numbers are listed in parentheses [167]. Text adapted from [145].

Part VI

Summary and concluding remarks

The main aim of this PhD project was to expand the current knowledge of ROS signalling and PCD in plant cells through the use of the barley aleurone layer as a biological model system. To overcome the limitations of end-point analyses, which are commonly employed for studies of ROS and PCD, and to enable time course studies on the same plant tissue, this project has focused on the use of methods that do not destroy cellular integrity. The first part of the project therefore focused on the optimisation and application of non-destructive detection techniques for living cells, whereas the second part focused primarily on the development of an incubation system for immobilised plant tissues and the possible applications of this system within time-dependent investigations in plant biology.
This section will summarise the answers obtained to the intermediate questions posed as part of the scientific aims (Section I.1, page 2).

VI.1 Results obtained by traditional aleurone layer incubations

- Can redox activity/redox homeostasis be measured in intact plant tissue?

A previously described method [79] for electrochemical detection of intracellular redox activity was successfully tested and optimised for use with barley aleurone layers (Figures II.2 and II.3, pages 32 and 33). This double mediator system had not previously been used in plant biology and provided new insight about the intracellular reducing capacity in living cells that has not previously been obtained with cell extracts. A comparison of measurements performed with either both or just one mediator showed that the reducing capacity was not solely intracellular but contained an extracellular component as well (Figure II.5, page 36). Investigations showed that this extracellular component was cell wall- or plasma membrane-associated and that it accounted for approximately two thirds of the total reducing capacity (Figure II.6, page 37).
A spectrophotometric redox activity assay [138] was tested as an alternative to the electrochemical assay, which yielded similar results but suffered from large deviations and a large work load, both probably due to a systematic error from the multiple pipetting steps necessary (Figure III.2, page 46).

- How does cell viability and redox activity correlate in the aleurone layer?

A previously described optical method [12] was used to monitor PCD to confirm the basal response of barley aleurone layers to GA- and ABA-treatments. A delay in the onset of PCD in response to GA was observed (Figure II.4B, page 35) compared to previous results [12], but this could have been caused by different seed batches, buffers, hormone concentrations, and physical

incubation conditions. As the general trend of increased PCD in the presence of GA and maintained levels of PCD in the presence of ABA was determined, this difference in time of onset of PCD was regarded as inconsequential.
The electrochemical redox assay was used to show that the reducing capacity of aleurone cells increase over time in parallel with the increase in cell death for GA-treated aleurone layers (Figure II.4A, page 35). This increased reducing capacity was hypothesised to be a mechanism by which the aleurone cells may counteract the oxidative stress resulting from increased levels of ROS, and thereby be a way to hold the previously proposed 'oxidative window' [61] open long enough to complete the synthesis and release of hydrolytic enzymes required for germination of the embryo.

- What is the role of the plasma membrane-bound NADPH oxidase in redox homeostasis?

Given the known involvement of NADPH oxidase in the redox environment [61], the effect of the unspecific flavoenzyme inhibitor DPI on both total and extracellular reducing capacity was explored, again using the electrochemical redox assay. DPI was found to have a decreasing effect on both total and extracellular reducing capacity of GA-treated aleurone layers, indicating that a GA-induced increase in reducing capacity is dependent on the NADPH oxidase (Figure II.7A, page 38). This was confirmed with the spectrophotometric redox activity assay (Figure III.3, page 47), but further work with the spectrophotometric assay was abolished, as the electrochemical assay yielded more reproducible results, possibly due to the high dilution factor of 20 necessary for the spectrophotometrical assay. DPI was also shown to increase cell death slightly of GA-treated aleurone layers in parallel to the observed decrease in reducing capacity (Figure II.7, page 38), supporting the hypothesis that increased reducing capacity could be a mechanism by which the aleurone cells hold the 'oxidative window' open.
A preliminary proteomics experiment was performed to further investigate the effect of DPI on the protein abundance profiles of barley aleurone layer extracts (Section III.2, page 49). The study suffered from a low amount of identified proteins and will require repetition, but as the basal response of barley aleurone layers to GA- and ABA-treatments was confirmed, data analysis was performed despite this. Interestingly, the abundance level of glyceraldehyde-3-phosphate dehydrogenase 2 (GAPDH2) was found to be 2.6-fold upregulated in the presence of GA+DPI compared to GA alone (Figure III.4, page 50). This was hypothesised to be an indirect effect of the inhibition of NADPH oxidase, as this would lead to reduced levels of $NADP^+$ and NAD^+, resulting in decreased activity of GAPDH2. This would then prompt the cell to upregulate the enzyme in an attempt to maintain cellular carbohydrate metabolism. This enzyme would therefore be an obvious candidate for further studies of the effect of DPI in ROS signalling and PCD. However, abundance levels of the paralogue glyceraldehyde-3-phosphate dehydrogenase 1 (GAPDH1) were unchanged in the presence of DPI, which could be caused by lower effect of DPI due to a higher probability of a mitochondrial location of GAPDH1 compared to GAPDH2. As the enzymes are highly similar, further studies are needed to determine if this is truly the case.

Also, further investigations, including a repetition of the proteomics experiment, of the effect of DPI would be needed to determine the full extent of this enzyme on protein abundance levels.

VI.2 Results obtained with the developed incubation system

- Can the same living plant tissue be studied over time using detection techniques that do not destroy cellular integrity?
- Can multiple non-destructive techniques be combined to measure multiple parameters in such time course studies?

Having verified the applicability of both the cell viability and the redox activity assay, the focus of the project then shifted to the development of an incubation system for immobilised plant tissues that would allow the use of both these non-destructive techniques in time course studies on the same tissue (Figures I.11 and IV.1, pages 22 and 65). Immobilisation of the tissues in the lid of a 24-well plate facilitated easy combination of multiple assays by movement of the plate lid (Figure IV.2, page 66), lessened the workload by decreasing the amount of samples fivefold and the amount of dissected aleurone layers 25-fold, and enabled a higher throughput. The immobilised approach was also amenable to transient gene expression analysis by particle bombardment.
The first experiments with the developed incubation system tested the time-dependent effect of immobilisation on both cell viability and redox activity in parallel, confirming the use of the system for time course studies combining multiple non-destructive assays. The additional handling required for immobilisation of tissues was found to result in increased basal levels of dead cells compared to non-immobilised whole aleurone layers (Figure IV.3A, page 67). The rates of cell death for GA-treated immobilised aleurone layers and punch-outs were found to be slower compared to non-immobilised aleurone layers (Figure IV.3B, page 67), which was hypothesised to be caused by the lower exposure of immobilised tissues to the incubation buffer. Similarly, the reducing capacity was found to be severely reduced for immobilised tissues compared to non-immobilised aleurone layers (Figure IV.4, page 68). This was not a biological change between non-immobilised and immobilised tissues, but rather resulted from the lower amount of cells present in the immobilised punch-outs (approximately 15 times). Despite this issue of sensitivity, a higher increase in reducing capacity over time could be detected for GA- compared to ABA-treatment for both immobilised and non-immobilised tissues. Optimisation of the spectrophotometrical redox activity assay for use with the developed incubation system might solve the sensitivity issue as described in Section III.1 (page 43).
The aim of combining multiple assays with the developed system was further tested using a commercial α-amylase activity assay [160] and a previously described phytase activity assay [162, 163]. From a practical point of view both assays were easy to use with the system, as the lid with the aleurone layers were simply moved to a different 24-well plate for the phytase assay, while required volumes of the incubation buffer was extracted from the original incubation plate

for the α-amylase assay. However, the measurements obtained with both assays suffered from low levels of activity and high variations (Figures V.3 and V.4, pages 67 and 68), which indicates that the enzyme levels were very close to the detection level of the assay, rendering confident analysis of the data almost impossible. Enabling enzyme activity measurements using the developed system will therefore require further optimisation of these assays as described in Sections V.2 and V.3 (pages 83 and 86).

- How does transient expression of GFP controlled by target enzyme promoters correlate with cell viability in the aleurone layer?

The developed system was used to transform aleurone layers by particle bombardment and to subsequently monitor transient expression and cell viability in parallel over time (Figure IV.6, page 71). The immobilised approach enabled single transformed cells to be followed over time and provided an insight into the cell-to-cell variability of the actual transformation event, yielding a more detailed picture of transient expression profiles of target enzymes compared to traditional approaches.

- How does cell viability and redox activity change in the aleurone layer in response to phytohormones or other effector compounds?

Time course studies of cell viability in the presence of a range of different effector compounds was also performed with the developed incubation system. Previous findings of the effects of the compounds T, cPTIO, SNP, and NaN_3 on GA- and ABA-treated aleurone layers were confirmed (Figures IV.5A, V.1 and V.2, pages 69, 79 and 81) [7, 47, 48, 52]. Neither dicoumarol, DPI, nor AsA was found to have an effect on the rate of cell death of GA-treated aleurone layers. However, cell death was induced earlier with both dicoumarol and DPI compared to GA alone, confirming previous observations with DPI (Figure II.7B, page 38), while AsA delayed cell death in agreement with its role as a ROS scavenger (Figure V.2, page 71).
Reducing capacity was observed in parallel to the time course study of cell viability for the compounds T, SNP and cPTIO. T, an inducer of protein unfolding in the endoplasmic reticulum, induced an increased level of reducing capacity, while the NO donor SNP prevented such an increase, mirroring their effects on cell viability. Opposite to its effect on cell viability, the NO scavenger cPTIO did not induce a change in the level of reducing capacity compared to GA alone (Figure IV.5B, page 69), which is surprising considering the known interactions between ROS and NO (Figure I.6, page 10). Novel information was thereby obtained with the developed incubation system regarding the different PCD-inducing mechanisms of T and cPTIO, as induction of PCD by T either causes or is dependent on increased reducing capacity, while cPTIO appears to have no connection to reducing capacity.

VI.3 Main conclusions

Using optical and electrochemical detection techniques, this project has obtained new knowledge of increases in intra- and extracellular reducing capacity taking place in parallel with increases in PCD, and proposed this increased reducing capacity as a mechanism for holding the 'oxidative window' for germination open. The involvement of the NADPH oxidase or other flavoenzymes in determining the level of GA-induced reducing capacity was also shown using the inhibitor DPI. A preliminary proteomics investigations revealed that GAPDH2 was upregulated in the presence of DPI, possibly due to DPI-induced lower levels of NAD^+, resulting in lower activity of GAPDH2. As mentioned above, further investigations of the effect of DPI would be needed to determine which other enzymes are affected by this compound.
A new incubation system for immobilised aleurone layers was also developed, which enabled simple, user-friendly handling of plant tissue incubations and facilitated transient expression studies in plant tissues by particle bombardment as well as time course studies on the same population of cells combining multiple non-destructive assays. Future applications of this type of setup could be used for other types of plant tissues such as leaves or germinating embryos for studying the effects of e.g. biotic and abiotic stresses or for screening of compounds for biological effects. Due to the ease of use and many possibilities of assay combinations, the setup has great potential in the area of plant science.

References

[1] De Pinto MC, Locato V, De Gara L (2012) Redox regulation in plant programmed cell death. Plant, Cell & Environment 35: 234–244.

[2] van Doorn WG (2011) Classes of programmed cell death in plants, compared to those in animals. Journal of Experimental Botany 62: 4749–4761.

[3] Van Hautegem T, Waters AJ, Goodrich J, Nowack MK (2014) Only in dying, life: programmed cell death during plant development. Trends in Plant Science .

[4] Gechev TS, Van Breusegem F, Stone JM, Denev I, Laloi C (2006) Reactive oxygen species as signals that modulate plant stress responses and programmed cell death. BioEssays 28: 1091–1101.

[5] Bozhkov PV, Lam E (2011) Green death: revealing programmed cell death in plants. Cell Death and Differentiation 18: 1239–1240.

[6] Lam E, Pontier D, del Pozo O (1999) Die and let live - programmed cell death in plants. Current Opinion in Plant Biology 2: 502–507.

[7] Barba-Espín G, Dedvisitsakul P, Hägglund P, Svensson B, Finnie C (2014) Gibberellic acid-induced aleurone layers responding to heat shock or tunicamycin provide insight into the *N*-glycoproteome, protein secretion, and endoplasmic reticulum stress. Plant Physiology 164: 951–965.

[8] Finnie C, Andersen B, Shahpiri A, Svensson B (2011) Proteomes of the barley aleurone layer: A model system for plant signalling and protein secretion. Proteomics 11: 1595–1605.

[9] Ishibashi Y, Tawaratsumida T, Kondo K, Kasa S, Sakamoto M, et al. (2012) Reactive oxygen species are involved in gibberellin/abscisic acid signaling in barley aleurone cells. Plant Physiology 158: 1705–1714.

[10] Bønsager BC, Shahpiri A, Finnie C, Svensson B (2010) Proteomic and activity profiles of ascorbate-glutathione cycle enzymes in germinating barley embryo. Phytochemistry 71: 1650–1656.

[11] Bush DS, Cornejo MJ, Huang CN, Jones RL (1986) Ca^{2+}-Stimulated Secretion of α-Amylase During Development in Barley Aleurone Protoplasts. Plant Physiology 82: 566–574.

[12] Fath A, Bethke PC, Jones RL (2001) Enzymes That Scavenge Reactive Oxygen Species Are Down-Regulated Prior to Gibberellic Acid-Induced Programmed Cell Death in Barley Aleurone. Plant Physiology 126: 156–166.

[13] Fath A, Bethke PC, Beligni V, Jones RL (2002) Active oxygen and cell death in cereal aleurone cells. Journal of Experimental Botany 53: 1273–1282.

[14] Ishibashi Y, Tawaratsumida T, Zheng Sh, Yuasa T, Iwaya-Inoue M (2010) NADPH Oxidases Act as Key Enzyme on Germination and Seedling Growth in Barley (*Hordeum vulgare* L.). Plant Production Science 13: 45–52.

[15] Jones RL, Jacobsen JV (1983) Planta of α-amylase isoenzymes and other proteins from barley aleurone layers. Planta 158: 1–9.

[16] Palma K, Kermode AR (2003) Metabolism of hydrogen peroxide during reserve mobilization and programmed cell death of barley (*Hordeum vulgare* L.) aleurone layer cells. Free Radical Biology & Medicine 35: 1261–1270.

[17] Ritchie S, Gilroy S (1998) Abscisic acid signal transduction in the barley aleurone is mediated by phospholipase D activity. Proceedings of the National Academy of Sciences of the United States of America 95: 2697–2702.

[18] Bethke PC, Lonsdale JE, Fath A, Jones RL (1999) Hormonally regulated programmed cell death in barley aleurone cells. The Plant Cell 11: 1033–1046.

[19] Fath A, Bethke PC, Jones RL (1999) Barley aleurone cell death is not apoptotic: characterization of nuclease activities and DNA degradation. The Plant Journal 20: 305–315.

[20] Baik BK, Ullrich SE (2008) Barley for food: Characteristics, improvement, and renewed interest. Journal of Cereal Science 48: 233–242.

[21] Sullivan P, Arendt E, Gallagher E (2013) The increasing use of barley and barley by-products in the production of healthier baked goods. Trends in Food Science & Technology 29: 124–134.

[22] Plantpro (2005) All about barley! Morphology. Accessed 2014.18.12: Leonardo da Vinci Programme, European Union. URL `http://www.plantprotection.hu/modulok/angol/barley/morf01_bar.htm`.

[23] Olsen OA (2001) Endosperm Development: Cellularization and Cell Fate Specification. Annual Review of Plant Physiology and Plant Molecular Biology 52: 233–267.

[24] Fath A, Bethke PC, Lonsdale JE, Meza-Romero R, Jones RL (2000) Programmed cell death in cereal aleurone. Plant Molecular Biology 44: 255–266.

[25] Finnie C, Svensson B (2009) Barley seed proteomics from spots to structures. Journal of Proteomics 72: 315–324.

[26] Buchanan BB, Balmer Y (2005) Redox regulation: a broadening horizon. Annual Review of Plant Biology 56: 187–220.

[27] Eckardt NA (2007) GA Signaling: Direct Targets of DELLA Proteins. The Plant Cell 19: 2970.

[28] Gómez-Cadenas A, Zentella R, Walker-Simmons MK, Ho ThD (2001) Gibberellin/Abscisic Acid Antagonism in Barley Aleurone Cells: Site of Action of the Protein Kinase PKABA1 in Relation to Gibberellin Signaling Molecules. The Plant Cell 13: 667–679.

[29] Guo WJ, Ho ThD (2008) An abscisic acid-induced protein, HVA22, inhibits gibberellin-mediated programmed cell death in cereal aleurone cells. Plant Physiology 147: 1710–1722.

[30] Gutierrez L, Van Wuytswinkel O, Castelain M, Bellini C (2007) Combined networks regulating seed maturation. Trends in Plant Science 12: 294–300.

[31] Hirano K, Ueguchi-Tanaka M, Matsuoka M (2008) GID1-mediated gibberellin signaling in plants. Trends in Plant Science 13: 192–199.

[32] Bethke PC, Fath A, Spiegel YN, Hwang Ys, Jones RL (2002) Abscisic acid, gibberellin and cell viability in cereal aleurone. Euphytica 126: 3–11.

[33] Bewley JD (1997) Seed Germination and Dormancy. The Plant Cell 9: 1055–1066.

[34] Maya-Ampudia V, Bernal-Lugo I (2006) Redox-sensitive target detection in gibberellic acid-induced barley aleurone layer. Free Radical Biology & Medicine 40: 1362–1368.

[35] Aoki N, Ishibashi Y, Kai K, Tomokiyo R, Yuasa T, et al. (2014) Programmed cell death in barley aleurone cells is not directly stimulated by reactive oxygen species produced in response to gibberellin. Journal of Plant Physiology 171: 615–618.

[36] Bethke PC, Jones RL (2001) Cell death of barley aleurone protoplasts is mediated by reactive oxygen species. The Plant Journal 25: 19–29.

[37] Hoeberichts FA, Woltering EJ (2003) Multiple mediators of plant programmed cell death: interplay of conserved cell death mechanisms and plant-specific regulators. BioEssays 25: 47–57.

[38] Kuriyama H, Fukuda H (2002) Developmental programmed cell death in plants. Current Opinion in Plant Biology 5: 568–573.

[39] Pennell RI, Lamb C (1997) Programmed Cell Death in Plants. The Plant Cell 9: 1157–1168.

[40] Jones A (2000) Does the plant mitochondrion integrate cellular stress and regulate programmed cell death? Trends in Plant Science 5: 225–230.

[41] Laloi C, Apel K, Danon A (2004) Reactive oxygen signalling: the latest news. Current Opinion in Plant Biology 7: 323–328.

[42] Sun YL, Zhao Y, Hong X, Zhai ZH (1999) Cytochrome *c* release and caspase activation during menadione-induced apoptosis in plants. FEBS Letters 462: 317–321.

[43] Avila JR (2015) Physiology and function of PCD in Vascular Plants. Accessed 2015.01.06. URL `http://jr-avila.com/bio/images/tamu/CellDeathjpg.jpg`.

[44] Lam E (2004) Controlled cell death, plant survival and development. Nature Reviews Molecular Cell Biology 5: 305–315.

[45] Stovall G (2013) Plant Cell. Published 2013.11.28, accessed 2015.01.07. URL `http://pulpbits.com/wp-content/uploads/2013/11/Unlabeled-Plant-Cell-pic-1.jpg`.

[46] Lamb C, Dixon RA (1997) The oxidative burst in plant disease resistance. Annual Review of Plant Physiology and Plant Molecular Biology 48: 251–275.

[47] Beligni MV, Fath A, Bethke PC, Lamattina L, Jones RL (2002) Nitric Oxide Acts as an Antioxidant and Delays Programmed Cell Death in Barley Aleurone Layers. Plant Physiology 129: 1642–1650.

[48] Bethke PC, Badger MR, Jones RL (2004) Apoplastic Synthesis of Nitric Oxide by Plant Tissues. American Society of Plant Biologists 16: 332–341.

[49] Chalmers JDC, Coleman JOD, Walton NJ (1984) Use of an electrochemical technique to study plasmamembrane redox reactions in cultured cells of *Daucus carota* L. Plant Cell Reports 3: 243–246.

[50] de Jong A, Yakimova E, Kapchina V, Woltering E (2002) A critical role for ethylene in hydrogen peroxide release during programmed cell death in tomato suspension cells. Planta 214: 537–545.

[51] Gilroy S, Jones RL (1992) Gibberellic acid and abscisic acid coordinately regulate cytoplasmic calcium and secretory activity in barley aleurone protoplasts. Proceedings of the National Academy of Sciences of the United States of America 89: 3591–3595.

[52] Park H, Park M, Yim Hk, Park S, Jin E, et al. (2010) Inhibition of Oxidative Phosphorylation Induces a Rapid Death of GA-Pretreated Aleurone Cells, But Not of ABA-Pretreated Aleurone Cells. Journal of Plant Biology 53: 205–213.

[53] Truernit E, Haseloff J (2008) A simple way to identify non-viable cells within living plant tissue using confocal microscopy. Plant Methods 4.

[54] Desikan R, Hancock JT, Coffey MJ, Neill SJ (1996) Generation of active oxygen in elicited cells of *Arabidopsis thaliana* is mediated by a NADPH oxidase-like enzyme. FEBS Letters 382: 213–217.

[55] Govrin EM, Levine A (2000) The hypersensitive response facilitates plant infection by the necrotrophic pathogen *Botrytis cinerea*. Current Biology 10: 751–757.

[56] Inoue H, Kamoda S, Terada T, Hamamoto H, Saburi Y (2007) Menadione-induced cell death in *Ginkgo biloba* cell cultures. Bulletin of the Tokyo University Forests 118: 25–43.

[57] Towill LE, Mazur P (1975) Studies on the reduction of 2,3,5-triphenyltetrazolium chloride as a viability assay for plant tissue cultures. Canadian Journal of Botany 53: 1097–1102.

[58] Winterbourn CC (2008) Reconciling the chemistry and biology of reactive oxygen species. Nature Chemical Biology 4: 278–286.

[59] Dietz KJ (2003) Redox Control, Redox Signaling, and Redox Homeostasis in Plant Cells. International Review of Cytology 228: 141–193.

[60] Navrot N, Finnie C, Svensson B, Hägglund P (2011) Plant redox proteomics. Journal of Proteomics 74: 1450–1462.

[61] Bailly C, El-Maarouf-Bouteau H, Corbineau F (2008) From intracellular signaling networks to cell death: the dual role of reactive oxygen species in seed physiology. Comptes Rendus Biologies 331: 806–814.

[62] Greenshields DL, Liu G, Selvaraj G, Wei Y (2005) Differential regulation of wheat quinone reductases in response to powdery mildew infection. Planta 222: 867–875.

[63] Foreman J, Demidchik V, Bothwell JHF, Mylona P, Miedema H, et al. (2003) Reactive oxygen species produced by NADPH oxidase regulate plant cell growth. Nature 422: 442–446.

[64] Schopfer P, Plachy C, Frahry G (2001) Release of Reactive Oxygen Intermediates (Superoxide Radicals, Hydrogen Peroxide, and Hydroxyl Radicals) and Peroxidase in Germinating Radish Seeds Controlled by Light, Gibberellin, and Abscisic Acid. Plant Physiology 125: 1591–1602.

[65] Vranová E, Inzé D, Van Breusegem F (2002) Signal transduction during oxidative stress. Journal of Experimental Botany 53: 1227–1236.

[66] Bailly C (2004) Active oxygen species and antioxidants in seed biology. Seed Science Research 14: 93–107.

[67] Bethke PC, Gubler F, Jacobsen JV, Jones RL (2004) Dormancy of *Arabidopsis* seeds and barley grains can be broken by nitric oxide. Planta 219: 847–855.

[68] Bolwell GP, Wojtaszek P (1997) Mechanisms for the generation of reactive oxygen species in plant defence - a broad perspective. Physiological and Molecular Plant Pathology 51: 347–366.

[69] El-Maarouf-Bouteau H, Bailly C (2008) Oxidative signaling in seed germination and dormancy. Plant Signaling & Behavior 3: 175–182.

[70] Bérczi A, Møller IM (2000) Redox enzymes in the plant plasma membrane and their possible roles. Plant, Cell & Environment 23: 1287–1302.

[71] Heyno E, Alkan N, Fluhr R (2013) A dual role for plant quinone reductases in host-fungus interaction. Physiologia Plantarum 149: 340–353.

[72] Schopfer P, Heyno E, Drepper F, Krieger-Liszkay A (2008) Naphthoquinone-dependent generation of superoxide radicals by quinone reductase isolated from the plasma membrane of soybean. Plant Physiology 147: 864–878.

[73] Rubinstein B, Stern AI, Chalmers JDC (1990) Measurements of redox activity at the plasmalemma. Physiologia Plantarum 80: 479–486.

[74] Liu B, Rotenberg SA, Mirkin MV (2000) Scanning electrochemical microscopy of living cells: Different redox activities of nonmetastatic and metastatic human breast cells. Proceedings of the National Academy of Sciences of the United States of America 97: 9855–9860.

[75] Rabinowitz JD, Vacchino JF, Beeson C, Mcconnell HM (1998) Potentiometric Measurement of Intracellular Redox Activity. Journal of the American Chemical Society 120: 2464–2473.

[76] Rahimi M, Youn HY, McCanna DJ, Sivak JG, Mikkelsen SR (2013) Application of cyclic biamperometry to viability and cytotoxicity assessment in human corneal epithelial cells. Analytical and Bioanalytical Chemistry 405: 4975–4979.

[77] Baronian KHR, Downard AJ, Lowen RK, Pasco N (2002) Detection of two distinct substrate-dependent catabolic responses in yeast cells using a mediated electrochemical method. Applied Microbiology and Biotechnology 60: 108–113.

[78] Heiskanen AR, Yakovleva J, Spégel C, Taboryski R, Koudelka-Hep M, et al. (2004) Amperometric monitoring of redox activity in living yeast cells: comparison of menadione and menadione sodium bisulfite as electron transfer mediators. Electrochemistry Communications 6: 219–224.

[79] Heiskanen AR, Spégel C, Kostesha N, Lindahl S, Ruzgas T, et al. (2009) Mediator-assisted simultaneous probing of cytosolic and mitochondrial redox activity in living cells. Analytical Biochemistry 384: 11–19.

[80] Heiskanen AR, Coman V, Kostesha N, Sabourin D, Haslett N, et al. (2013) Bioelectrochemical probing of intracellular redox processes in living yeast cells–application of redox polymer wiring in a microfluidic environment. Analytical and Bioanalytical Chemistry 405: 3847–3858.

[81] Zór K, Vergani M, Heiskanen AR, Landini E, Carminati M, et al. (2011) Real-time monitoring of cellular dynamics using a microfluidic cell culture system with integrated electrode array and potentiostat. In: 15th International Conference on Miniaturized Systems for Chemistry and Life Sciences, October 2-6, Seattle, Washington, USA. pp. 1532–1535.

[82] Coman V, Gustavsson T, Finkelsteinas A, von Wachenfeldt C, Hägerhäll C, et al. (2009) Electrical wiring of live, metabolically enhanced *Bacillus subtilis* cells with flexible osmium-redox polymers. Journal of the American Chemical Society 131: 16171–16176.

[83] Kondo T, Ikeda T (2000) Rapid Detection of Substrate-Oxidising Activity of *Hiochi* Bacteria Using Benzoquinone-Mediated Amperometric Method. Journal of Bioscience and Bioengineering 90: 217–219.

[84] Harvey D (2009) Electrochemical Methods. In: Analytical Chemistry 2.0: An Electronic Textbook for Introductory Courses in Analytical Chemistry, Accessed 2015.01.06, chapter 11. pp. 667–782. URL `http://acad.depauw.edu/harvey_web/eText%Project/AnalyticalChemistry2.0.html`.

[85] Chareonthiphakorn N, Wititsuwannakul D, Golan-Goldhirsh A, Wititsuwannakul R (2002) Purification and characterization of NAD(P)H quinone reductase from the latex of *Hevea brasiliensis* Müll.-Arg. (Euphorbiaceae). Phytochemistry 61: 123–128.

[86] Lüthje S, Möller B, Perrineau FC, Wöltje K (2013) Plasma membrane electron pathways and oxidative stress. Antioxidants & Redox Signaling 18: 2163–2183.

[87] Trost P, Foscarini S, Preger V, Bonora P, Vitale L, et al. (1997) Dissecting the Diphenylene Iodonium-Sensitive NAD(P)H:Quinone Oxidoreductase of Zucchini Plasma Membrane. Plant Physiology 114: 737–746.

[88] Valenti V, Guerrini F, Pupillo P (1990) NAD(P)H-Duroquinone Reductase in the Plant Plasma Membrane. Journal of Experimental Botany 41: 183–192.

[89] Viljoen CC, Cloete F, Botes DP, Kruger H (1983) Isolation and characterization of NAD(P)H-dehydrogenases from seeds of the castor bean. Phytochemistry 22: 365–370.

[90] Rao AQ, Bakhsh A, Kiani S, Shahzad K, Shahid AA, et al. (2009) The myth of plant transformation. Biotechnology Advances 27: 753–763.

[91] Rivera AL, Gómez-Lim M, Fernández F, Loske AM (2012) Physical methods for genetic plant transformation. Physics of Life Reviews 9: 308–345.

[92] Hansen G, Wright MS (1999) Recent advances in the transformation of plants. Trends in Plant Science 4: 226–231.

[93] Fischer R, Vaquero-Martin C, Sack M, Drossard J, Emans N, et al. (1999) Towards molecular farming in the future: transient protein expression in plants. Biotechnology and Applied Biochemistry 116: 113–116.

[94] Potrykus I (1991) Gene Transfer To Plants: Assessment of Published Approaches and Results. Annual Review of Plant Physiology and Plant Molecular Biology 42: 205–225.

[95] Bio-Rad Laboratories (2015) Biolistic Deliviry Systems. Accessed 2015.01.06. URL `http://www.bio-rad.com/webroot/web/pdf/lsr/literature/Bulletin_5443.pdf`.

[96] Bio-Rad Laboratories (2015) Biolistic PDS-1000/He Particle Delivery System. Accessed 2015.01.06. URL `http://www.bio-rad.com/webroot/web/pdf/lsr/literature/M1652249.pdf`.

[97] Casaretto J, Ho ThD (2003) The Transcription Factors HvABI5 and HvVP1 Are Required for the Abscisic Acid Induction of Gene Expression in Barley Aleurone Cells. The Plant Cell 15: 271–284.

[98] Cercós M, Gómez-Cadenas A, Ho ThD (1999) Hormonal regulation of a cysteine proteinase gene, *EPB-1*, in barley aleurone layers: cis- and trans-acting elements involved in the coordinated gene expression regulated by gibberellins and abscisic acid. The Plant Journal 19: 107–118.

[99] Gómez-Cadenas A, Verhey SD, Holappa LD, Shen Q, Ho THD, et al. (1999) An abscisic acid-induced protein kinase, PKABA1, mediates abscisic acid-suppressed gene expression in barley aleurone layers. Proceedings of the National Academy of Sciences of the United States of America 96: 1767–1772.

[100] Gubler F, Raventos D, Keys M, Watts R, Mundy J, et al. (1999) Target genes and regulatory domains of the GAMYB transcriptional activator in cereal aleurone. The Plant Journal 17: 1–9.

[101] Harris LJ, Martinez SA, Keyser BR, Dyer WE, Johnson RR (2013) Functional analysis of TaABF1 during abscisic acid and gibberellin signalling in aleurone cells of cereal grains. Seed Science Research 23: 89–98.

[102] Lanahan M, Ho ThD, Rogers SW, Rogers JC (1992) A Gibberellin Response Complex in Cereal α-Amylase Gene Promoters. The Plant Cell 4: 203–211.

[103] Mena Mn, Cejudo FJ, Isabel-Lamoneda I, Carbonero P (2002) A Role for the DOF Transcription Factor BPBF in the Regulation of Gibberellin-Responsive Genes in Barley Aleurone. Plant Physiology 130: 111–119.

[104] Shen Q, Uknes SJ, Ho ThD (1993) Hormone Response Complex in a Novel Abscisic Acid and Cycloheximide-inducible Barley Gene. The Journal of Biological Chemistry 268: 23652–23660.

[105] Stacy RAP, Munthe E, Steinum T, Sharma B, Aalen RB (1996) A peroxiredoxin antioxidant is encoded by a dormancy-related gene, *Perl*, expressed during late development in the aleurone and embryo of barley grains. Plant Molecular Biology 31: 1205–1216.

[106] Xie Z, Zhang ZL, Zou X, Huang J, Ruas P, et al. (2005) Annotations and Functional Analyses of the Rice *WRKY* Gene Superfamily Reveal Positive and Negative Regulators of Abscisic Acid Signaling in Aleurone Cells. Plant Physiology 137: 176–189.

[107] Zou X, Neuman D, Shen QJ (2008) Interactions of two transcriptional repressors and two transcriptional activators in modulating gibberellin signaling in aleurone cells. Plant Physiology 148: 176–186.

[108] Furtado A, Henry R, Scott K, Meech S (2003) The promoter of the asi gene directs expression in the maternal tissues of the seed in transgenic barley. Plant Molecular Biology 52: 787–799.

[109] Hong YF, Ho ThD, Wu CF, Ho SL, Yeh RH, et al. (2012) Convergent starvation signals and hormone crosstalk in regulating nutrient mobilization upon germination in cereals. The Plant Cell 24: 2857–2873.

[110] Isabel-LaMoneda I, Diaz I, Martinez M, Mena Mn, Carbonero P (2003) SAD: a new DOF protein from barley that activates transcription of a cathepsin B-like thiol protease gene in the aleurone of germinating seeds. The Plant Journal 33: 329–340.

[111] Martínez M, Rubio-Somoza I, Fuentes R, Lara P, Carbonero P, et al. (2005) The barley cystatin gene (*Icy*) is regulated by DOF transcription factors in aleurone cells upon germination. Journal of Experimental Botany 56: 547–556.

[112] Moreno-Risueno MA, Díaz I, Carrillo L, Fuentes R, Carbonero P (2007) The HvDOF19 transcription factor mediates the abscisic acid-dependent repression of hydrolase genes in germinating barley aleurone. The Plant Journal 51: 352–365.

[113] Rubio-Somoza I, Martinez M, Diaz I, Carbonero P (2006) HvMCB1, a R1MYB transcription factor from barley with antagonistic regulatory functions during seed development and germination. The Plant Journal 45: 17–30.

[114] Rubio-Somoza I, Martinez M, Abraham Z, Diaz I, Carbonero P (2006) Ternary complex formation between HvMYBS3 and other factors involved in transcriptional control in barley seeds. The Plant Journal 47: 269–281.

[115] Jefferson Ra (1987) Assaying chimeric genes in plants: The GUS gene fusion system. Plant Molecular Biology Reporter 5: 387–405.

[116] Jacobsen JV, Knox RB (1973) Cytochemical localization and antigenicity of α-amylase in barley aleurone tissue. Planta 112: 213–224.

[117] DiCosmo F, Misawa M (1995) Plant cell and tissue culture: Alternatives for metabolite productions. Biotechnology Advances 13: 425–453.

[118] Ramachandra Rao S, Ravishankar GA (2002) Plant cell cultures: Chemical factories of secondary metabolites. Biotechnology Advances 20: 101–153.

[119] Sajc L, Grubisic D, Vunjak-Novakovic G (2000) Bioreactors for plant engineering: an outlook for further research. Biochemical Engineering Journal 4: 89–99.

[120] Hillmer S, Gilroy S, Jones RL (1992) Visualizing Enzyme Secretion from Individual Barley (*Hordeum vulgare*) Aleurone Protoplasts. Plant Physiology 102: 279–286.

[121] Swanson SJ, Jones RL (1996) Gibberellic Acid lnduces Vacuolar Acidification in Barley Aleurone. The Plant Cell 8: 2211–2221.

[122] Bourgaud F, Gravot A, Milesi S, Gontier E (2001) Production of plant secondary metabolites: a historical perspective. Plant Science 161: 839–851.

[123] Vanisree M, Lee Cy, Lo Sf, Nalawade SM, Lin CY, et al. (2004) Studies on the production of some important secondary metabolites from medicinal plants by plant tissue cultures. Botanical Bulletin of Academia Sinica 45: 1–22.

[124] Sabourin D (2010) Bridging Flows: Microfluidic End-User Solutions. Ph.D. thesis, Technical University of Denmark.

[125] Yetisen aK, Jiang L, Cooper JR, Qin Y, Palanivelu R, et al. (2011) A microsystem-based assay for studying pollen tube guidance in plant reproduction. Journal of Micromechanics and Microengineering 21: 054018.

[126] Meier M, Lucchetta EM, Ismagilov RF (2010) Chemical stimulation of the *Arabidopsis thaliana* root using multi-laminar flow on a microfluidic chip. Lab on a Chip 10: 2147–2153.

[127] Bu M, Perch-Nielsen IR, Sun Y, Wolff A (2011) A microfluidic control system with reusable micropump/valve actuator and injection moulded disposable polymer Lab-On-A-Slide. In: 16th International Solid-State Sensors, Actuators and Microsystems Conference (TRANSDUCERS), June 5-9, Beijing, China. pp. 1244–1247.

[128] Zór K, Heiskanen A, Caviglia C, Vergani M, Landini E, et al. (2014) A compact multifunctional microfluidic platform for exploring cellular dynamics in real-time using electrochemical detection. RSC Advances 4: 63761–63771.

[129] González-Sánchez MI, González-Macia L, Pérez-Prior MT, Valero E, Hancock J, et al. (2013) Electrochemical detection of extracellular hydrogen peroxide in *Arabidopsis thaliana*: A real-time marker of oxidative stress. Plant, Cell and Environment 36: 869–878.

[130] Landini G (2010) Colour Deconvolution (plugin for ImageJ software). Acquired 2013.01.10. URL `http://www.mecourse.com/landinig/software/cdeconv/cdeconv.html`.

[131] Oracz K, El-Maarouf-Bouteau H, Kranner I, Bogatek R, Corbineau F, et al. (2009) The mechanisms involved in seed dormancy alleviation by hydrogen cyanide unravel the role of reactive oxygen species as key factors of cellular signaling during germination. Plant Physiology 150: 494–505.

[132] Lozano RM, Wong JH, Yee BC, Peters A, Kobrehel K, et al. (1996) New evidence for a role for thioredoxin *h* in germination and seedling development. Planta 200: 100–106.

[133] Jones RL (1969) The Effect of Ultracentrifugation on Fine Structure and α-Amylase Production in Barley Aleurone Cells. Plant Physiology 44: 1428–1438.

[134] Neill S, Desikan R, Hancock J (2002) Hydrogen peroxide signalling. Current Opinion in Plant Biology 5: 388–395.

[135] Koyachi E, Kojima K, Qiu X, Satake T, Suzuki H (2013) Electrochemical microdevice for on-site determination of rice freshness. Biosensors and Bioelectronics 42: 640–645.

[136] Nyholm L (2005) Electrochemical techniques for lab-on-a-chip applications. Analyst 130: 599–605.

[137] Xu X, Zhang S, Chen H, Kong J (2009) Integration of electrochemistry in micro-total analysis systems for biochemical assays: Recent developments. Talanta 80: 8–18.

[138] May JM (2010) Assessing the Reductive Capacity of Cells by Measuring the Recycling of Ascorbic and Lipoic Acids. In: Uppu RM, Murthy SN, Pryor WA, Parinandi NL, editors, Free Radicals and Antioxidant Protocols, Humana Press, volume 610 of *Methods in Molecular Biology*, chapter 14. 2 edition, pp. 229–243.

[139] Montás-Ramírez L, Claassen N, Moawad AM (2003) Determination of Fe2+ in Rice Leaves (Oryza sativa L.) by Using the Chelator BPDS Alone or Combined with the Chelator EDTA. Journal of Plant Nutrition 26: 2023–2030.

[140] Piagnani C, Zocchi G (1997) Physiological responses of grapevine callus cultures to iron deficiency. Journal of Plant Nutrition 20: 1539–1549.

[141] Avron M, Shavit N (1963) A Sensitive and Simple Method for Determination of Ferrocyanide. Analytical Biochemistry 6: 549–554.

[142] Korithoski B, Lévesque CM, Cvitkovitch DG (2007) Involvement of the detoxifying enzyme lactoylglutathione lyase in *Streptococcus mutans* aciduricity. Journal of Bacteriology 189: 7586–7592.

[143] UniProt (2015) UniProt Knowledgebase (UniProtKB). Accessed 2015.01.28. URL `http://www.uniprot.org/`.

[144] EMBL-EBI (2015) Ensembl Plants. Accessed 2015.01.28. URL `http://plants.ensembl.org/`.

[145] Center for Biological Sequense Analysis (2015) TargetP 1.1 Server. Accessed 2015.02.14: Technical University of Denmark. URL `http://www.cbs.dtu.dk/services/TargetP/`.

[146] Kishor PBK, Hong Z, Miao GH, Hu CAA, Verma DPS (1995) Overexpression of Δ^1-Pyrroline-5-Carboxylate Synthetase Increases Proline Production and Confers Osmotolerance in Transgenic Plants. Plant Physiology 108: 1387–1394.

[147] Taiz L, Zeiger E (2010) Secondary Metabolites and Plant Defense. In: Plant Physiology, chapter 13. 5 edition, pp. 369–400. URL `http://5e.plantphys.net/`.

[148] Goyal K, Walton LJ, Tunnacliffe A (2005) LEA proteins prevent protein aggregation due to water stress. The Biochemical Journal 388: 151–157.

[149] McAlister GC, Nusinow DP, Jedrychowski MP, Wühr M, Huttlin EL, et al. (2014) MultiNotch MS3 enables accurate, sensitive, and multiplexed detection of differential expression across cancer cell line proteomes. Analytical Chemistry 86: 7150–7158.

[150] Mark C, Zór K, Heiskanen A, Dufva M, Emnéus J, et al. (2015) Electrochemical measurement of the intra- and extracellular redox environment in intact plant tissue responding to phytohormones. Bioelectrochemistry (Submitted) .

[151] Nielsen K, Olsen O, Oliver R (1999) A transient expression system to assay putative antifungal genes on powdery mildew infected barley leaves. Physiological and Molecular Plant Pathology 54: 1–12.

[152] Finnie C, Sultan A, Grasser KD (2011) From protein catalogues towards targeted proteomics approaches in cereal grains. Phytochemistry 72: 1145–1153.

[153] Madsen CK, Dionisio G, Holme IBk, Holm PB, Brinch-Pedersen H (2013) High mature grain phytase activity in the Triticeae has evolved by duplication followed by neofunctionalization of the purple acid phosphatase phytase (*PAPhy*) gene. Journal of Experimental Botany 64: 3111–3123.

[154] Bethke PC, Swanson SJ, Hillmer S, Jones RL (1998) From Storage Compartment to Lytic Organelle: The Metamorphosis of the Aleurone Protein Storage Vacuole. Annals of Botany 82: 399–412.

[155] Christensen AH, Sharrock Ra, Quail PH (1992) Maize polyubiquitin genes: structure, thermal perturbation of expression and transcript splicing, and promoter activity following transfer to protoplasts by electroporation. Plant Molecular Biology 18: 675–689.

[156] Fu D, Huang B, Xiao Y, Muthukrishnan S, Liang GH (2007) Overexpression of barley *hva1* gene in creeping bentgrass for improving drought tolerance. Plant Cell Reports 26: 467–477.

[157] Brinch-Pedersen H, Olesen A, Rasmussen SrK, Holm PB (2000) Generation of transgenic wheat (*Triticum aestivum* L.) for constitutive accumulation of an *Aspergillus* phytase. Molecular Breeding 6: 195–206.

[158] Wosilait WD, Nason A (1954) Pyridine Nucleotide-Menadione Reductase from *Escherichia coli*. The Journal of Biological Chemistry 208: 785–798.

[159] Päpke C, Ramirez-Aguilar S, Antonio C (2014) Oxygen Consumption Under Hypoxic Conditions. In: van Dongen JT, Licausi F, editors, Low-Oxygen Stress in Plants, Springer Vienna, volume 21 of *Plant Cell Monographs*. pp. 185–208.

[160] Sigma-Aldrich Co (2014) Amylase Activity Assay Kit: Technical Bulletin. Accessed 2015.01.11. URL `http://www.sigmaaldrich.com/content/dam/sigma-aldrich/docs/Sigma/Bulletin/1/mak009bul.pdf`.

[161] BioVision Inc (2015) Amylase Activity Colorimetric Assay Kit. Accessed 20115.02.08. URL `http://www.biovision.com/amylase-activity-colorimetric-assay-kit-3732.html`.

[162] Engelen AJ, van der Heeft FC, Randsdorp PHG, Somers WAC, Schaefer J, et al. (2001) Determination of Phytase Activty in Feed by a Colorimetric Enzymatic Method: Collaborative Interlaboratory Study. Journal of AOAC INTERNATIONAL 84: 629–633.

[163] Sanikommu S, Pasupuleti M, Vadalkonda L (2014) Comparison of phosphate estimating methods in the presence of phytic acid for the determination of phytase activity. Preparative Biochemistry & Biotechnology 44: 231–241.

[164] Asmar F (1997) Variation in activity of root extracellular phytase between genotypes of barley. Plant and Soil 195: 61–64.

[165] Centeno C, Viveros A, Brenes A, Canales R, Lozano A, et al. (2001) Effect of Several Germination Conditions on Total P, Phytate P, Phytase, and Acid Phosphatase Activities and Inositol Phosphate Esters in Rye and Barley. Journal of Agricultural and Food Chemistry 49: 3208–3215.

[166] Dilger RN, Onyango EM, Sands JS, Adeola O (2004) Evaluation of Microbial Phytase in Broiler Diets. Poultry Science 83: 962–970.

[167] Dionisio G, Madsen CK, Holm PB, Welinder KG, Jø rgensen M, et al. (2011) Cloning and characterization of purple acid phosphatase phytases from wheat, barley, maize, and rice. Plant Physiology 156: 1087–1100.

[168] Bush DS, Hedrich R, Schroeder JI, Jones RL (1988) Channel-mediated K^+ flux in barley aleurone protoplasts. Planta 176: 368–377.

[169] Hwang Ys, Bethke PC, Gubler F, Jones RL (2003) cPrG-HCl a potential H^+/Cl^- symporter prevents acidification of storage vacuoles in aleurone cells and inhibits GA-dependent hydrolysis of storage protein and phytate. The Plant Journal 35: 154–163.

Appendices

A Presentations

A.1 Oral presentations

Programmed cell death: The life ambition of the barley aleurone layer, 1st INPPO World Congress on Plant Proteomics: Methodology to Biology, Hamburg, Germany, August 31^{st} to September 4^{th} 2014 (selected from abstract)

Using microfluidics to study programmed cell death: A new approach, 25th Congress of the Scandinavian Plant Physiology Society, Elsinore, Denmark, August 11^{th} to 15^{th} 2013 (selected from abstract)

Monitoring programmed cell death of living plant tissues in microfluidics using electrochemical and optical techniques, Annual Plant Biotech Denmark Meeting, Copenhagen, Denmark, January 31^{st} to February 1^{st} 2013 (selected from abstract)

A.2 Poster presentations

Christina Mark[1], Kinga Zór[2], Arto Heiskanen[2], Jenny Emnéus[2], Martin Dufva[3], and Christine Finnie[1]: **Programmed cell death: The life ambition of the barley aleurone layer**, 1st INPPO World Congress on Plant Proteomics: Methodology to Biology, Hamburg, Germany, August 31^{st} to September 4^{th} 2014 (selected for oral presentation from abstract)

Christina Mark[1], Kinga Zór[2], Arto Heiskanen[2], Jenny Emnéus[2], Martin Dufva[3], and Christine Finnie[1]: **Monitoring programmed cell death of living plant tissues in microfluidics using electrochemical and optical techniques**, Plant Biology Congress, Dublin, Ireland, June 22^{nd} to 26^{th} 2014

Christina Mark[1], Kinga Zór[2], Arto Heiskanen[2], Jenny Emnéus[2], Martin Dufva[3], and Christine Finnie[1]: **Electrochemical monitoring of reducing capacity during programmed cell death of plant tissue**, Annual Plant Biotech Denmark Meeting, Copenhagen, Denmark, January 29^{th} to 30^{th} 2014

Christina Mark[1], Kinga Zór[2], Arto Heiskanen[2], Birte Svensson[4], Jenny Emnéus[2], Martin Dufva[3], and Christine Finnie[1]: **Using microfluidics to study programmed cell death: A new approach**, 25th Congress of the Scandinavian Plant Physiology Society, Elsinore, Denmark, August 11^{th} to 15^{th} 2013 (selected for oral presentation from abstract)

Christina Mark[1], Kinga Zór[2], Arto Heiskanen[2], Birte Svensson[4], Jenny Emnéus[2], Martin Dufva[3], and Christine Finnie[1]: **Using microfluidics to study programmed cell death: A new approach**, 9th Protein.DTU Workshop, Kongens Lyngby, Denmark, May 22nd 2013

Christina Mark[1], Kinga Zór[2], Arto Heiskanen[2], Birte Svensson[4], Jenny Emnéus[2], Martin Dufva[3], and Christine Finnie[1]: **Monitoring programmed cell death of living plant tissues in microfluidics using electrochemical and optical techniques**, Annual Plant Biotech Denmark Meeting, Copenhagen, Denmark, January 31st to February 1st 2013 (selected for oral presentation from abstract)

Christina Mark[1], Arto Heiskanen[2], Kinga Zór[2], Birte Svensson[4], Jenny Emnéus[2], Martin Dufva[3], and Christine Finnie[1]: **Microfluidic monitoring of programmed cell death in living plant seed tissue**, Symposium for Biotech Research, Kongens Lyngby, Denmark, November 14th 2012

Christina Mark[1], Kinga Zór[2], Arto Heiskanen[2], Birte Svensson[3], Jenny Emnéus[2], Martin Dufva[4], and Christine Finnie[1]: **Monitoring programmed cell death of living plant tissues in microfluidics using electrochemical and optical techniques**, 8th Protein.DTU Workshop, Kongens Lyngby, Denmark, November 1st 2012

Christina Mark[1], Arto Heiskanen[2], Kinga Zór[2], Birte Svensson[3], Jenny Emnéus[2], Martin Dufva[4], and Christine Finnie[1]: **Microfluidic monitoring of programmed cell death in living plant tissue**, Plant Biology Congress, Freiburg, Germany, July 29th to August 3rd 2012

[1] Agricultural and Environmental Proteomics, Department of Systems Biology, Technical University of Denmark
[2] Bioanalytics, Department of Micro- and Nanotechnology, Technical University of Denmark
[3] Fluidic Array Systems and Technology, Department of Micro- and Nanotechnology, Technical University of Denmark
[4] Enzyme and Protein Chemistry, Department of Systems Biology, Technical University of Denmark

B Materials and Methods

B.1 Chemicals

ABA, acetic acid, acetonitrile, Amersham ECL Western Blotting Reagent, Amido Black staining solution, ampholytes, ampicillin, Amylase Activity Assay Kit, AsA, $CaCl_2$, CHAPS, cPTIO, dicoumarol, DPI, dithiothreitol, ECL Western Blotting Detection Reagents, ethanol, FDA, FiC, GA, Goat anti-rabbit IgG conjugated Alkaline Phosphatase, M, methanol, NaN_3, nystatin, phytic acid, sodium acetate, SNP, succinic acid, T, tetraethylammonium bromide, thiourea, trifluoroacetic acid, Trizma base, urea, and vanadate-molybdate reagent were obtained from Sigma-Aldrich Co. (St. Louis, MO, USA), while MM 4-64 was obtained from Biomol GmbH (Hamburg, Germany). cOmplete Mini EDTA-free Protease Inhibitor Cocktail Tablets were obtained from Roche (Basel, Switzerland), and Amine-reactive 6-plex TMT Reagents were obtained from Thermo Scientific (Pierce Protein Biology Products, Thermo Fisher Scientific Inc., Rockford, IL, USA).

B.2 Multiwell plate setup

The 24 cylindrical pillars were fabricated by casting PDMS in a 48-well flat-bottomed multiplate (Nunc, Nunclon Delta Surface, Thermo Scientific, Waltham, MA, USA) and cured at 50°C overnight. After removal, the cylinders were immobilised on the inside of the lid of a 24-well multiwell flat-bottomed culture plate (Nunc, Nunclon Delta Surface, Thermo Scientific, Waltham, MA, USA) with cut-outs of double-sided adhesive silicone tape (INT TA106, Intertronics, Oxfordshire, UK) cut using laser ablation (48-5S Duo Lase carbon dioxide laser from Synrad Inc., Mukilteo, WA, USA). The pillars were immobilised on the lid to have one pillar in each well with approximately 1 mm space between the end of the pillars and the bottom of the wells. Double-sided adhesive silicone tape was also placed at the bottom of the pillars (facing the bottom of the wells) for aleurone layer immobilisation.

B.3 Plant material and incubation buffer

Barley grains (*Hordeum vulgare* cv. Himalaya, 2003 harvest, Washington State University, Pullman, USA) from a batch previously used to study production of secreted hydrolases [7] were de-embryonated, surface sterilised with 70% ethanol, rinsed four times with sterile H_2O, and imbibed in sterile H_2O with 50 μg mL^{-1} ampicillin and 5 μg mL^{-1} nystatin for 4 days in the dark at 4°C. Aleurone layers were isolated by gently scraping away the starchy endosperm with the blunt side of a metal scalpel.
For the non-immobilised, original experimental setup, 5 aleurone layers (approximately 50 mg fresh weight) were incubated in separate wells of 12-well multiplates placed at room temperature on a shaker at 150 rpm for the indicated time. Each well held 1 mL incubation buffer with phytohormones or effector compounds as indicated elsewhere. For liquid N_2-treated samples, freshly isolated aleurone layers were immersed in liquid nitrogen for 1 min and allowed to thaw at room

temperature, prior to assay of redox activity. All incubations were set up in at least triplicates.
For the immobilised 24-well multiplate setup (Appendix B.2, page 109) the outside of the aleurone layers (facing outwards *in vivo*) were dried shortly by placing them on filter paper for 5 seconds, after scraping away the endosperm. Subsequently, 4 mm circular punch-outs were made with a biopsy puncher (Disposable Biopsy Punch, 4.0 mm w/Plunger, Miltex, Integra LifeSciences, Plainsboro, NJ, USA). The aleurone layer punch-outs were immobilised on the pillars of the 24-well multiplate lid by lightly pressing the outside of the aleurone layer punch-outs onto the silicone tape, thus facing the inside of the aleurone layer punch-outs (facing the endosperm *in vivo*) towards the bottom of the wells. To prevent drying of already immobilised punch-outs during immobilisation of the remaining punch-outs, a drop of sterile H_2O was applied on top of each punch-out. Incubation was started by placing the lid with the immobilised aleurone layer punch-outs in a 24-well multiwell plate and placing the plate at room temperature on a shaker at 150 rpm for the indicated time. Each well held 0.5 mL incubation buffer with phytohormones or effector compounds as indicated elsewhere. All incubations were set up in four replicates within each multiwell plate lid. For Part IV: Article Manuscript #2 (page 61) two identical plate lids were set up, yielding eight replicates of each treatment.
For both setups, the incubation buffer was composed of 20 mM succinic acid, 20 mM $CaCl_2$, 20 mM Trizma base, pH 5 with 50 μg mL^{-1} ampicillin and 5 μg mL^{-1} nystatin. Concentrations of phytohormones and effector compounds: ABA, 10 μM; GA, 10 μM; DPI, 10 μM; T, 20 mg mL^{-1}; SNP, 100 μM; cPTIO, 100 μM; AsA, 50 μM; dicoumarol, 100 μM; NaN_3, 5 mM.

B.4 Cell viability assay

Cell viability of intact aleurone layers was based on a previously described method [12].
For the non-immobilised, original experimental setup, the incubation buffer was removed and aleurone layers were washed with 20 mM $CaCl_2$ before staining with fluorescein diacetate (2 μg mL^{-1} in 20 mM $CaCl_2$) and MM 4-64 (2 μM in 20 mM $CaCl_2$). Each staining step was followed by washing with 20 mM $CaCl_2$. The aleurone layers were immobilised with cover glass on microscope slides. The aleurone layers were observed with a microscope (AXIO OBSERVER.Z1 with EC Plan-Neofluar 10x/0.30 Ph 1 objective and AxioCamMR3 camera with the AxioVision LE 4.8.2.0 software, Carl Zeiss Microscopy GmbH, Jena, Germany) and digital images were taken of three different regions of three different aleurone layers for each sample.
For the immobilised 24-well multiplate setup (Appendix B.2, page 109) the lids with the immobilised aleurone layer punch-outs were transferred to new multiwell plates for washing in 20 mM $CaCl_2$ before being transferred to a second set of plates for staining with fluorescein diacetate (2 μg mL^{-1} in 20 mM $CaCl_2$, 0.5 mL per well) and to a third set of plates for staining with MM 4-64 (2 μM in 20 mM $CaCl_2$, 0.5 mL per well). Each staining step was followed by washing with 20 mM $CaCl_2$ in a new multiwell plate each time. After staining and a last washing step, the lids were transferred back to the original multiwell plates with the incubation buffer. The aleu-

rone layers were then observed with a microscope (AXIO OBSERVER.Z1 with EC Plan-Neofluar (10x or 5x)/0.16 Ph 1 M27 objective and AxioCamMR3 camera with the AxioVision LE 4.8.2.0 software, Carl Zeiss Microscopy GmbH, Jena, Germany) and digital images were taken of three separate regions of each aleurone layer (10x optical zoom) or of the middle of each punch-out (5x optical zoom). The position of each region was stored in the microscope software to enable imaging of the same region for each punch-out throughout the time course study.
For both setups, the size of the photographed regions were 872x655 μm for 10x optical zoom and 1784x1310 μm for 5x optical zoom. Percentages of dead cells were determined using the Colour Deconvolution plugin [130] for the ImageJ 1.45s software (National Institutes of Health, USA).

B.5 Redox activity assay

Redox activity measurements were based on the method previously described for yeast cells [79]. For the non-immobilised, original experimental setup, the redox mediators M and/or FiC were added to the incubation buffer after incubation of the intact aleurone layers in the presence or absence of phytohormones and/or DPI to obtain final concentrations of 20 mM FiC and 100 μM M in the incubation buffer. The aleurone layers were incubated in the presence of redox mediators for 1 h at room temperature on a shaker unless otherwise specified. The spent incubation buffer with the redox mediators was transferred to Eppendorf tubes and centrifuged (14800 rpm for 10 min; SIGMA 1-14 Microfuge, SIGMA Laborzentrifugen GmbH, Osterode am Harz, Germany). The clarified supernatant was transferred to new tubes, frozen in liquid nitrogen and stored at -80°C until electrochemical analysis. The aleurone layers were transferred to aluminium weighing boats, and dried for a minimum of 24 h at 80°C for determination of dry weight.
For the immobilised 24-well multiplate setup (Appendix B.2, page 109) the lids with the immobilised aleurone layer punch-outs were transferred to new multiwell plates for washing in sterile H_2O before being transferred to two identical new plates containing 0.5 mL redox mediator mix (20 mM FiC and 100 μM M in fresh incubation buffer) in each well. After 1 h incubation at room temperature on a shaker at 150 rpm, both lids were washed in sterile H_2O in separate new plates and then transferred back to the original plates with the incubation buffer. The spent redox mediator mix was transferred to separate Eppendorf tubes, frozen in liquid nitrogen and stored at -80°C until electrochemical analysis.

B.6 Electrochemical detection of redox activity

The setup consisted of a peristaltic pump (Minipuls 2, Gilson, Inc., Middleton, WI, USA) providing a continuous flow (500 μL min^{-1}) of incubation buffer to define the baseline, an injection port (Model 7010, Rheodyne, Inc., Cotati, CA, USA) with a sample loop of 50 μL, an electrochemical cell designed and fabricated for commercial screen printed electrodes (Dropsense) and a potentiostat (Model CHI 1010A, CH Instrument Inc., Austin, TX, USA). 50 μL of each sample was injected in carrier buffer flow through the injection port to the electrochemical cell containing a

screen printed electrode (DS 250 AT, DropSense, Asturias, Spain). The FoC present in the samples was electrochemically oxidised on the Au working electrode at +400 mV vs. an Au reference electrode. Each of the three biological replicates was injected three times and peak currents were averaged. The FoC content was calculated using a calibration curve of FoC standard solutions.

B.7 Spectrophotometrical detection of redox activity

Spectrophotometrical determination of redox activity was based on a previously described method [138].
Prior to incubation with redox mediators (Appendix B.5, page 111, non-immobilised setup), 50 μL supernatant was extracted from all samples and clarified to act as background absorbance measurements to be subtracted from the actual sample absorbance measurements, and remaining samples ($\approx$1 mL incubation buffer with five aleurone layers) were incubated with redox mediators. Clarified supernatants (both exposed and not exposed to redox mediators) were diluted 20 times with fresh incubation buffer, and triplicate volumes of 100 μL diluted supernatant from each sample was transferred to separate cuvettes (Two-Sided Disposable Plastic Cuvettes, VWR International, Radnor, PA, USA) containing 600 μL MilliQ water [138]. Immediately prior to use the BPDS reaction mix was prepared by mixing 10 mL 3 M sodium acetate buffer (pH 6-6.5), 10 mL 0.2 M citric acid, 5 mL 3.3. mM ferric chloride, and 5 mL 6.2 mM BDPS, and 300 μL of this mix was transferred to each cuvette with precise time intervals [138]. The red Fe^{2+}-$(BPDS)_3$-complex was allowed to form for 5 min for each sample before the absorbance at 535 nm was measured (Ultrospec 2100 pro UV/Visible Spectrophotometer, GE Healthcare Life Sciences, UK) [138]. The FoC content (c) was determined by Lambert Beers law:

$$c = \frac{A_{sample} - A_{background}}{\epsilon \cdot l} \cdot D$$

using the difference in absorbance between the sample and the background ($A_{sample} - A_{background}$), the molar extinction coefficient of BPDS ($\epsilon = 20.500$ M^{-1} cm^{-1} [138,141]), the length of the spectrophotometer cuvette ($l = 1$ cm), and the dilution factor ($D = 20$).

B.8 Western blotting

After incubation (Appendix B.3, page 109, non-immobilised setup), the incubation buffer was centrifuged, frozen in liquid nitrogen and stored at -80°C until Western blotting. 25 μL thawed samples were separated on a NuPAGE 4-12% BisTris 12-well gel (Invitrogen, Thermo Scientific, Waltham, MA, USA) before blotting onto a nitrocellulose membrane (Hybond-ECL, Amersham, GE Healthcare Life Sciences, UK). The blot was probed with rabbit polyclonal antibodies raised against barley α-amylase (Søgaard and Svensson, 1990). Secondary goat anti-rabbit IgG antibodies conjugated to alkaline phosphatase, and Amersham ECL Western Blotting Reagent and ECL Western Blotting Detection Reagents were used to detect binding. Detection was performed on

an AutoChemi Darkroom Imaging System (UVP, Upland, CA, US).

B.9 α-amylase activity assay

α-amylase activity determinations followed the protocol provided by the manufacturer (Amylase Activity Assay Kit, Sigma-Aldrich Co., St. Louis, MO, USA) but applied halved volumes. After incubation of immobilised aleurone layer punch-outs (Appendix B.3, page 109, immobilised setup), duplicates of 24 μL from each well of the 24-well incubation plate were transferred to separate wells of a 96-well plate, before the lid with the immobilised aleurone layer punch-outs was placed back in the original plate for continued incubation. To one set of duplicates in the 96-well plate, 1 μL fresh buffer was added, while the other set of duplicates was spiked with 1 μL 25 U mL^{-1} U pure α-amylase solution per well. 50 μL Master Reaction Mix was added to the separate wells of the 96-well plate and a series of standard solutions, positive and negative controls, and a pure spike (1 μL α-amylase and 24 μL buffer) were added to empty wells of the plate. The plate was incubated in the dark at room temperature and the absorbance measured with 10 min intervals for 1 h at 405 nm (PowerWave XS Microplate Spectrophotometer, BioTek Instruments, Winooski, VT, US). A linear standard curve based on the standard dilutions was used to calculate the actual activity of the pure spike using a blank of pure buffer as follows:

$$\Delta nitrophenol = \frac{(Abs_{pure\ spike} - Abs_{blank}) - intercept_{std.\ curve}}{slope_{std.\ curve}}$$

$$Activity\ in\ pure\ spike = \frac{\Delta nitrophenol \cdot Dilution\ Factor}{Reaction\ Time \cdot Volume}$$

The activities in the unspiked samples were then calculated as follows using absorbance measurements on both samples and spiked samples:

$$Activity\ in\ sample = \frac{Activity\ in\ pure\ spike \cdot (Abs_{sample} - Abs_{blank})}{(Abs_{spiked\ sample} - Abs_{blank}) - (Abs_{sample} - Abs_{blank})}$$

The results were converted to α-amylase activity units (U), as one unit is defined as the amount of α-amylase that cleaves ethylidene-pNP-G7 to generate 1.0 μmol of *p*-nitrophenol per minute at 25°C [160].

B.10 Phytase activity assay

Phytase activity determination was based on a previously described method [163].
After incubation of immobilised aleurone layer punch-outs (Appendix B.3, page 109, immobilised setup), the lid with the punch-outs was transferred to a new multiwell plate for washing in sterile H_2O. Subsequently, the lid was transferred to a second plate containing 200 μL substrate solution (10 mM phytic acid in 0.1 M sodium acetate buffer, pH 5.0) in each well, and incubated for 1 h at 37°C. Subsequently, the lid to a new multiwell plate for washing in sterile

H_2O and then transferred back to the original plate for continued incubation. 300 μL vanadate-molybdate reagent was added to each well of the plate containing the substrate solution and the absorbance measured at 415 nm (PowerWave XS Microplate Spectrophotometer, BioTek Instruments, Winooski, VT, US). A series of standard solutions of dibasic phosphate potassium ranging from 0 to 10 μM was prepared in a separate plate with 200 μL in each well before addition of 300 μL vanadate-molybdate reagent and subsequent absorbance measurements at 415 nm. Based on a polynomial standard curve of the phosphate dilutions [162], measured absorbances were translated to activities and expressed in phytase activity units (FTU). One FTU is defined as the amount of phytase that liberates 1.0 μmol of *ortho*-phosphate per minute at 37°C [165,166].

B.11 Transient expression

Transformation of aleurone layer punch-outs were performed immediately after immobilisation by bombardment in a DuPont Biolistic PDS-1000/He Particle Delivery System (Bio-Rad, USA) using 650 psi rupture discs and 0.6 μm gold particles coated with plasmid DNA as detailed by the supplier. Three or four PDMS pillars were placed in the bombardment area per shot, and the pillars were placed at the lowest level of the bombardment system to increase the chance of the plasmid-coated gold particles penetrating the cell walls of the aleurone cells and decrease the risk of the particles ricocheting off of the cell walls. To prevent drying of already transformed aleurone layer punch-outs during transformation of the remaining punch-outs, a drop of sterile H_2O was applied on top of each punch-out immediately after re-mounting of the PDMS pillars in the lid of the multiwell plate system. Aleurone layers were transformed with naked gold particles (negative control) or with particles coated with one of three constructs. The α-amylase construct (pAMY-αGFP-N) comprised an α-amylase promoter fused to a synthetic GFP-sequence, the phytase construct (ScPAPb-pro-GFP) a phytase promoter (*ScPAPhy*_b, as described by [153]) fused to a synthetic GFP-sequence, and the positive control construct (pUhGFPC3N, as described by [151]) the maize ubiquitin 1 gene (*Ubi-1*) fused to a synthetic GFP-sequence. pAMY-αGFP-N and pScPAPb-pro-GFP-N were constructed by replacing the PstI-EcoRI ubiquitin promoter of pU-hGFP-C3-N with a 745 bp or 2687 bp PstI-EcoRI fragment of the α-amylase and rye *PAPhy*_b promoter, respectively. For pAMY-αGFP-N the α signal peptide from pUSPPhyN [157] was ligated into the PstI site downstream the α-amylase promoter.
Observations of GFP-expression was performed similarly to the cell viability assay, as cells were stained with MM 4-64 (Appendix B.4, page 110) at the first imaging session and then every 24 h to ease identification of dead cells. After staining and washing, the transformed aleurone layers were observed with a microscope (AXIO OBSERVER.Z1 with EC Plan-Neofluar 5x/0.16 Ph 1 M27 objective and AxioCamMR3 camera with the AxioVision LE 4.8.2.0 software, Carl Zeiss Microscopy GmbH, Jena, Germany) and digital, two-channel (red, green) images were taken of the middle of each punch-out (5x optical zoom). The position of each region was saved with the microscope software to enable imaging of the same region for each aleurone layer through-

out the time course study. For digital image analysis, 600x600 μm regions containing visually identified GFP-expressing cells were excised. To ensure correct determination of fluorescence levels for GFP-expressing cells and non-GFP-expressing autofluorescent (green [116]) cells without interference from dead cells (orange-red), only the green channel of the images were used for the subsequent analysis. Using the ImageJ 1.45s software (National Institutes of Health, USA), fluorescence levels of GFP-expressing cells in the excised 600x600 μm regions were determined by measuring intensity per area for visually GFP-expressing cells and comparing to an average of four visually non-GFP-expressing cells per image. Visually identified GFP-expressing cells were only accepted as truly GFP-expressing cells, if the fluorescence level exceeded 115% of the average of the non-GFP-expressing cells at minimum one time point throughout the time course study. This requirement was not relevant for the negative control for which random non-GFP-expressing cells were chosen for analysis. For data analysis the average of the background/autofluorescence was subtracted from GFP-expression values.

B.12 Statistical analysis

All data was analysed using the GraphPad Prism 6.04 software (GraphPad Software, Inc., San Diego, CA, USA) by first subjecting datasets to the ROUT (Robust regression and Outlier removal) outlier analysis with a false discovery rate of 1%. Subsequently, outlier analysed data was then subjected to Fisher's LSD (Least Significant Difference) two-way ANOVA test at a confidence level of 95%.

B.13 Proteomics preparations

Data obtained with proteomics analysis is presented in Section III.2: Proteomics analysis of protein abundance levels (page 49).
Mass spectrometry-based proteomics analysis was performed on cell extracts of five non-immobilised aleurone layers (approximately 50 mg) incubated with GA, GA+DPI, ABA, ABA+DPI, or GA+ABA for 48 h as described in Appendix B.3 (109). Each sample was produced in four replicates. Aleurone layers were frozen in liquid nitrogen and stored at -80°C until proteomics analysis.

Protein extraction and gel filtration

Total protein content was extracted by grinding of the frozen aleurone layers with quartz sand in a chilled mortar in 250 μL extraction buffer (7 M urea, 2 M thiourea, 2% 3-((3-cholamidopropyl) dimethylammonio)-1-propanesulfonate (CHAPS), 0.5% ampholytes pH 3-10, 5 mM dithiothreitol, cOmplete Mini EDTA-free Protease Inhibitor Cocktail Tablets (one tablet per 10 mL). The extracts were transferred to Eppendorf tubes and the mortar washed with 250 μL extraction buffer, which was transferred to the same tubes. Subsequently, sample extracts were placed on an Eppendorf shaker at room temperature for 2 h, centrifuged for 30 min (14800 rpm, SIGMA 1-14

Microfuge, SIGMA Laborzentrifugen GmbH, Osterode am Harz, Germany), and 200 μL of supernatant from each sample transferred to fresh tubes. All samples were kept at $-20°$C, during extraction of other samples.
For gel filtration, Illustra NAP-10 columns were placed over suitable waste containers for collection of flow through, and the excess liquid was allowed to drain through the columns. 15 mL gel filtration buffer (8 M urea, 50 mM tetraethylammonium bromide, pH 8.0) was used for equilibration of the columns, before the total sample volume (200 μL) was added and allowed to enter the gel bed completely. Subsequently, 800 μL gel filtration buffer was added and allowed to enter the gel bed completely, before elution of the samples with 500 μL gel filtration buffer into fresh Eppendorf tubes. Samples were stored at $-20°$C.

Popov determination of protein content
Triplicates of 5 μL from each sample were mixed with 45 μL H_2O and 300 μL staining solution (26 mg Amido Black per 100 mL, 10% acetic acid, 90% methanol, filtered) before vortexing and 5 min incubation at room temperature. Samples were then centrifuged for 10 min (14800 rpm), and the supernatant was discarded before addition of 500 μL washing solution (10% acetic acid, 90% ethanol) to the protein precipitate and vortexing of the samples. The samples were then centrifuged for 10 min (14800 rpm), the supernatant discarded and the protein precipitate washed, vortexed and centrifuged again (same conditions). The supernatant was again discarded and the protein precipitate allowed to air-dry for a few minutes before being dissolved in 300 μL 0.1 M NaOH. 250 μL of each dissolved sample was transferred to a 96well multiwell plate along with a standard curve of bovine serum albumin (0, 0.5, 1.0, 1.5, 2.0 and 2.5 μg), and the absorbance at 615 nm was measured (PowerWave XS Microplate Spectrophotometer, BioTek Instruments, Winooski, VT, US). Determined protein contents can be found in Table B.1.

Table B.1: Popov determination of protein content

Sample	GA #1	GA #2	GA #3	GA #4
Concentration [μg μL^{-1}]	0.6258	0.7700	1.0421	0.8287
Sample	GA+DPI #1	GA+DPI #2	GA+DPI #3	GA+DPI #4
Concentration [μg μL^{-1}]	0.8854	0.8768	0.8796	0.9412
Sample	ABA #1	ABA #2	ABA #3	ABA #4
Concentration [μg μL^{-1}]	0.7374	0.7518	0.8047	0.8316
Sample	ABA+DPI #1	ABA+DPI #2	ABA+DPI #3	ABA+DPI #4
Concentration [μg μL^{-1}]	1.0354	0.9421	0.9286	1.0709
Sample	GA+ABA #1	GA+ABA #2	GA+ABA #3	GA+ABA #4
Concentration [μg μL^{-1}]	0.8296	1.0700	0.8498	0.9739

Reduction, alkylation, precipitation, and digestion
All samples were diluted to 200 μL of 0.5 μg μL^{-1} with gel filtration buffer. Reduction was performed by addition of 4 μL 450 mM dithiothreitol in 100 mM tetraethylammonium bromide with

1 h incubation at room temperature. Subsequently, alkylation was performed by addition of 8 μL freshly made 500 mM iodoacetamide in 100 mM tetraethylammonium bromide with 45 min incubation in the dark at room temperature. The samples were then precipitated by addition of 6x volume of ice cold 100 % acetone (1272 μL), mixing and incubation overnight at $-20°$C. Subsequently, samples were allowed to obtain room temperature and then vortexed to allow urea precipitates to dissolve before centrifugation for 15 min (14800 rpm). The supernatants were discarded and the protein precipitates washed in 500 μL 80 % acetone before vortexing and centrifugation for 5 min (14800 rpm). The supernatant was again discarded and the protein precipitates allowed to air-dry for a few minutes, before resuspension in 100 μL 100 mM tetraethylammonium bromide and shaking for 1 h at room temperature. In preparation for digestion, 20 μL trypsin storage buffer was added to 20 μg lyophilised trypsin and left for 5 min before addition of 2.5 μL to each sample. Samples were mixed, centrifuged shortly to collect all liquid at the bottom of the tubes, and left to digest overnight at 37°C. Finally, all samples were centrifuged for 5 min (14800 rpm) to collect undissolved and therefore undigested protein in the bottom of the tubes.

Peptide labelling

Immediately before use the TMT label reagents were equilibrated to room temperature, 41 μL anhydrous acetonitrile were added to each 0.8 mg vial, and the reagents were allowed to dissolve for 5 min with occasional vortexing before being centrifuged shortly to collect all liquid at the bottom of the tubes. The samples (minus pelleted, undigested protein) were then transferred to the relevant TMT reagent vials (Table B.2), mixed and incubated for 1 h at room temperature. Subsequently, quenching the labelling reaction was performed by addition of 8 μL 5% hydroxyalamine in 100 mM tetraethylammonium bromide was added to each sample followed by 15 min incubation at room temperature. All label vials now contained 100 μg labelled peptides in 151.5 μL (0.66 μg μL^{-1}).

38 μL (25 μg) of each sample were then mixed as detailed in Table B.3 to obtain four mixes of 150 μg peptides in 228 μL, before addition of 2 μL 20% trifluoroacetic acid to each mix for acidification. All peptide mixes thus contained a replicate of each sample, all labelled with a different TMT label.

Stage tip purification

Stage tip columns were prepared by punching two disks of C18 solid phase extraction material (3M Empore Solid Phase Extraction Disks, C18, thickness 0.50±0.05 mm, Fisher Scientific,

Table B.2: Peptide labelling

Sample	GA	GA+DPI	ABA	ABA+DPI	GA+ABA
Label	TMT126	TMT127	TMT128	TMT129	TMT130

Table B.3: Peptide mixes

Mix #1	Mix #2	Mix #3	Mix #4
GA #1	GA #2	GA #3	GA #4
GA+DPI #1	GA+DPI #2	GA+DPI #3	GA+DPI #4
ABA #1	ABA #2	ABA #3	ABA #4
ABA+DPI #1	ABA+DPI #2	ABA+DPI #3	ABA+DPI #4
GA+ABA #1	GA+ABA #2	GA+ABA #3	GA+ABA #4
IS #1	IS #2	IS #3	IS #4

Waltham, MA, USA) with a sampling tool with a 1 mm diameter and gently placing the disks on top of each other in a DL-10 tip (Diamond Tower Pack, 10 μL tips, Gilson, Middleton, WI, USA). The stage tip was mounted on the P1000 pipette setup, 10 μL wetting solution (80% acetonitrile, 0.1% trifluoroacetic acid) was placed on top of the disks and gently pressed through, before addition of 20 μL equilibration solution (0.1% trifluoroacetic acid) was placed on top of the disks and also pressed through. 5 μg (7.7 μL) of each acidified peptide mix was added to the top of the disks in separate stage tips and slowly pressed through, before 20 μL washing solution (5% acetonitrile, 0.1% trifluoroacetic acid) was placed on top of the disks and also pressed through. Washing was repeated twice. Finally, 10 μL elution solution (50% acetonitrile, 0.1% trifluoroacetic acid) was placed on top of the disks with care to avoid air bubbles between the elution solution and the column bed, the solution was gently pressed through to elute the purified peptides into a fresh tube, and the tube was centrifuged shortly to collect all liquid at the bottom of the tube. The purified peptide mixes should have been lyophilised in a speed-vacuum, but the equipment was out of order, and samples were therefore left to dry in an airing cupboard at room temperature for a few hours and then stored at -80°C until further use. Each purified peptide mix of 5 μg was redissolved in 2.5 μL 10% formic acid (yielding 2 μg μL^{-1} peptides in 10% formic acid), and subsequently all samples were diluted 20x with H_2 (yielding 0.1 μg μL^{-1} peptides in 0.5% formic acid) before loading onto the LC-MS system.
For stage tip purification, all solutions were made with MS-grade reagents, and all handling of 100% acetonitrile and 100% trifluoroacetic acid were carried out with glass pipettes only. All tubes and pipette tips were made of polypropylene, and the entire procedure was carried out in a LAF bench to avoid any contamination of the samples.

LC-MS setup

The LC-MS setup consisted of an EASY-nLC Liquid Chromatograph with Easy-Spray column (ES802: 25 cm x 75 μm ID, PepMap C18, 2 μm particles, 100 Å pore size, 120 min gradient) connected to an Orbitrap Fusion Mass Spectrometer operated in MultiNotch MS3-mode (all from Thermo Scientific, Waltham, MA, USA). Each biological replicate was run three times. Documents regarding applied analysis settings can be found on the enclosed data disc (Appendix C, page 119).

C Data disc

The data disc enclosed here contains documents regarding setup and analysis of the proteomics LC-MS analysis.

DTU Systems Biology
Department of Systems Biology
Technical University of Denmark

Søltofts Plads
2800 Kgs. Lyngby

www.bio.dtu.dk